Development of Polyolefin Nanocomposites for Electrical Applications

Dissertation

With the aim of achieving the doctoral degree
at the Faculty of Mathematics, Informatics and Natural Sciences

submitted to the
Department of Chemistry
University of Hamburg

Sven Käselau

Hamburg 2019

The experimental work described in this thesis has been carried out between October 2013 and June 2017 at the Institute of Technical and Macromolecular Chemistry of the University of Hamburg in the research group of Professor Dr. Gerrit A. Luinstra.

Date of Disputation: 30.08.2019

Approval for Printing: 30.08.2019

The following referees recommend the acceptance of this doctoral thesis:

1. Evaluator: Professor Dr. Gerrit A. Luinstra

2. Evaluator: Professor Dr. Hans-Ulrich Moritz

In Gedanken an Heinz Käselau

Für meine Familie

List of Publications

Original article

S. Käselau, S. Scheel, L. Petersson, C.-H. Ho, and G.A. Luinstra, *Polym. Int.*, **67**, 1359 (2018).

S. Käselau, S. Scheel, L. Petersson, C.-H. Ho, and G.A. Luinstra, *Polym. Int.*, **68**, 946 (2019).

Patents

ABB TECHNOLOGY LTD., 2017, *Next Level Nanocomposites for Electrical Insulation*, Inventors: C.-H. Ho, S. Scheel, L. Petersson, S. Käselau, G. Luinstra, 12.01.2017. Filing date: 03.07.2015. CH, Patent WO2017005280

Symbols and Abbreviations

aPP	atactic polypropylene
CGC	constrained geometry catalyst
CMR	carcinogenic, mutagenic, or toxic for reproduction
CNT	carbon-nanotube
DBM	dibutyl magnesium
DSC	differential scanning calorimetry
EDX	energy-dispersive X-ray spectroscopy
HDPE	high density polyethylene
ICI	Imperial Chemical Industries
iPP	isotactic polypropylene
LDPE	low-density polyethylene
LLDPE	linear low-density polyethylene
MAO	methylaluminoxane
MASS	magic angle solid state
NMR	nuclear magnetic resonance spectroscopy
Đ	dispersity
PE	polyethylene
PET	polyethylene terephthalate
PFT	polymerization-filling technique
PP	polypropylene
PS	polystyrene
PUR	polyurethane
PVC	polyvinylchloride
rac	*racemic*
SEC	size exclusion chromatography
SEM	scanning electron microscopy
sPP	syndiotactic polypropylene
TEM	transmission electron microscopy
TGA	thermogravimetric analysis
TIBA	triisobutylaluminum
TMA	trimethylaluminum
WAXD	wide-angle X-ray diffraction

Compounds used in this work

Bis(*n*-butylcyclopentadienyl)zirconium(IV) dichloride **1**

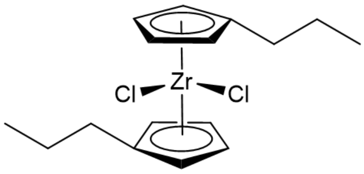

[dimethylsilane diyl-bis(2-methyl-4-phenylindenyl)]zirconium(IV) dichloride **2**

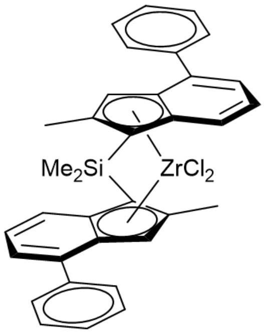

Table of contents

1 Summary

Polyolefins, like polyethylene (PE), linear low-density polyethylene (LLDPE) or polypropylene (PP) are among the most widely used polymers at present time. By incorporating nanofillers into those polymer composites, extended or novel polymer properties can be obtained. However, it is very challenging to incorporate highly polar oxidic nanofillers into a nonpolar polymer without the appearance of agglomeration by common melt mixing strategies.

In this work, a modified *in situ* co-polymerization of 1-octene and ethylene in the presence of polar core/shell-like MgO@Mg$(OH)_2$ nanoparticles is presented. In this way, LLDPE-C6/MgO@Mg$(OH)_2$ nanocomposites with up to 25 wt% filler content were obtained. (*n*-BuCp)$_2$ZrCl$_2$/methylaluminoxane (MAO) as catalyst system was supported on the nanosized core-shell MgO@Mg$(OH)_2$ particles, which transferred the catalyst system from a homogeneous to a heterogeneous system. A method to reduce the MAO content was developed, as free charge carrier are disadvantages for insulation applications. It was found that the pre-impregnation of the MgO@Mg$(OH)_2$ nanoparticles with 0.6 mmol dibutyl magnesium (DBM) per gram MgO@Mg$(OH)_2$ before MAO impregnation allows to reduce the amount of MAO significantly by 50% without any influence in the average catalyst activity of about 50-60 t·mol^{-1}·h^{-1}. ^{27}Al-MAS-NMR indicated covalent bonds of Mg-O-Al between MAO and the MgO@Mg$(OH)_2$ surface. SEM and EDX mapping showed homogeneous dispersed filler in the nanocomposites obtained by *in situ* polymerization. These are present as single encapsulated nanoparticles at 100 nm scale. A prior surface modification of the filler was thus avoided to reduce the surface energy.

The established synthesis route was successfully transferred from 20 g laboratory scale to 500 g pilot plant scale. LLDPE/MgO@Mg$(OH)_2$ nanocomposites with 7 wt% nanoparticles were synthesized as masterbatches with and without DMB impregnation. The average catalytic activity of 50 t·mol^{-1}·h^{-}1 was comparable to small scale experiments. As reference, LLDPE/MgO@Mg$(OH)_2$ nanocomposites were obtained by conventional melt extrusion. AFM, SEM and EDX mapping showed homogeneous particle distribution for samples from *in situ* polymerization, whereas samples from melt extrusion showed heterogeneous particle distribution with micro sized agglomerates and voids near the filler indicating weak filler polymer matrix interaction. Filler distribution were more homogeneous, and the mechanical performance was better for samples with DBM pre-impregnations relative to MAO only impregnation.

Summary

Nanocomposites made of isotactic polypropylene and MgO@$Mg(OH)_2$, silicon dioxide or barium titanate were developed based on the established *in situ* polymerization of LLDPE/MgO@$Mg(OH)_2$ nanocomposites applying the same synthesis strategy. As catalyst system [dimethylsilane diyl-bis(2-methyl-4-phenylindenyl)]zirconium(IV) dichloride and MAO were used and supported on the oxidic nanofiller. The original agglomerates of the nanoparticles were broken up by treatment with dibutyl magnesium for MgO@$Mg(OH)_2$, and with ultrasound in the presence of MAO for SiO_2 and $BaTiO_3$. The tacticity (98% mmmm) of the *in situ* formed iPP was not influenced by the presence of the nanofillers. The obtained materials were diluted by melt extrusion to obtain composites with 0.5 wt% filler content. SEM and EDX mapping indicated that after melt extrusion agglomerates of primary particles disappeared and composites with a fine filler distribution were obtained. A significant reinforcing effect could not be detected for nanocomposites with 0.5 wt% filler.

2 Zusammenfassung

Polyolefine, wie Polyethylen (PE), *Linear Low-Density* Polyethylen (LLDPE) oder Polypropylen (PP), sind heute die am häufigsten verwendeten Polymeren. Durch die Kombination von Nanofüllstoffen mit diesen Polymeren können Verbundwerkstoffe mit erweiterten oder auch neuartigen Materialeigenschaften erhalten werden. Es ist jedoch sehr herausforderend polare oxidische Nanofüllstoffe in ein unpolares Polymer zu mischen, ohne dass es dabei bei gängigen Schmelzmischverfahren zu einer Füllstoffagglomeration kommt.

In dieser Arbeit wird eine modifizierte *in situ* Co-Polymerisation von 1-Octen und Ethylen in Gegenwart von polaren $MgO@Mg(OH)_2$ *Core-Shell*-Nanopartikeln vorgestellt. Auf diese Weise konnten LLDPE-C6/$MgO@Mg(OH)_2$ Nanokomposite mit bis zu 25 Gew.-% Füllstoffgehalt erhalten werden. Das Katalysatorsystem (*n*-BuCp)$_2$ZrCl$_2$/Methylaluminoxan (MAO) wurde hierbei auf nanoskalige *Core-Shell* $MgO@Mg(OH)_2$ Teilchen geträgert. Dadurch konnte das Katalysatorsystem von einem homogenen in ein heterogenes Katalysatorsystem transferiert werden. Aufgrund der für die Polymerisation notwendigen hohen Menge an Co-Katalysator MAO, wurde ein Verfahren zur Reduzierung des MAO-Gehaltes in den erhaltenen Kompositen entwickelt. Es wurde festgestellt, dass die Behandlung der $MgO@Mg(OH)_2$ Nanopartikel mit 0.6 mmol Dibutylmagnesium (DBM) pro Gramm $MgO@Mg(OH)_2$ vor der MAO-Imprägnierung die Menge an MAO um 50% signifikant reduziert, ohne dass dabei die durchschnittliche Katalysatoraktivität von 50-60 $t \cdot mol^{-1} \cdot h^{-1}$ negativ beeinflusst wird. ^{27}Al-MAS-NMR zeigte, dass MAO an der $MgO@Mg(OH)_2$ Oberfläche kovalent als Mg-O-Al gebundenen ist. REM- und EDX-Mapping zeigen, dass der Füllstoff in den durch *in-situ*-Polymerisation erhaltenen Nanokompositen homogen dispergiert ist. Diese lagen somit als einzelne, eingekapselte Nanopartikel von 100 nm-Maßstab vor. Eine weitere Oberflächenmodifizierung des Füllstoffes war so nicht mehr notwendig, um die Oberflächenenergie zu reduzieren.

Die zuvor etablierte Synthesestrategie wurde erfolgreich von 20 g Labormaßstab auf den 500 g Technikumsmaßstab übertragen. LLDPE/$MgO@Mg(OH)_2$ Nanokomposite mit 7 wt% Nanopartikeln mit und ohne DMB-Imprägnierung wurden so als *Masterbatches* synthetisiert. Die durchschnittliche katalytische Aktivität war vergleichbar mit denen aus dem Laborexperiment von 50 $t \cdot mol^{-1} \cdot h^{-1}$. Als Referenz wurden LLDPE/$MgO@Mg(OH)_2$ Nanokomposite konventionell durch Schmelzextrusion hergestellt. AFM, REM und EDX-Kartierung zeigten eine homogene Partikelverteilung für Proben der *in situ* Polymerisation, während Proben aus der Schmelzextrusion heterogene

Partikelverteilung mit Agglomeraten und Hohlräume zeigten, welches auf eine schwache Wechselwirkung des Füllstoffs mit der Polymermatrix hindeutet. Proben, die mit DBM vorimprägniert wurden, zeigten eine homogenere Füllstoffverteilung und höhere mechanische Eigenschaften im Vergleich zu Proben, die nur mit MAO behandelt wurden.

Nanokomposite aus isotaktischem Polypropylen und MgO@Mg(OH)$_2$, Siliziumdioxid oder Bariumtitanat wurden auf Basis der etablierten *in situ* Polymerisation von LLDPE/MgO@Mg(OH)$_2$-Nanokompositen mit der gleichen Synthesestrategie entwickelt. Als Katalysatorsystem wurden [Dimethylsilandiyl-bis(2-methyl-4-phenylindenyl)] Zirkonium(IV)dichlorid und MAO verwendet, welches auf den oxidischen Nanofüllstoffen geträgert wurde. Die ursprünglichen Agglomerate der Nanopartikel wurden durch Behandlung mit Dibutylmagnesium für MgO@Mg(OH)$_2$ und mit Ultraschall in Gegenwart von MAO für SiO_2 und $BaTiO_3$ aufgebrochen. Die Taktizität (98% mmmm) des *in situ* gebildeten iPP wurde durch die Anwesenheit der Nanofüller nicht beeinflusst. Die erhaltenen Materialien wurden in einem zweiten Schritt durch Schmelzextrusion verdünnt, um Komposite mit 0.5 Gew.-% Füllstoffgehalt zu erhalten. Die REM- und EDX-Analyse zeigte, dass nach der Schmelzextrusion Agglomerate von Primärpartikeln verschwanden und Verbundwerkstoffe mit einer feinen Füllstoffverteilung erhalten wurden. Ein signifikanter mechanischer Verstärkungseffekt konnte bei Nanokompositen mit 0.5 Gew.-% Füllstoff nicht nachgewiesen werden.

3 Introduction

Since the discovery of synthetic polymers in the 1920s by STAUDINGER, polymers have spread their way into more or less every aspect of today's life.[1, 2] Polymers have a low density, are cheap in production and can be easily processed. Driven by continuous innovation and based on the broad spectrum of polymer properties, materials like metal or wood were substituted to an ever higher degree.[3, 4] This process is ongoing and is reflected by the high growing rate of polymer production (Figure 3.1).

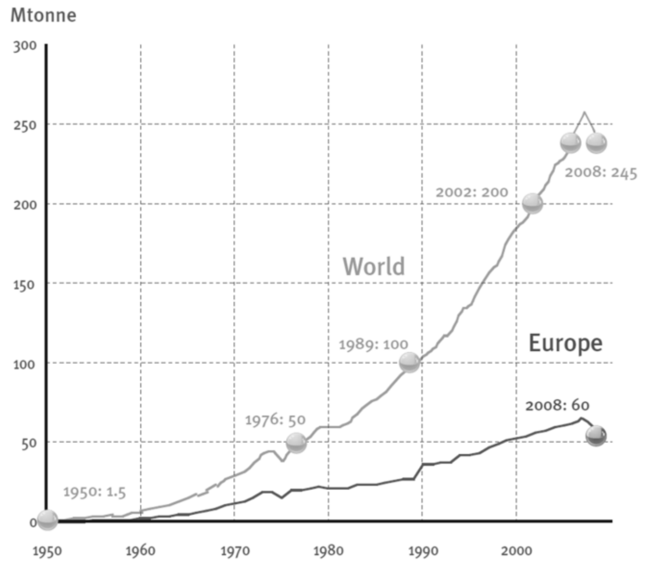

Figure 3.1 Growth of polymer production in Europe and worldwide from 1950-2008.[5]

Since the beginning of industrial polymer production in the 1950s, the polymer production has grown about 9% in average per year.[5] From 1.5 Mt in 1950, the total global polymer production has reached 311 Mt in 2014.[6] Packaging is the largest volume end-use for plastics (39.5%) followed by application in building and construction (20.1%), automotive (8.6%) and electrical and electronic industry (5.7%).[6]

80% of "European's" polymer production activities may be divided into five high-volume plastic families (Figure 3.2); polyethylene (including low-density (LDPE), linear low-density (LLDPE) and high density (HDPE)), polypropylene (PP), polyvinylchloride (PVC), polystyrene (solid PS and expandable EPS), polyurethane (PUR) and polyethylene terephthalate (PET).

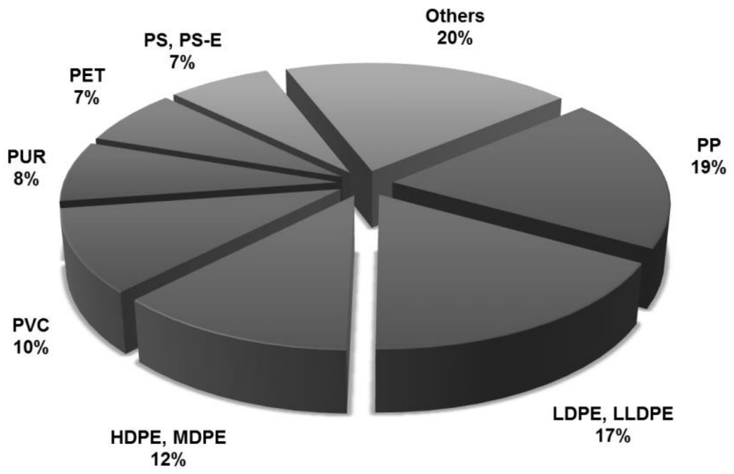

Figure 3.2 European plastics demand (47.8 Mt) by polymer type 2014.[6]

With a proportion of 49%,[6] polyolefins are the most important commodity polymers in volume and applications.[7–10] Optimized production processes and the availability of different catalysts make polyolefins cheap and easy to access.[11, 12] Depending on the microstructure, polyolefins can be soft and elastic or tough and hard. LLDPE with its good balance of rigidity and strength, and the range of processing conditions has seen the most rapid growth within the PE family.[13, 14] Custom-made polyolefins are substituting more and more expensive polymers made for special applications.[15] With the incorporation of micro or nano sized fillers, polymer composites with a new range of properties can be achieved. The development of polymer composites gives access to completely new materials or increases the cost efficiency by reducing the amount of material without a lack of polymer properties.

3.1 Catalytic Olefin Polymerization

3.1.1 ZIEGLER-NATTA-Catalysts

Polyethylene was first obtained by the polymerization of diazomethane in 1898.[16, 17] FAWCETT and GIBSON developed in 1933 the first industrial method to produce polyethylene (ICI-process).[18] In this process, ethylene is polymerized by a radical reaction with traces of oxygen at pressures of 1500-3000 bar and temperatures between 170-320 °C.[19] Highly branched polyethylene (low-density polyethylene; LDPE) with short and long-chain branches can be obtained by this way.[3] LDPE is characterized by a low crystallinity (40-45%), a density of 0.915-0.935 g·cm^{-3} and a melt temperature at 100-110 °C.[20]

In 1953, ZIEGLER reported a catalytic route to polymerize ethylene at low pressure (5-100 bar) and room temperature for the first time.[21] A mixture of titanium tetrachloride and triethylaluminum was used as catalytic system.[21–23] The obtained polyethylene (high density polyethylene; HDPE) is highly linear, crystalline, has a density of 0.94-0.965 g·cm^{-3} and a melt temperature in the range of 125-135 °C.[20] Due to the different micro structure of HDPE, HDPE is tougher and harder compared to LDPE.[3]

Since the beginning of 1970s, a new class of polyethylene was introduced by the co-polymerization of ethylene with 1-alkenes. Polyethylene with branching on the main chain was obtained (linear low-density polyethylene; LLDPE). Compared to HDPE, the density can be reduced to 0.92-0.94 g·cm^{-3} when side chains are introduced. The crystallinity can be reduced to 55-60% and the melt temperature is in the range of 120-130 °C. Depending on the co-monomer and content of co-monomer in the LLDPE, polymer properties can be designed for specific applications.[20]

COSSÉE and ARLMAN performed at that time sophisticated calculations on the heterogeneous catalytic system and concluded on a coordination-insertion-mechanism (Figure 3.3) for the catalytic polymerization. This proposal is overall accepted today as a useful description.[24] In a first step, the monomer is coordinated on a free coordination site on the active titane-(III)-species.[24] In a second step, coordinated monomer undergoes a migratory insertion reaction into a Ti-C-bound. This migration opens up another neighboring free coordination site. The reaction continues and the polymer chain can grow. The chain may be terminated when 1,2-hydrogen elimination occurs and polymerization is stopped.[24]

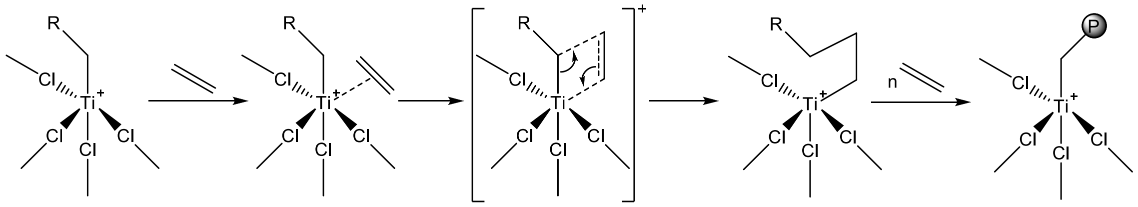

Figure 3.3 COSSÉE-ARLMAN-mechanism for ZIEGLER-NATTA-polymerization.[24]

An alternative catalytic system to polymerize ethylene to HDPE was developed by the *Phillips Petroleum Company* in the 1950s. They discovered a chromium oxide based catalyst (0.1-3 wt% CrO_3), which is supported on silicon dioxide. Compared to the

ZIEGLER-catalysts, the PHILLIPS-catalysts does not need to be activated by aluminum alkyls.[25, 26]

Based on the work of ZIEGLER, NATTA showed 1954 the polymerization of propylene and higher α-olefins on ZIEGLER-catalysts.[21, 27, 28] By analyzing different fractions of the polymer products with the help of X-ray diffraction, NATTA discovered the stereospecific polymerization of propylene to atactic (aPP), isotactic (iPP) and syndiotactic (sPP) polypropylene.[21, 29] Since those discoveries, catalyst systems from transition metal halogenides of group IV and main group metal alkyls are called ZIEGLER-NATTA-catalysts. The importance of ZIEGLER and NATTA'S work was awarded with the Nobel Prize in Chemistry in 1963.[21, 30]

The first ZIEGLER-NATTA-catalysts (generation I) had a low productivity with 0.8-1.2 $kg \cdot g^{-1}$.[31] Continued development of the catalyst system increased the productivity more and more. Supporting titanium tetrachloride on magnesium chloride and activating this system with aluminum alkyls increased the productivity dramatically. Modern ZIEGLER-NATTA-catalysts of generation V have a productivity in the range of 50-120 $kg \cdot g^{-1}$.[31] Residuals of the catalyst do not need to be extracted anymore on account of the low concentration in the produced polymer. Those supported catalyst systems are made of agglomerates with a size in the range of 10-100 µm. These primary particles consist of smaller particles with a high surface area. Today, 1,3-diethers such as 2,2-disubstituted-1,3-dimethoxypropane are present during the preparation of the supported catalyst. The presence of Lewis bases is no longer required during aluminum alkyl addition and the stereocontrol for polypropylene was increased.[26] This catalyst concept allowed the development of specific morphology control of polymer particles (*Reactor Granule Technology* by *Basell*).[32]

3.1.2 Single-Site Catalysts

ZIEGLER-NATTA and PHILLIPS-catalysts belong to the group of multi-site catalysts, which have various types of catalytic centers. They produce polymers with a broad molecular weight distribution and the incorporation of a co-monomer depends on the molecular weight.[26] To investigate the polymerization mechanism for enabling a specific catalyst design, homogeneous single site catalysts were developed. NATTA and BRESLOW reported the polymerization of polyethylene in 1957 for the first time with a single site catalyst.[28, 33]

As catalyst, they used titanocene dichloride activated by mixed aluminum alkyl halides ($Cp_2TiCl_2/AlEt_3$ or $AlEt_2Cl$). This system presented low activity compared to Ziegler-Natta-catalysts.[28, 33] A break through in homogeneous metallocene catalysts was the discovery of methylaluminoxane (MAO) as co-catalyst by Sinn and Kaminsky in 1976.[34, 35] MAO activated zirconocenes showed a high activity for ethylene polymerization ($10^8\ g\cdot g^{-1}\cdot mol^{-1}\cdot Zr^{-1}\cdot h^{-1}$) and yielded products with a narrow molar weight distributions (dispersity of about 2) typical for single site catalysts.[35, 36] MAO $[\text{-AlMe-O-}]_n$ (n = 5-20) can be prepared by the partial hydrolysis of trimethylaluminum (TMA). MAO is believed to consist of oligomers ($M \approx 1\ 000\ g\cdot mol^{-1}$) in a linear, ring or cage-like structure (Figure 3.4). A comprehensive description of MAO has yet not been reached.

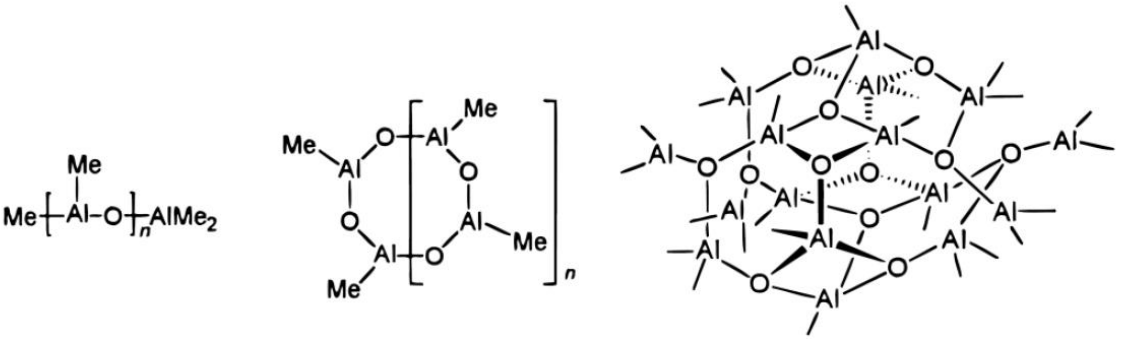

Figure 3.4 Possible structures of methylaluminoxane (MAO).[37]

It is believed that the cage-like structure of MAO, complexing TMA inside, is the catalyst activating species.[38] MAO forms cationic metallocene alkyl complexes containing a weakly or non-coordinating anion, which is complexed by the cage-like MAO molecule. The activation process of a metallocene (Figure 3.5) takes place in several steps. Firstly, the metallocene coordinates on the MAO and a methylation takes place. Secondly, a chloride ligand is abstracted forming the active 14 electron cationic d^0-complex $[Cp_2Zr(CH_3)]^+$. With larger amounts of MAO, a dimethyl complex can be formed, which is activated by transferring a methyl anion to the MAO.[39–41] Brookhart and Green proposed in 1983 a modified version of the Cossée-Arlman-mechanism (Figure 3.3) as polymerization mechanism for MAO activated metallocene.[42] This mechanism includes an α-agostic interaction, which helps to facilitate 1,2-insertion by reducing the steric inhibition to the carbon-carbon bond forming step.[42, 43] Besides the chain propagation reaction, chain termination and chain transfer reactions can take place (Figure 3.6). β-Hydride transfer is the dominant chain termination mechanism under usual experimental conditions. An H^- anion is transferred from the growing polymer chain to an incoming olefin.[44] Furthermore, β-hydrogen elimination, β-methyl transfer and chain transfer to the aluminum can take place.[44–47]

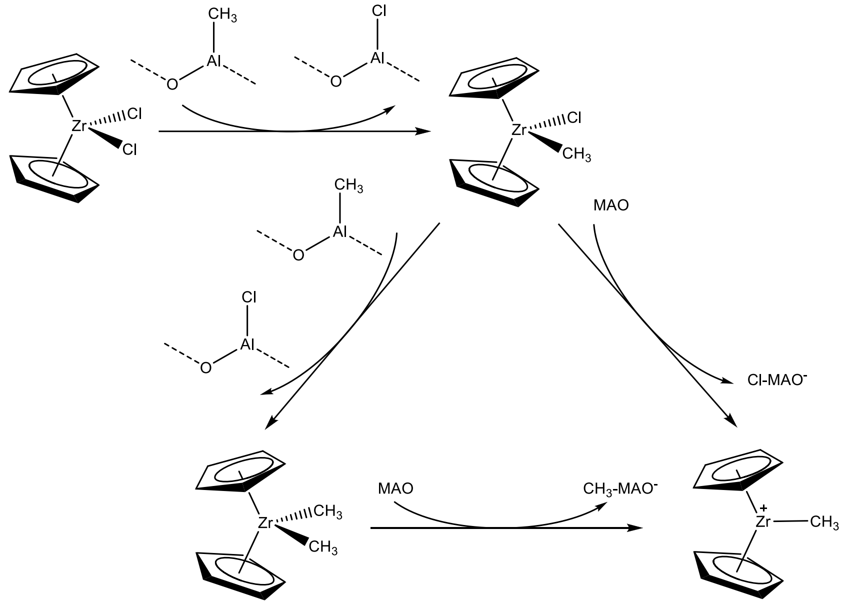

Figure 3.5 Activation of metallocene by methylaluminoxane (MAO).[41, 48]

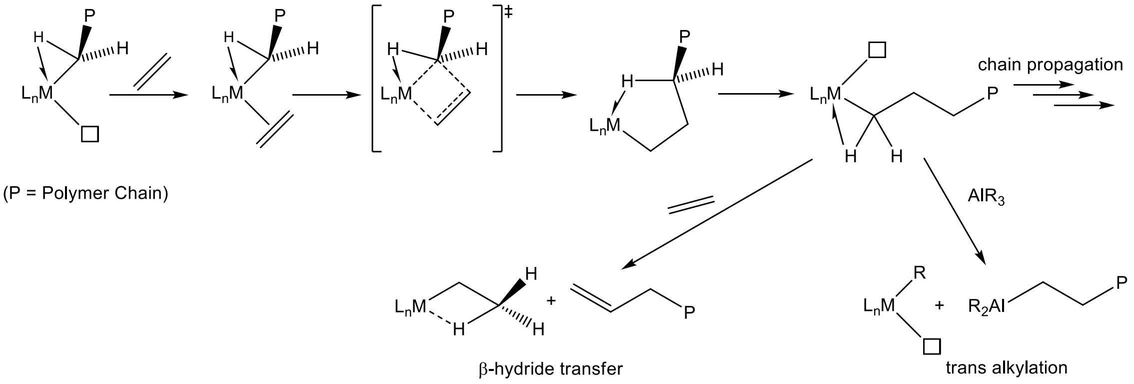

Figure 3.6 Chain propagation mechanism proposed by BROOKHART and GREEN, chain termination and transalkylation for metallocene.[43, 44]

In the 1980s, SINN and KAMINSKY developed metallocene based and MAO activated catalysts, which polymerized propylene to atactic polypropylene (aPP) for the first time.[36] BRINTZINGER and co-workers synthesized bridged, chiral metallocene (*ansa*-metallocene).[49] With those *ansa*-bis(indenyl) complexes in a *racemic* (rac) mixture, it was possible to obtain isotactic polypropylene (iPP) with a single side catalyst.[50, 51] Years later (1988), EWEN and RAZAVI synthesized an *ansa*-metallocene catalyst, which made it possible to obtain syndiotactic polypropylene (sPP).[52] The tacticity of polyolefins can be controlled by customizing ligand structure and symmetry of the catalyst shown in Figure 3.7. Unbridged metallocene with C_{2v}-symmetry and the *meso*-diasteromer of bridged C_2-metallocene polymerize pro-chiral monomers to aPP. iPP can be polymerized using bridged metallocene with C_2-symmetry. Metallocene of C_S-symmetry give sPP. Hemiisotactic or stereoblock polymers can be obtained by asymmetric C_1-metallocene.[53]

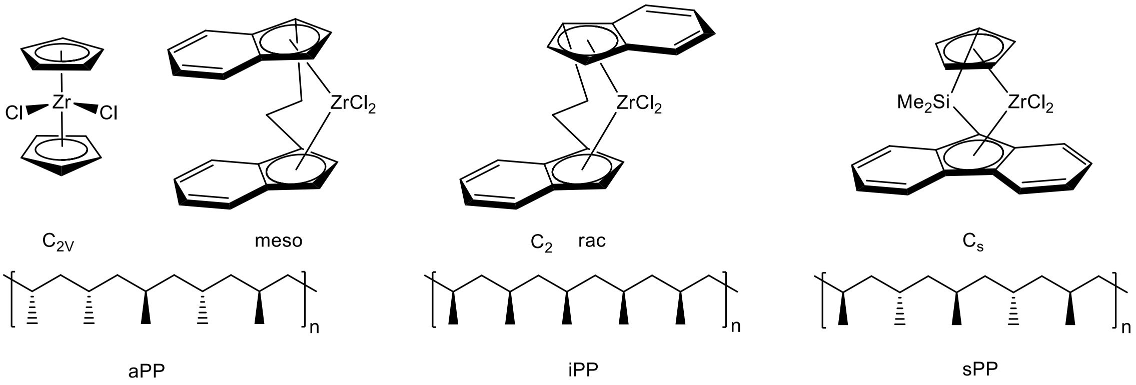

Figure 3.7 Metallocene based catalysts for stereo specific 1-olefin polymerization.[53, 54]

The stereochemistry of a polymerization is influenced by the growing polymer chain and the set of catalyst ligand.[53] During the polymerization, the chain end remains coordinated on the active metal center during monomer enchainment. The stereo information of the last enchained monomer unit influences the stereochemistry of monomer addition. This mode of stereochemical regulation is called "*polymer chain-end control"*.[53] In the case of bridged single site catalysts, where the set of ligands is chiral, the regulation is called *"enantiomorphic-site control"*. The chiral information of the ligands is transferred to the chain orientation and this effect directs the orientation of the polymer chain end.[53] Thus, the chain end control appears as a enantiomorphic control.

Ansa-metallocene with C_2-symmerty are built of π-ligands, frequently bridged by a silicon or carbon entity. Bulky ligands sterically block the upper right and the lower left area of the complex (Figure 3.8). The pro-chiral monomer and the polymer chain are forced into the remaining free areas. 1,2-insertion takes place and the polymer chain is now on the opposite side. Coordination of the prochiral monomer takes always place in the same way. Repeating this process leads to iPP. Thus, the chirality of the ligand is transferred to the monomer through the β-carbon of the metal-alkyl group.[53]

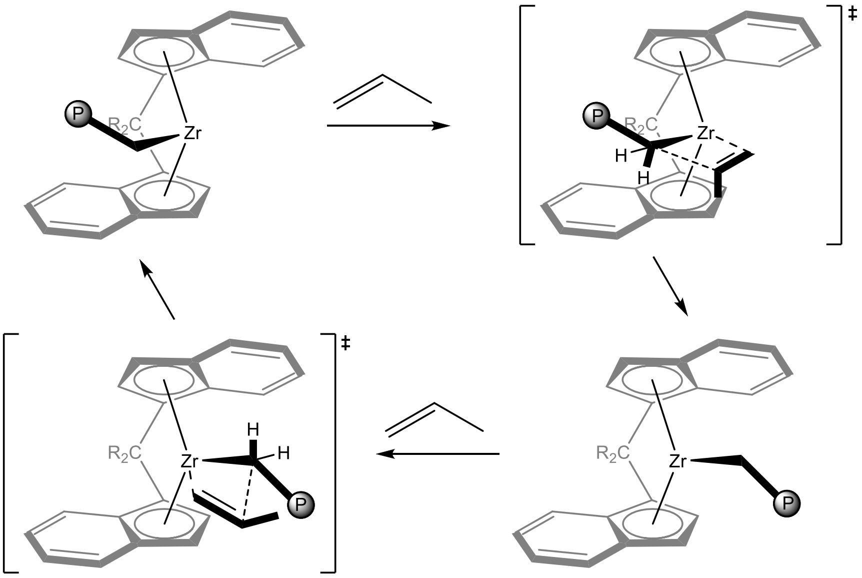

Figure 3.8 Proposed mechanism of propylene polymerization with a C_2-symmetric metallocene catalyst under *enantiomorphic-site control*.[53]

The same mechanism of stereocontrol is related to C_2-symmetric *ansa*-metallocene for sPP polymerization. The bulky fluorenyl-ligand blocks both lower areas forcing polymer chain away from the ligands, and the smaller propylene to slip in between ligand and polymer chain at the β-carbon. sPP is formed by the alternating coordination of propylene from the *si* and the *re* side.[53]

3.1.3 Post-Metallocene Catalysts

Further developments in ZIEGLER-NATTA and metallocene-catalysts improved the productivity and material properties of polyolefins. New types of catalyst were obtained leading to customized or new types of polyolefins. A milestone was the discovery of high active half sandwich titanamide catalysts (Figure 3.9) by DOW CHEMICAL and EXXON.[55, 56] These types of catalysts are called *constrained geometry catalysts* (CGC). CGC-catalysts are very suitable for co-polymerization of sterically demanding co-monomers such as 1-octene. Styrene, propylene or cycloolefins can also be co-polymerized by CGC-catalysts.[57, 58]

Metallocene complexes of group IV are very sensitive to polar groups. Catalysts of late transition metals are less sensitive to hetero atoms, which make them interesting for co-polymerization of polar co-monomers. In 1995, the BROOKHART group reported on a new class of catalysts. They synthesized Pd(II) and Ni(II) complexes with sterically demanding diimine ligands (Figure 3.9).[59] High branched and high molecular weight polyolefins can be obtained with those catalysts. The productivity is comparable with those of metallocene catalysts.[60, 61] *Chain walking,* caused by repeated β-hydride elimination and reinsertion at a high rate is responsible for the branching.[26, 61] Polar monomers such as acrylates can be co-polymerized with those catalysts. By introducing Ni(II) catalysts with N,O-ligands, GRUBBS and coworkers were able to co-polymerize hydroxynorbornene.[62]

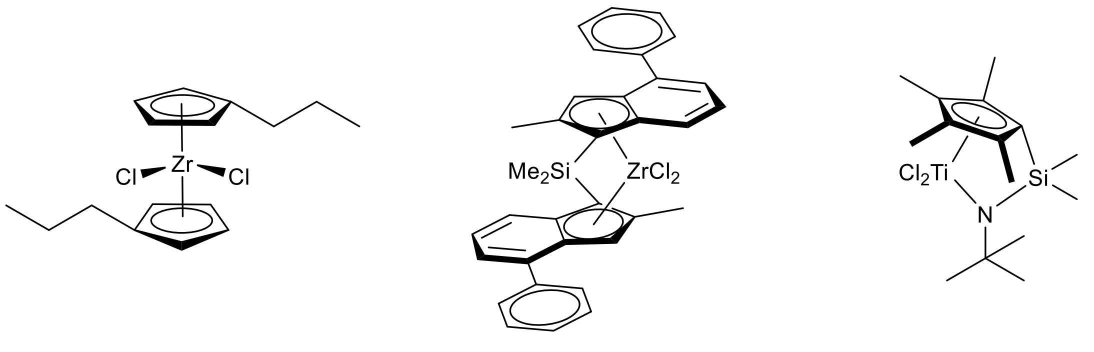

Metallocene **ansa-metallocene** **CGC-Catalyst**

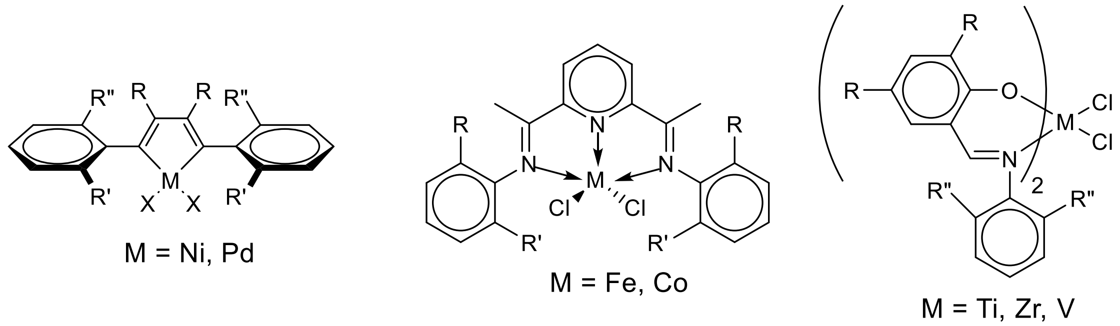

Diimine-catalyst **Bis(imino)pyridine-catalyst** **Phenoxyimine-catalyst**

Figure 3.9 Metallocene and non-metallocene precursors for olefin polymerization.[54]

Bis(imino)pyridine complexes of iron and cobalt (Figure 3.9) for olefin polymerization were discovered independently from each other by BROOKHART and GIBSON.[63–65] Those high active catalysts give linear polyolefin in opposite to the Ni(II)- and Pd(II)-catalysts. By customizing the *ortho*-aryl substituent, the molecular weight can be controlled.[66, 67]

For the selective construction of special microstructures, living polymerization is necessary. Due to chain termination and chain transfer reactions, living polymerization is often only possible with metallocene at temperatures at or under 0 °C.[68] An important development in the field of living polymerization was the discovery of phenoxy-imine-catalysts (Figure 3.9) by FUJITA.[69] This type of catalyst is able to produce polyolefins with ultra-high molecular weight and a dispersity (Đ) in the range of 1.1. Furthermore, block copolymers can be obtained. However, these catalysts are expensive, not very active and are not used on an industrial scale.[70]

3.2 Supported Catalysts

Homogeneous single-site catalysts tend to show *reactor fouling* in solvent polymerization. Polymer adheres to the reactor wall, which causes boiler scale effects. A continuous reaction under those circumstances on an industrial scale is not feasible. To avoid the reactor fouling, single-site catalysts ,e.g. metallocene-based ones, are commonly immobilized on inorganic materials.[71] Supports like silica, alumina or magnesium dichloride are most representative examples of inorganic materials used for ZIEGLER-NATTA and PHILLIPS catalysts.[72–83] The immobilization of a catalyst on a support can influence or change the nature of active sites on the catalyst. Polymer properties such as molecular weight, Đ or stereospecificity for PP may be different.[83] The catalyst thermal stability may advantageously be improved after heterogenization.[84] A large advantage of inorganic supports is the possibility to control the morphology of the obtained product and thus avoid the associated reactor fouling which is drastically changing the mass and heat transfer in the reactor.[85–87]

The heterogenization of the catalytic system can be achieved by several methods.[71, 85–88] Functional groups of catalyst ligands and the supports surface can covalently linked. However, this method is usually quite complex and expensive. A second method is to immobilize the co-catalyst MAO on the supports surface followed by physical fixation of the catalyst complex. Using latter heterogeneous catalysts is the most common method in industry to produce polyolefins.[83] Fixation is reached by electrostatic interactions between the complex and the immobilized MAO as counterion. The direct binding of the catalyst on the supports surface is another method, but the activity is often decreased by this approach.

3.3 Polymer Composites

3.3.1 Composites

Polymer composites are multiphase systems made of a polymer matrix and an organic or inorganic filler. Fillers can modify the properties of the polymer matrix such as electrical conductivity, thermal properties or dimensional stability. Often, fillers are only used as dilutant for reducing the material costs. Furthermore, the processing properties of a polymer melt can be influenced by fillers.[89] Examples for fillers used in the industry are $CaCO_3$, wollastonite, kaolinite, clay, magnesium oxide, aluminum oxide, silicon dioxide or talc.[90]

To improve the mechanical properties of polymer composites, functional fillers with a high aspect ratio (length/diameter) are of particular importance. Spherical particles with an aspect ratio of one basically influence the hardness only, and their application goes along with a loss of toughness. On the other hand, orientated fillers such as glass or carbon fibers show an enhancement in mechanical properties.[89]

Besides the aspect ratio of the filler, a good interaction between filler and polymer matrix is advantageous for a reinforcing effect. Phase separation often leads to mechanical failure. Surface modification with silanes, titanates or oleic acids is one way to improve the filler polymer interaction.[89, 91] Another method is to graft polymers or block-co-polymers on the filler surface.[92] Those modifications and the use of compatibilizers also improve the filler dispersion in the polymer matrix. Mechanical failure due to agglomerates can be avoided by this way.[93]

3.3.2 Nanocomposites

The interest in nanoscopic fillers has been increased with their availability over the last decades. The fine dispersion of inorganic fillers - especially nanosized fillers – into a polymer matrix can favorably enhance polymer properties. More and more, nanofillers are used instead traditional micron-sized fillers.[94, 95] Nanofillers have an advantage over micron-sized fillers. Desired filler effects can be achieved with smaller amounts, i.e. a few weight percent of nanofillers. This effect may be related to the properties of the filler and often more so to the resulting large contact area between filler and matrix with the concomitant impact on properties of the matrix polymer.[96–102]

To define the material as nanocomposite at least one dimension of the filler has to be smaller than 100 nm.[103] When nanoparticles are used instead of micron-sized particles, the number of particles is increased by a factor of 10^9 at the same volume content. As consequence, much more of the polymer matrix is located near the nanoparticle surface. The polymer is transferred from a *“bulk”*-polymer to an *“interface”* polymer. Thus, only small amounts of nanofillers are necessary to achieve the desired properties.[94] Normally, large amounts of conventional micron-size fillers are used, which results in deterioration of processability and change the surface appearance. Main disadvantage of nanoparticles as fillers is the high specific surface energy, which causes the formation of agglomerates. Latter, better be deagglomerated and their reformation are better inhibited by suitable processing methods.[104] Nanocomposites have increased the spectrum of polymer application to a new level. For example the mechanical properties[95], chemical resistance[105], barrier properties[106–108], flame resistance[94, 109–111], thermal stability[112], scratch resistance[113–116] and dielectric properties[95, 117–120] have been improved significantly.

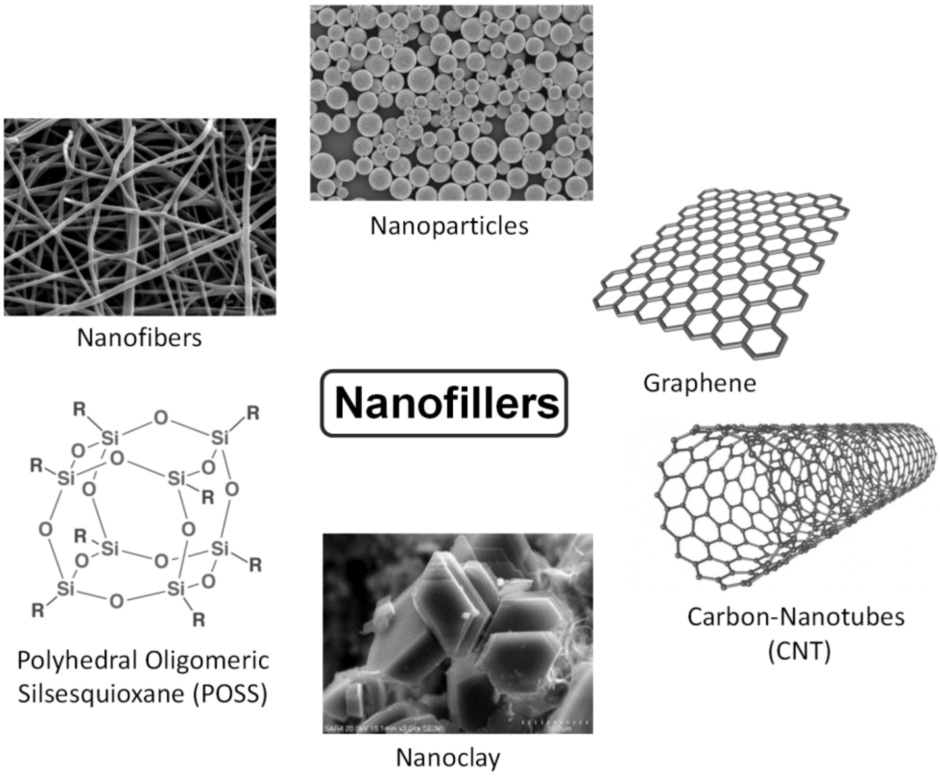

Figure 3.10 Nanofiller families including molecules and inorganic nanoparticles.

3.3.3 Methods of Nanocomposite Preparation

Reaching a fine dispersion of an inorganic nanofiller in a (thermoplastic olefinic) polymer is usually a challenge on account of the larger differences in polarity.[121] To prepare nanocomposites, various methods such as melt compounding, solution and dispersion blending and *in situ* polymerization were used.[37, 97, 122–124] Melt compounding, where a mixture of polymer and filler is mechanically mixed at elevated temperatures, is the most common one. Advantage of this method is that it does not require the use of a solvent or monomer, making it simple, economical and environmentally friendly. If polymer-filler interactions are larger than filler-filler interactions a homogeneous dispersion can be obtained. Polymer-filler interactions can be increased by surface modification to reduce the specific surface energy.[125] However, this method often leads to an insufficient nanofiller dispersion due to the highly viscous polymer melts. Filler-aggregates are often present, causing deterioration of general physical properties.

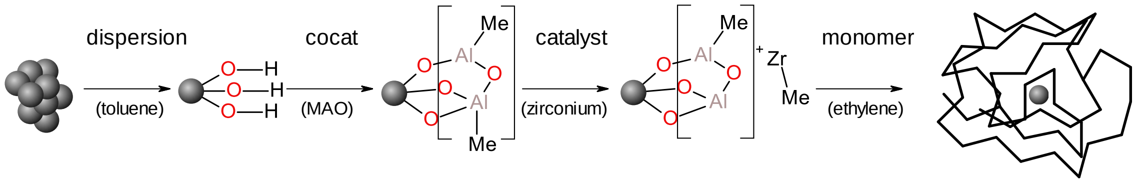

Figure 3.11 Schematic illustration of *in situ* polymerization on catalyst/MAO supported nanofillers.

Such disadvantages can be resolved by *in situ* polymerization, where the co-catalyst methylaluminoxane (MAO) and the catalyst are supported on the filler (Figure 3.11). The concomitant "*wrapping*" of the filler particle with polyolefin is changing the filler surface to a hydrophobic one.[126, 127] The reaction suspension in the *in situ* polymerization is saturated by the polymer-monomer generating the polymer in the presence of the filler near the filler surface.[128, 129] This method has been shown to yield composites with finely dispersed nanofiller[128–130], also for polyolefins[131]. The polymerization process starts at the nanofiller surface and separates the nanoparticles effectively by the force of polymer growth in between. Thus, deagglomeration and effective nanoparticle dispersion is taking place. PE/graphite oxide composites,[132] PE and iPP carbon nanotube composites,[133–135] iPP/layered silica nanocomposites[136, 137] and PE/boehmite nanorod composites[97] are only a few examples, where an *in situ* polymerization technique was successfully applied.[138–144] This type of *in situ* polymerization is also often called "*polymerization-filling technique*" (PFT).[145, 146] Homogeneous filler dispersion and the wrapping of the filler by polymer are the main advantages. Furthermore, nanocomposites with a high filler content can be obtained by *in situ* polymerization, which is not possible with melt compounding.[145] Such materials can be used as "*masterbatches*". Combined with melt compounding, nanocomposites with a defined filler content and homogeneous dispersed nanofillers can be obtained.[147] The combination of the methods is only possible if the polymer and filler can be processed at high temperatures (230 °C).

Another method to obtain nanocomposites is the solution blending. The polymer nanocomposite is prepared by blending the filler with the polymer into a solution. This requires a suitable solvent that can both solubilize the polymer and disperse the filler.

The nanocomposite is obtained by removal of the solvent when the filler is dispersed into the polymer solution.[148, 149] Solution and dispersion blending is limited to soluble polymers and the polymer solvent must be capable of dispersing the fillers. Large amounts of solvents are necessary, which has the disadvantage of high costs and the environmental impact.

4 Motivation

The need for enhanced insulation materials in electrical appliances with all of their requirements led to this investigation. In the first part of the project, LLDPE was used as the designated matrix and magnesium oxide nanoparticles with a size of ± 50 nm as filler. Target of the project was to develop and optimize the polymerization process for obtaining a polyolefinic composite material, which shows a higher electrical resistance than standard materials today. Such polymers are needed to face today's and future challenges in the energy market. Combining industrial polymers like LLDPE with nanofillers gives the possibility to obtain composite materials with new or advanced properties compared to neat polymers or composites made of micro sized fillers. Therefore, suitable polymerization techniques and reaction conditions need to be developed to prevent nanoparticles from agglomeration and to obtain a nanocomposite with homogeneous particle distribution in 500 g scale. Chapter 5.1 focuses on the developing process of a LLDPE/MgO composites in 20 g scale along a pseudo-PFT with the aim to keep the amount of MAO co-catalyst as low as possible.

After finding a method to obtain LLDPE/MgO@$Mg(OH)_2$ nanocomposites in small scale experiments, the polymerization process should be adapted to 500 g scale to obtain masterbatches of LLDPE/MgO@$Mg(OH)_2$ nanocomposite with about 10 wt% filler content. The composite is to be bench-marked against to composites obtained by standard melt extrusion process.

In the second part of the project, iPP nanocomposites with enhanced electrical properties should be developed based on the previous research. Those materials could be used as dielectric material in capacitor applications. A capacitor can temporally store energy and is built of two electrical conductors separated by a dielectric. For this project, MgO@$Mg(OH)_2$, SiO_2 and $BaTiO_3$ nanoparticles were chosen as nanofillers for the preparation of polypropylene nanocomposites. Those should be diluted with commercial iPP by melt extrusion to obtain nanocomposites with 0.5 wt% filler.

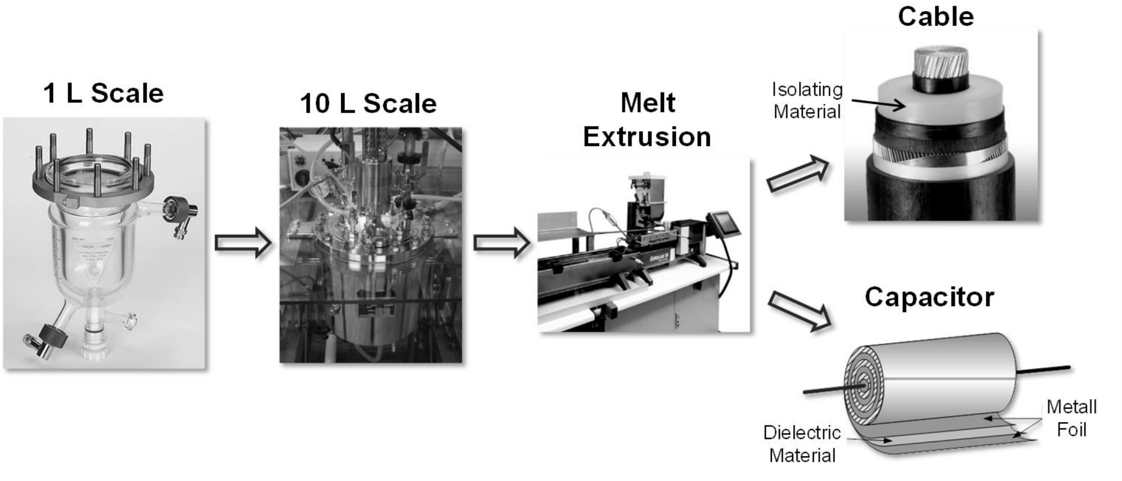

Figure 4.1 Flow chart of project developing process.

5 Results and Discussion

5.1 Synthesis of Linear Low-Density Polyethylene $MgO@Mg(OH)_2$ Nanocomposite using modified *in situ* Polymerization

The present chapter reports the preparation of linear low-density polyethylene LLDPE/$MgO@Mg(OH)_2$ nanocomposites using pseudo-PFT with the aim of keeping the amount of MAO co-catalyst as low as possible. The surface of $MgO@Mg(OH)_2$, containing protonic entities, was also pre-treated with dibutyl magnesium (DBM), generating a more inert surface without changing the character of the filler (Figure 5.1). As little as necessary, MAO was added for obtaining a reasonable active olefin polymerization catalyst from bis(*n*-butyl cyclopentadienyl)zirconium(IV) dichloride **1**. Polymerization at the surface of nanoparticles affords the additional option of preparing polyolefin composites with well-distributed particles.[150–153] Such LLDPE/ $MgO@Mg(OH)_2$ nanocomposites were prepared with the objective to study the enhancement in dielectric properties.[153, 154] The synthesis was performed as a one pot procedure with the option of an easy scaling up.

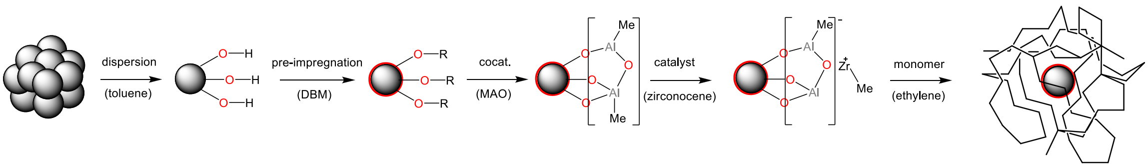

Figure 5.1. Preparation of LLDPE/MgO nanocomposites by a pseudo-polymerization filling technique.

5.1.1 Characterization of MgO

The preparation of nanocomposites of polyolefins with a good distribution of particles using *in situ* polymerization or polymerization filling technique profits strongly from the preparation of a fine suspension of the nanoparticles in the polymerization medium.[155] MgO is a filler that is quite sensitive to pressure and temperature and tends to agglomerate in the solid state. Not all available qualities of MgO nanoparticles (treated or untreated) were found useful for preparing nanocomposites by the method used here. The quality selected for preparing composites with finely dispersed nanoparticles turned out as a core-shell mixed oxide/hydroxide of magnesium (*vide infra*). MgO nanoparticles can enhance the electrical performance of PE; no reports for the mixed oxide/hydroxide particles were found in that regard, further motivating to continue research on them.[156, 157] The bulk material consists of agglomerated primary particles in the solid state. The primary particles are more or less rectangular in shape with a largest dimension of about 100 nm. Agglomerated particles may be separated to primary particles under the specific conditions of polymerization. Indeed, the agglomerates are easily broken up, for example after suspending in ethanol as was found in the preparation of TEM samples (Figure 5.2). It was expected that the pressure resulting from growing polymer chains on the surface of the primary particles would also be sufficient to break up the agglomerates.[158, 159]

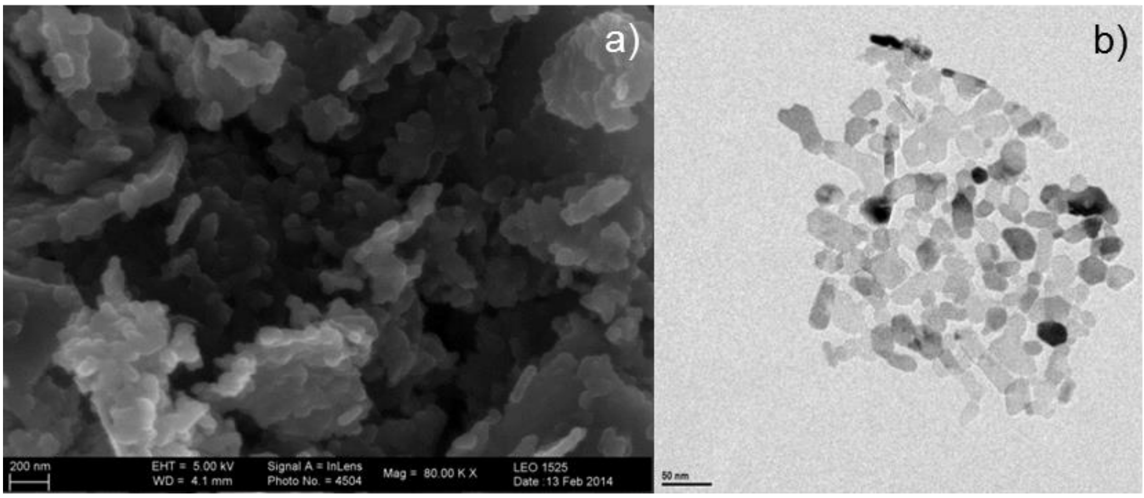

Figure 5.2. (a) SEM image with a magnification of 80 000 of $MgO@Mg(OH)_2$ nanoparticles agglomerate. (b) TEM micrograph after deposition at a TEM substrates from ethanol.

TGA of the nanoscopic MgO shows a weight loss of 9.5 wt% during heating to 600 °C. The weight loss can be attributed to the presence of $Mg(OH)_2$, losing water on heating. This was confirmed by XRD (Figure 5.3b).[160, 161] The “MgO” nanoparticles thus consist of 30 mol% in form of $Mg(OH)_2$ (Figure 5.3a). $Mg(OH)_2$ is mainly in the bulk of the particles. Treating these nanoparticles with the maximum amount of DBM that would react with the surface ($0.6\ mmol\cdot g^{-1}$) led to no significant reduction in $Mg(OH)_2$ content (Figure 5.3a). Calcination at 400 °C in contrast leads to a full conversion of $Mg(OH)_2$ to MgO as shown by a decrease in $Mg(OH)_2$ content (Figure 5.3a). The calcination, however, promotes the formation of larger and robust agglomerates that cannot be suspended in toluene.[162] The calcined MgO is not useful for preparing composites with nanoscopic MgO filler, and therefore the core-shell were used; these are referred as MgO@Mg(OH)$_2$. The particles were dried before use at 80 °C under a dynamic vacuum overnight in order to have comparable starting conditions (i.e. conditioned MgO@Mg(OH)$_2$). Calcination to MgO does not proceed under those conditions; instead only residual coordinated water is removed (Figure 5.3a).

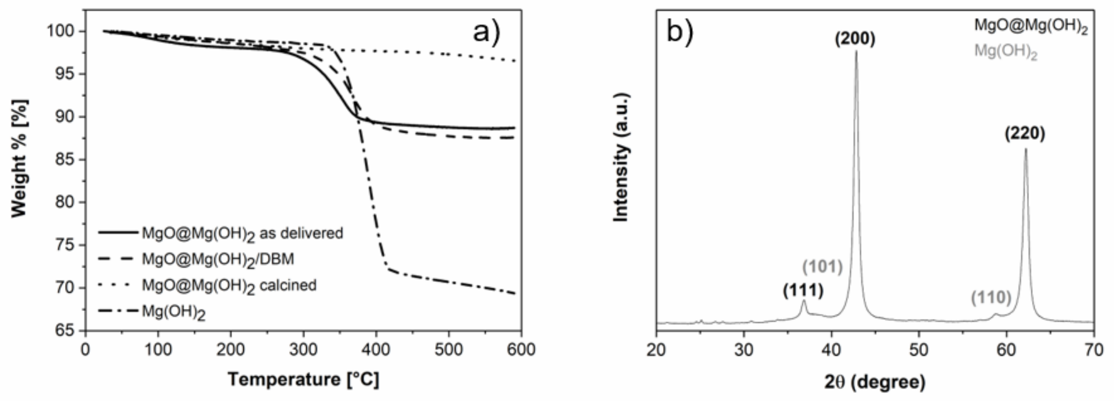

Figure 5.3. a) TGA of MgO@Mg(OH)$_2$ nanoparticles, MgO@Mg(OH)$_2$ impregnated with DBM for 15 min (0.6 mmol·g^{-1}), MgO@Mg(OH)$_2$ calcined for 1 h at 400 °C and Mg(OH)$_2$ nanoparticles (100 nm). b) XRD pattern of MgO@Mg(OH)$_2$.

5.1.2 Suspension of MgO@Mg(OH)$_2$ in Toluene/MAO

The conditioned MgO@Mg(OH)$_2$ precipitates readily after suspending in dry toluene. The addition of MAO to the mixture leads to a more stable suspension (Figure 5.4). This is usually observed; MAO will adhere and/or react with the relatively polar surface of fillers and thus decrease the surface energy of the particles in toluene. MAO contains anionic methyl groups that will react with hydroxyl groups at the MgO@Mg(OH)$_2$ surface to liberate methane and probably building covalent bonds to the surface.[163–166] The layer formed will additionally take up oligomeric MAO, leading to an impregnated surface (*vide infra*). The toluene suspension of the filler obtained this way was used to prepare LLDPE nanocomposites after an impregnation time of 45 min.

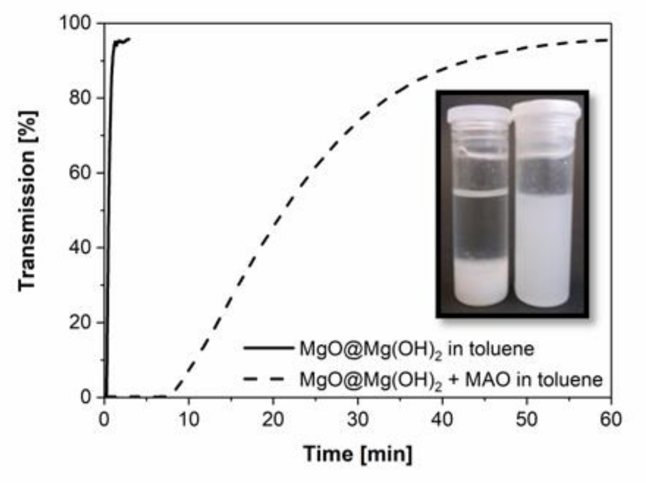

Figure 5.4. Sedimentation of $MgO@Mg(OH)_2$ nanoparticles in toluene suspension with (right) and without MAO (left) impregnation.

The result of a solid-state ^{27}Al MAS NMR study of the $MgO@Mg(OH)_2$ filler treated with MAO and with DBM and consecutively MAO is consistent with the view that the co-catalyst is associated and covalently bound to the surface (Figure 5.5). Samples were prepared analogously to the procedure for preparing the composites. Thus, $MgO@Mg(OH)_2$ nanoparticles were allowed to react with MAO or DBM and MAO and isolated after contacting to water-saturated toluene and filtration. A sample of hydrolysed MAO – designated Al(O)OH - was used as reference (Table 5.1).

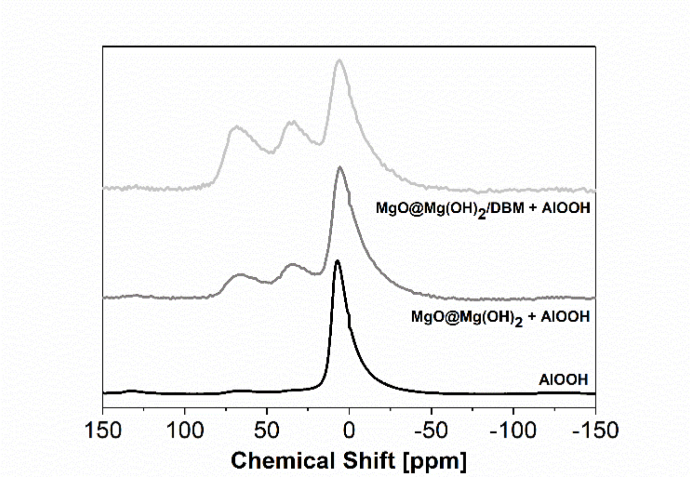

Figure 5.5. Solid-state ^{27}Al MAS NMR of hydrolyzed MAO and hydrolyzed MAO impregnated $MgO@Mg(OH)_2$ nanoparticles with and without DBM pre-impregnation.

Table 5.1 Data obtained from solid-state ^{27}Al MAS NMR.

Sample	Al_{octa} [ppm / %]	Al_{penta} [ppm / %]	Al_{tetra} [ppm / %]
Al(O)OH	6.8 / 100	-	-
$MgO@Mg(OH)_2$ + Al(O)OH	6.1 / 66.2	34.0 / 20.1	65.7 / 13.7
$MgO@Mg(OH)_2$/DBM + Al(O)OH	6.5 / 45.5	34.1 / 26.8	68.9 / 27.7

The spectra show the presence of aluminum in three kinds of environments. Well-defined six-coordinated aluminum is found with a characteristic resonance at 7 ppm.[167] This peak is also found in hydrolyzed MAO and in clays like boehmite with six oxygen atoms surrounding a central aluminum ion.[167] A second peak is present at 34 ppm, which corresponds to a fivefold-coordinated Al atom.[168, 169] A third peak at 69 ppm indicates the presence of a tetrahedral-coordinated Al atom.[170] The second and third resonances are only found for the treated $MgO@Mg(OH)_2$ and are assigned to aluminum atoms associated with the surface of the filler, i.e. Mg–O–Al_{penta} or Mg–O–Al_{tetra} could be possible anchoring spots to the $MgO@Mg(OH)_2$ nanoparticle surface and/or a second layer of bridging atoms to the six-coordinate aluminum atoms. Aluminum ions (with oxo bridges or hydroxide ligands) may not be able to coordinate six-fold manner to the Mg-O surface on account of the different bound lengths/angles of Al-O and Mg-O entities. In addition, it is found that the relative intensity of the six-coordinated aluminum atoms in $MgO@Mg(OH)_2$ treated with DBM and MAO is lower than in that treated with MAO only. This may be a natural result of a lower aluminum amount. However, the ratio of Mg–O–Al_{penta} to Mg–O–Al_{tetra} also changes (decreases) after the reaction of the filler with DBM, indicating that the surface entities are different (Figure 5.5). Thus, reacting the filler particles with MAO or consecutively with DBM and MAO leads to a surface with a lower polarity and with aluminum ions closely associated to it.

5.1.3 LLDPE Composites of $MgO@Mg(OH)_2$ impregnated with MAO

The formation of LLDPE in the presence of $MgO@Mg(OH)_2$ impregnated with MAO was reached after addition of the catalyst **1** to the toluene suspension containing ethylene and 1-octene at 60 °C. The pressure of ethylene was held constant at 2 bar and the ethylene feed was limited to 500 $mL\cdot min^{-1}$ in order to keep the temperature in the range of 60-70 °C. Reaction was terminated after 30 min; the apparent limitation of the average activity is thus related to the limitation in the feed (Figure 5.6b).

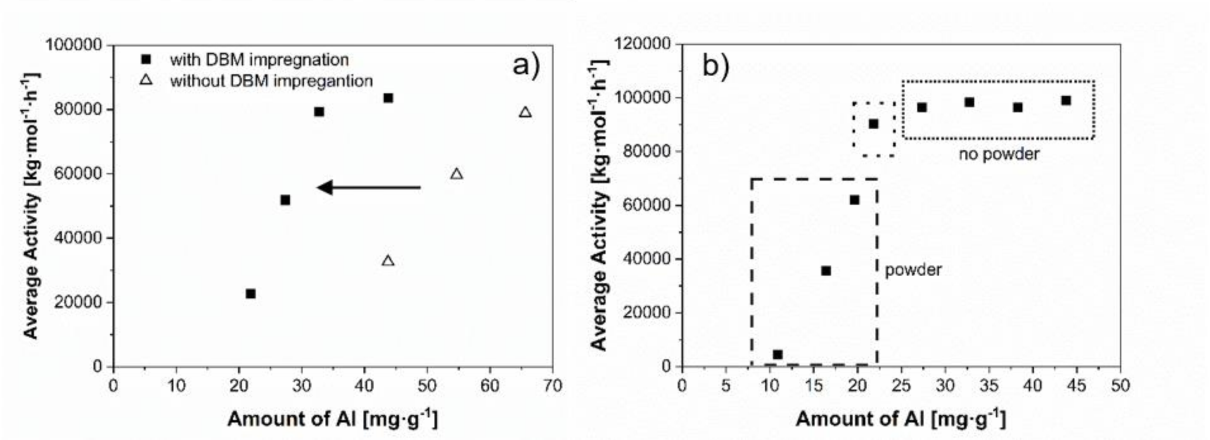

Figure 5.6. (a) Average activity of **1** as function of the amount of MAO (1 g $MgO@Mg(OH)_2$, 0.6 mmol DBM, 0.5 µmol of **1** at 60 °C and 2 bar of ethylene pressure, 30 min). (b) Average activity as a function of the amount of Al (MAO) (2 g $MgO@Mg(OH)_2$, 1.2 mmol of DBM, 0.5 µmol 1 at 60 °C and 2 bar for 30 min; see Table 5.2 and Figure 5.7.

It was found essential for obtaining a product with a powdery morphology and preventing reactor fouling to tune the amount of MAO to the amount of filler in the range corresponding to 10-20 milligrams of aluminum per gram of $MgO@Mg(OH)_2$. The MAO then is mostly close to the filler surface. This has a noticeable impact on the polymer-filler interface (*vide infra*). If the amount of MAO is over 20 milligrams of aluminum per gram of $MgO@Mg(OH)_2$, a cloddy product will result (Figure 5.6b, Figure 5.7, Table 5.2), indicative of substantial polymer formation in the solvent. The composites that are obtained, contain up to 65 mg aluminum per gram of $MgO@Mg(OH)_2$ (Figure 5.7; Table 5.3).

Systematically decreasing the amount of MAO allows one to obtain a powdery product that is easy to handle. Thus, the polymerization process may have changed from an *in situ* polymerization to one that is more like a PTF polymerization process with the (majority of the) co-catalyst associated with the $MgO@Mg(OH)_2$ filler particles. The average activity of the catalyst over the 30 min of polymerization decreases with the amount of MAO: less catalyst precursor **1** is activated for co-polymerization. A lower yield leads to a composite with a higher filler content as the amount of filler in the reactor was kept constant. Polymer formation becomes impractically slow if the amount of MAO is lower than 11 $mg{\cdot}g^{-1}$: the catalyst will then be active only for a short period of time. This may lead to composites with filler particles visually sticking to polymer and are obviously not embedded.

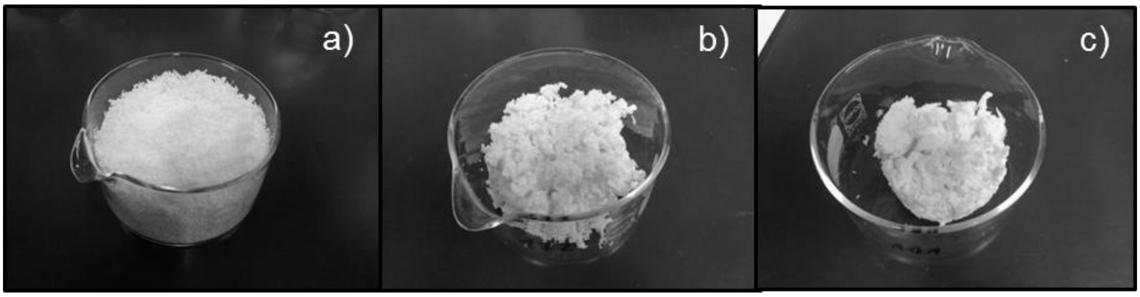

Figure 5.7. LLDPE/MgO nanocomposites obtained with (a) an amount of 10-20 mg Al per gram of MgO@Mg$(OH)_2$ as delivered leads to a powdery product, (b) the product with amount of 22.5 mg per gram Al and more (c) leads to ever more clumpy products.

Table 5.2 Average activity of the *in situ* ethylene/1-octene co-polymerization on MgO@Mg$(OH)_2$ filler.

Amount of Al [mmol·g^{-1}]	**Amount of Al [mg·g^{-1}]**	**Yield [g]**	**Average activity [kg·mol^{-1}·h^{-1}]**	**Filler content [wt%]**
1.6	43.75	24.8	98955	7.5
1.4	38.3	24.2	96482	7.6
1.2	32.8	24.7	98214	7.5
1	27.35	24.2	96295	7.6
0.8	21.9	22.6	90173	8.1
0.7	19.7	15.6	61984	11.4
0.6	16.4	8.9	35493	18.3
0.4	10.95	1.1	2170	64.5

(2 g MgO@Mg$(OH)_2$, 1.2 mmol DBM, 8 mL 1-octene, 0.5 µmol cat. at 60 °C and 2 bar for 30 min).

5.1.4 LLDPE Composites of MgO@Mg$(OH)_2$ impregnated with DBM and MAO

The amount of MAO per gram of MgO@Mg$(OH)_2$ can be reduced by first contacting the filler with DBM (Figure 5.6a). DBM will react with active protons on the filler to generate Mg oxides and butane. This reaction is apparently fast, and a contact time of 15 min was considered satisfactory (Figure 5.8). It was inferred, keeping the amount of MAO constant at 0.72 mmol Al per gram filler, then about 0.6 mmol of DBM will react per gram of $MgO@Mg(OH)_2$ (Table 5.3). This number was found for loadings of 1 and 2 g of $MgO@Mg(OH)_2$ per 300 mL of toluene. The activity of the catalyst increases to this number, implying that more active sites are formed as less MAO is deactivated, and decreases when more DBM is added (Figure 5.9a). (Excess) DBM will putatively coordinate to the Lewis acidic sites in MAO and/or to the active catalyst leading to a lower amount of polymer. Indeed, the co-catalytic potential of MAO is completely lost after adding of 0.6 mmol DBM to 0.72 mmol Al in MAO in the absence of $MgO@Mg(OH)_2$. Basically, the same amount of DBM was found useful in the case of calcined MgO, leading to the conclusion that the drying procedure in the polymerization reactor leads to a similar surface constitution, independent of the calcining (Figure 5.9b). The calcining thus, affects the inner of the particles more than that it changes the surface.

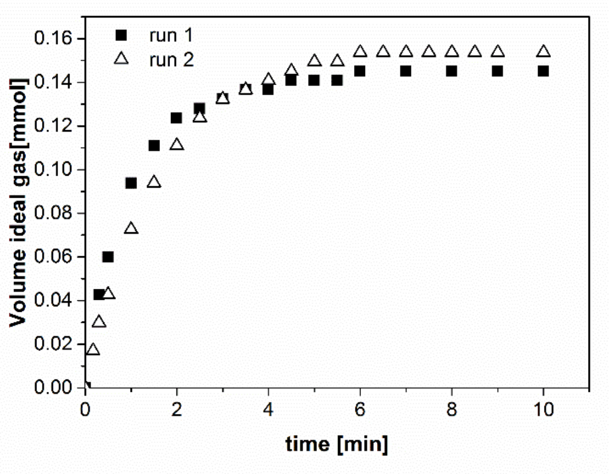

Figure 5.8 Formation of *n*-butane vs. time in the reaction of 0.6 mmol DBM with 1 g $MgO@Mg(OH)_2$ nanoparticles in 20 mL of toluene.

Pretreatment of the $MgO@Mg(OH)_2$ with 0.6 mmol DBM per gram of $MgO@Mg(OH)_2$ allows to offset MAO by the equivalent of 1-1.2 mmol Al-based units per gram $MgO@Mg(OH)_2$ for a polymerization with the same average catalytic activity of **1** (Figure 5.9a). That is about twice the amount of DBM, and that is reminiscent of the number of alkyls moieties that the respective organometallics DBM and MAO carry per metal atom. DBM and MAO thus, seem to react with the same entities on the surface, apparently by a protonation of alkyl groups (Figure 5.6). No reactor fouling was observed, which indicates that a (pseudo) supported catalyst system has been formed. MAO thus, still coordinates to the now modified nanofiller surface.[171]

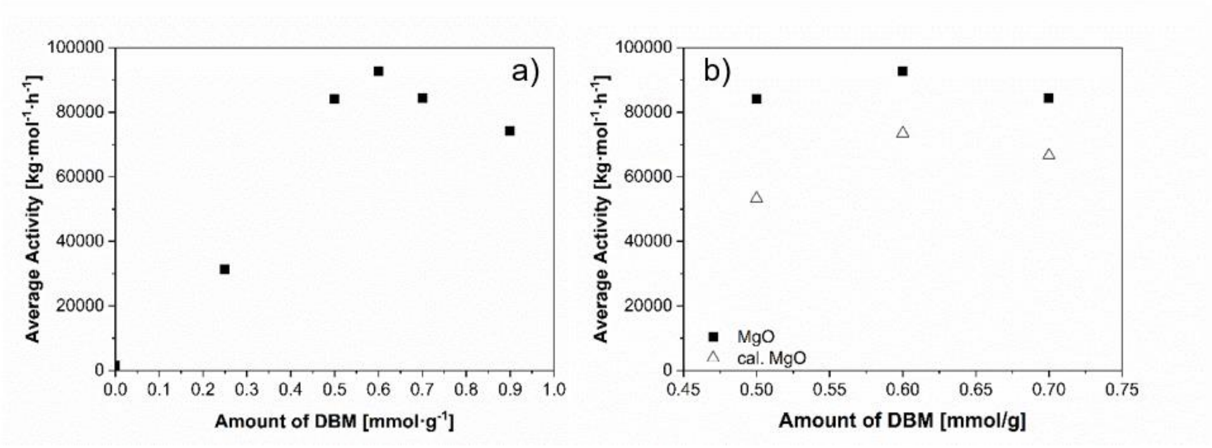

Figure 5.9. (a) Average activity in dependency of the amount DBM (2 g MgO@Mg$(OH)_2$, 0.9 mL MAO (1.46 mmol Al), 0.5 µmol of 1, 60 °C and 2 bar of ethylene pressure, 30 min). (b) Average activity in dependency of the amount of dibutyl magnesium (DBM) for MgO@Mg$(OH)_2$ and calcined MgO@Mg$(OH)_2$ nanoparticles showing a maximum at 0.6 mmol DBM per g MgO@Mg$(OH)_2$, 0.9 mL MAO (1.46 mmol Al), 0.5 µmol cat. at 60 °C and 2 bar for 30 min).

Table 5.3. Ethylene/1-octene co-polymerization in the presence of $MgO@Mg(OH)_2$ nanoparticles.

Amount of DBM [$mmol \cdot g^{-1}$]	Amount of Al [$mmol \cdot g^{-1}$]	Amount of Al [$mg \cdot g^{-1}$]	Yield [g]	Average activity [$kg \cdot mol^{-1} \cdot h^{-1}$]	Filler content [wt%]
without DBM[a]					
0	1.6	43.8	8.2	32 570	10.9
0	2.0	54.7	15.0	59 660	6.2
0	2.4	65.6	19.9	78 890	4.8
with DBM[a]					
0.6	0.8	21.9	5.7	22 630	14.9
0.6	1.0	27.3	13.1	51 830	7.1
0.6	1.2	32.8	20.0	79 360	4.8
0.6	1.6	43.8	21.0	83 490	4.5
with DBM[b]					
0	0.73	20.0	0.4	1 670	82.7
0.25	0.73	20.0	7.8	31 415	20.3
0.5	0.73	20.0	21.0	84 120	8.7
0.6	0.73	20.0	23.1	92 690	8.0
0.7	0.73	20.0	21.0	84 240	8.7
0.9	0.73	20.0	20.6	74 270	8.9

[a] 1 g $MgO@Mg(OH)_2$, 8 mL 1-octene, 0.5 µmol of **1** at 60 °C and 2 bar of ethylene pressure, 30 min.

[b] 2 g $MgO@Mg(OH)_2$, 0.9 mL MAO (1.46 mmol Al), 8 mL 1-octene, 0.5 µmol of **1** at 60 °C and 2 bar of ethylene pressure, 30 min.

5.1.5 Morphology

The *in situ* polymerization process, taking place near the nanofiller surface, separates the nanoparticles efficiently, thus, promoting deagglomeration and leading to an effective nanoparticle dispersion.[97] Composite morphologies were investigated by SEM (Figure 5.10). The nanoparticles seem homogeneously distributed and mostly separated as primary particles with a size of 100 nm. The $MgO@Mg(OH)_2$ nanoparticles appear encapsulated with polymer and voids are not observed in cryo-broken samples.

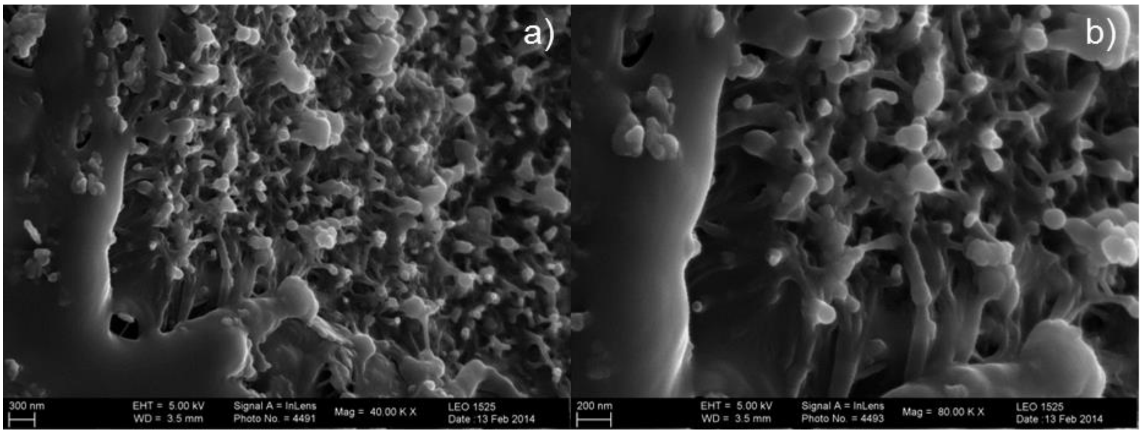

Figure 5.10. SEM images of LLDPE/MgO nanocomposite cross sections (10 wt% $MgO@Mg(OH)_2$) at a magnification of (a) 40k and (b) 80k.

EDX mapping of composite with 8 wt% (Figure 5.11a) and 20.3 wt% of $MgO@Mg(OH)_2$ (Figure 5.11c) again indicate well-distributed particles over the polymer matrix together with some cloudy areas of higher concentration. The dispersion of aluminum within the composites follows that of the $MgO@Mg(OH)_2$ to some extend (Figure 5.11b, d, Figure 5.13) indicating that appreciable amounts of the co-catalyst are indeed associated with the $MgO@Mg(OH)_2$ filler. The nature of the polymerization apparently had changed from an *in situ* polymerization to a predominantly polymerization filling process.

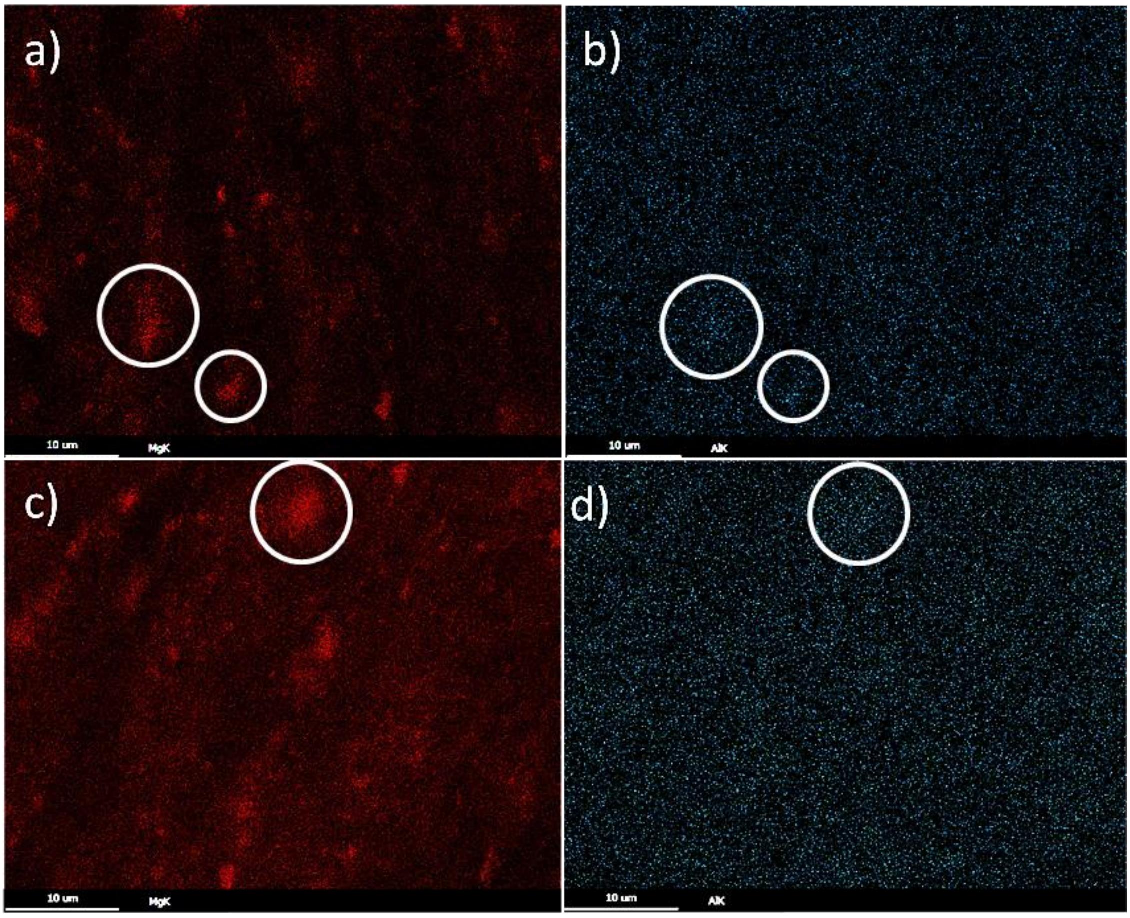

Figure 5.11. EDX mapping of LLDPE/MgO nanocomposites indicating a distribution of a) MgO@Mg(OH)$_2$ and b) Al for a sample with 8 wt% filler and c) MgO@Mg(OH)$_2$ and d) Al for a sample with 20.3 wt% filler. SEM overview is given at Figure 5.12.

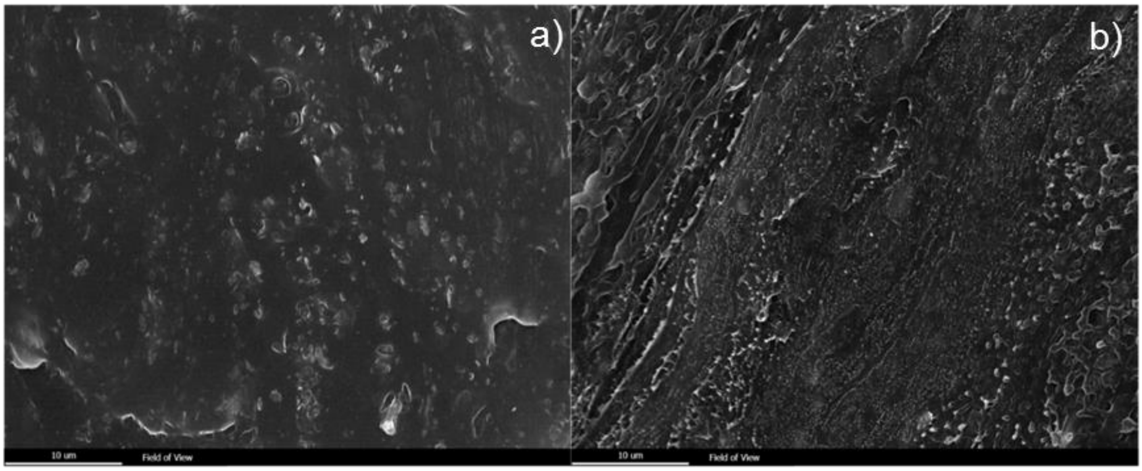

Figure 5.12 SEM overview (magnification: 5k) of LLDPE/MgO@Mg(OH)$_2$ nanocomposite 8 wt% (a) and 20.3 wt% (b).

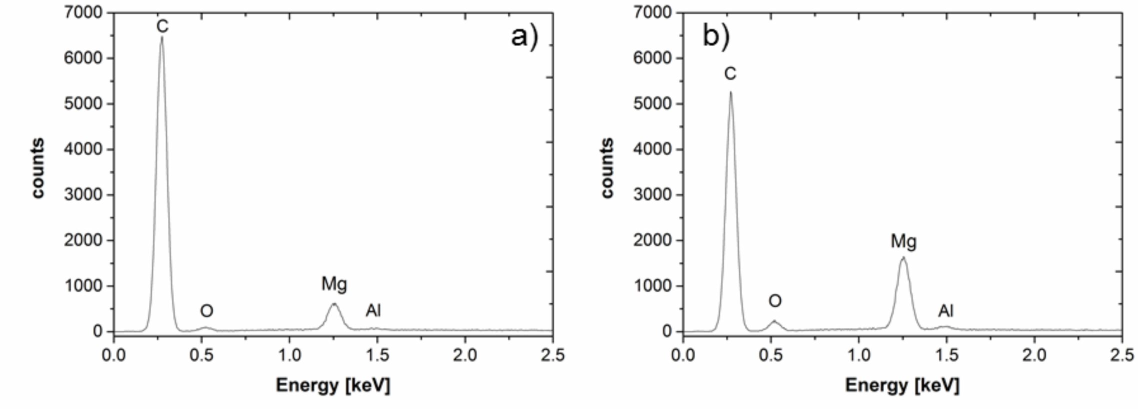

Figure 5.13. EDX spectrum of a LLDPE/MgO composite containing (a) 8 wt% and (b) 20.3 wt% filler.

5.1.6 Properties of LLDPE/MgO Nanocomposites

The 1-octene content of the obtained LLDPE composite is not influenced by the presence of MgO@$Mg(OH)_2$ nanoparticles (Figure 5.14). ^{1}H-NMR and ^{13}C-NMR measurements show an incorporation of 1-octene into the ethylene backbone in the range of 2 – 3 mol% (Figure 5.14, Table 5.4), making them fairly comparable. The products of lower filler content, resulting from experiments with a high polymer yield may have a small gradient in the composition resulting from a compositional drift of the feed. Depending on the total yield of polymer, the initial concentration of 1-octene of 16.6 $mmol \cdot L^{-1}$ is decreased to the range of 14 – 9 $mmol \cdot L^{-1}$. This corresponds to a 1-octene consumption between 10 – 40 mol%.

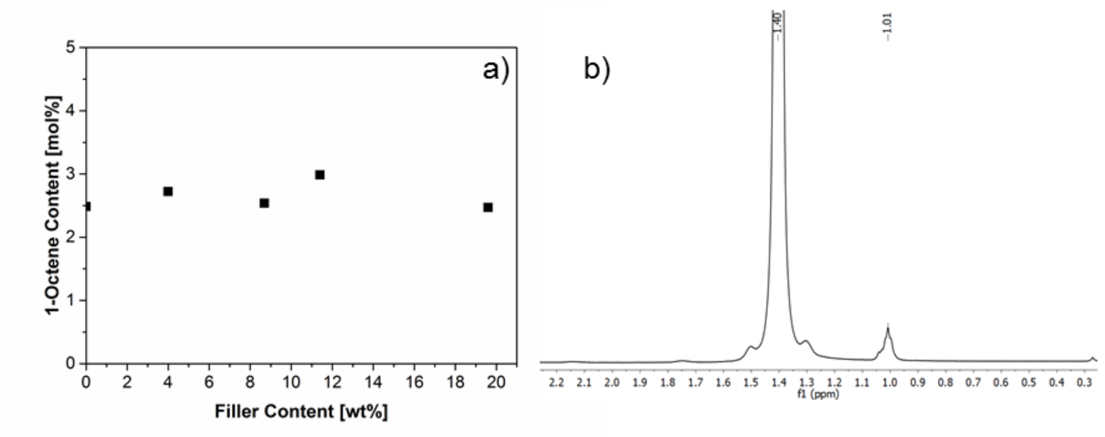

Figure 5.14. a) 1-Octene content of LLDPE/MgO nanocomposites measured by ^{1}H-NMR b). Representative ^{1}H-NMR of obtained LLDPE/MgO nanocomposites with 8.7 wt% MgO@Mg(OH)$_2$ (2.5 mol% 1-octene). A Representative ^{13}C-NMR is given at Figure 6.1.

Table 5.4 1-Octene/branch content of obtained composites determined by ^{1}H-NMR and ^{13}C-NMR.

Filler content [wt%]	1-Octene content [mol%]^a	Branch content [per 1000 C]^b
0	2.5	12.3
4	2.7	13.8
8.7	2.5	12.5
11.4	3.0	13.7
19.6	2.5	10.1

a) from ^{1}H-NMR b) from ^{13}C-NMR[172]

The crystallinity of the matrix LLDPE tends to decrease somewhat with the filler content (Figure 5.15, Table 5.5), and the melt temperature of the composites seems to increase a couple of degrees with the filler content up to 24.6 wt% - despite the tentatively higher number of butyl side chains in these low yield products. Larger crystals with associated higher melting points form, when more filler is present. The self-nucleation of the PE apparently becomes of lesser importance in the composites with more filler, and the formed larger crystals decrease with the extent of crystallization.[173] The crystallization in polyolefin composites with nanofiller that nucleate crystallization can be complex.[174–178] DUBOIS and co-workers found - in congruence - a decreasing crystallinity for CNT composites with increasing CNT load in PE/CNT composites.[179] The CNTs act here as strong nucleating agents, and the crystallization from the surface is decisive for obtaining larger crystals. This leads to larger volumes of amorphous domains between the crystals. It must be noted that the surface of MgO@Mg(OH)$_2$ nanoparticles is covered with a small layer of MAO decomposition products (alumina derivatives), related to the process of preparation.[153] Alumina is a known to nucleate the crystallization of PE.[180] The formation of larger crystals in LLDPE composites with a higher filler content may thus also be related to the dominant nucleation at the filler surface. The greater super cooling corresponding to a lower crystallization temperature with at a higher concentration of filler is indicative of a higher state of energy in the melt when the MgO@Mg(OH)$_2$ filler is present, and is consistent with the higher rate of crystallization at higher filler content.

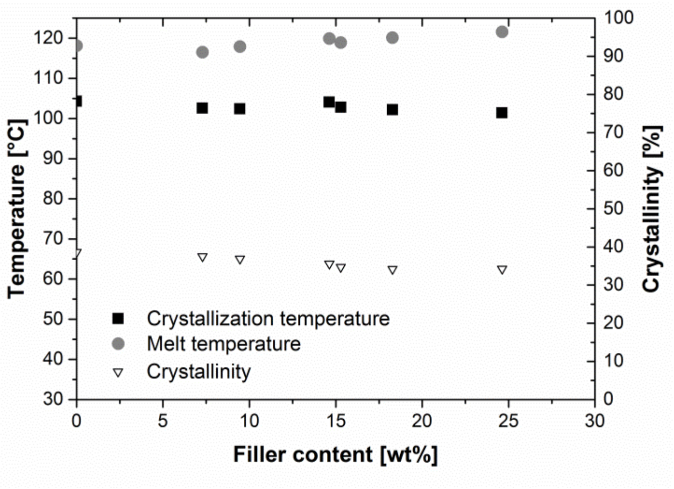

Figure 5.15 Crystallinity, melting and crystallization temperature in non-isothermal crystallization of LLDPE and LLDPE/MgO@Mg(OH)$_2$ nanocomposites.

Table 5.5. Thermal properties of obtained LLDPE/MgO nanocomposites measured by DSC (illustrated at Figure 5.15).

Filler content [wt%]	**Crystallinity [%]**	**Crystallization temperature T_c [°C]**	**Melt temperature T_m [°C]**
0	38.6	104.3	118.1
7.3	37.6	102.6	116.5
9.5	36.9	102.4	117.9
14.6	35.6	104.1	119.9
15.3	34.7	102.8	118.9
18.3	34.2	102.5	120.1
24.6	34.3	101.4	121.6

The two sharp characteristic reflections at 2θ = 21.5° and 23.9° of neat LLDPE can be observed in the normalized wide-angle X-ray scattering pattern [181] of LLDPE and the nanocomposites with 8.1 and 11.4 wt% $MgO@Mg(OH)_2$ (Figure 5.16). These do not change with increasing filler content. The broader background scattering observed in the region of 2θ = 18.5 – 20.5° is typical for the presence of amorphous parts and becomes more intense with an increasing amount of filler. The lower crystallinity at higher filler content is in accordance with the DSC measurements. The intensity of the $MgO@Mg(OH)_2$ reflections increases with the filler content and becomes well recognizable in the diffractograms of composites with 11.4 wt% $MgO@Mg(OH)_2$. Reflections of α-Al_2O_3 or other Al species cannot be observed.

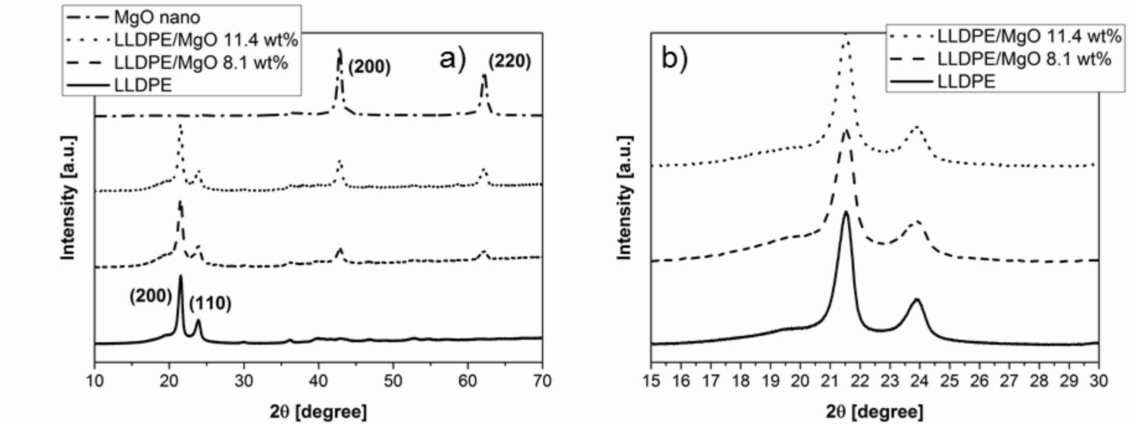

Figure 5.16 (a) Wide-angle X-ray scattering patterns of LLDPE, MgO@Mg(OH)$_2$ and LLDPE/MgO nanocomposites obtained by supported *in situ* polymerization (b) Wide-angle X-ray scattering patterns of LLDPE and LLDPE/MgO nanocomposites in the region between 2θ = 15° and 30°.

5.1.7 Conclusion

The core-shell MgO@Mg(OH)$_2$ was selected from several commercially offered "*nanoscopic*" magnesium oxides. It seems to have a true MgO surface, and the parent agglomerates can readily be broken up into primary particles. A corresponding nanosized magnesium core-shell hydroxide/oxide supported (*n*-BuCp)$_2$ZrCl$_2$/MAO catalyst system was generated *in situ* to obtain well-dispersed LLDPE-C6/MgO@Mg(OH)$_2$ nanocomposites with a filler content up to 25 wt%. MgO@Mg(OH)$_2$ nanoparticles were also surface modified by reacting them with DBM before absorbing MAO to the surface. The amount of DBM of 0.6 mmol per gram of MgO@Mg(OH)$_2$ was necessary to passivate the surface towards deactivating MAO in terms of its co-catalytic activity. It was shown that it is important to keep the amount of MAO under a certain limit in order to control the morphology of the composite. SEM and EDX mapping indicated homogeneously distributed and separated encapsulated nanoparticles at a 100 nm scale. This showed that the *in situ* procedure has led to an almost complete deagglomeration of the MgO@Mg(OH)$_2$ agglomerates into the primary particles. The melting temperature increases with filler content and the crystallinity decreases along the temperature of crystallization. This was interpreted as resulting from a higher rate of crystallization after nucleation from the alumina-covered MgO@Mg(OH)$_2$ particles.

5.2 Linear Low-Density Polyethylene MgO@Mg(OH)$_2$ Nanocomposites from *in situ* Synthesis and Melt Compounding: Morphology and Mechanical Properties

The next chapter reports on the preparation on a larger scale and material properties of LLDPE/MgO@Mg(OH)$_2$ nanocomposites. The impact of three procedures of synthesis is studied on the filler distribution and the material property profile (Figure 5.17). These comprise the pseudo supported polymerization of the MAO/**1** system, the analogous DBM/MAO/**1** system and melt compounding of LLDPE and MgO@Mg(OH)$_2$ nanoparticles.

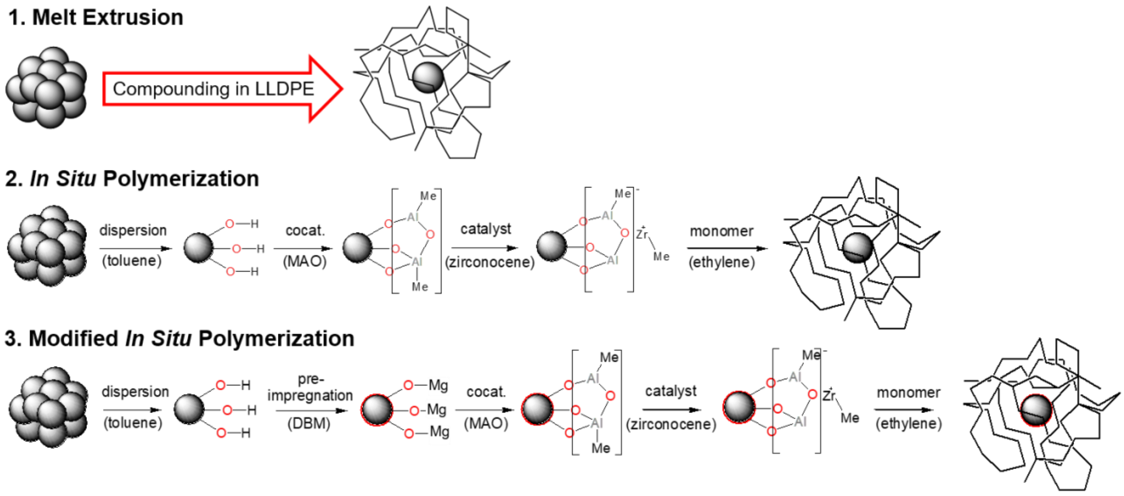

Figure 5.17. Three different routes of composite preparation.

The MgO@Mg(OH)$_2$ used in this study, is a core-shell particle with a MgO shell and a Mg(OH)$_2$ core.[182] An incomplete calcination of Mg(OH)$_2$ has presumably led to this type of core-shell particles.[158, 159, 182] The amount of residual Mg(OH)$_2$ in the core makes up about 31 wt% of the sample. The particles in solid state are an agglomerate of primary particles with a roughly rectangular shape and the largest dimension is smaller than 100 nm (see Figure 5.2) The agglomerates are loose ensembles of the primary particles that can be separated by ultrasonic treatment.[182]

5.2.1 Synthesis and Characterization

LLDPE/MgO@Mg(OH)$_2$ nanocomposites were prepared by the tailored *in situ* polymerization on a scale of a few hundred grams in a 10 L steel reactor (Table 5.6, Table 5.7, Figure 5.17).[182] The scale up from a 1 L reactor (see chapter 5.1) was unproblematic in the sense that the procedure led to the same type of products. The experiments have a good reproducibility, which is advantageous for a further scale up (Table 5.7). The procedure of synthesis starts by conditioning the filler in a defined way. The $MgO@Mg(OH)_2$ particles were dried in the reactor under vacuum and suspended in a toluene/1-octene mixture. MAO (1.5 mmol $Al{\cdot}g^{-1}$ $MgO@Mg(OH)_2$) was subsequently allowed to interact with the surface of the filler for at least 45 min. A part of the MAO reacts with protonic entities at the surface of the $MgO@Mg(OH)_2$ to liberate methane, the rest is majorly absorbed onto the *in situ* formed surface. This was concluded from the powdery morphology of the product that is formed after addition of ethylene and catalyst **1**. Reactor fouling was not observed, contradictory to experiments leading to a reference LLDPE. Its preparation was carried out analogously - in the absence of a support -, and leads to a clumpy product that partly sticks to the reactor interior and stirrer. This is a common observation in olefin polymerization homogenously catalyzed by metallocenes.[9, 14, 183]

A similar series of LLDPE/$MgO@Mg(OH)_2$ nanocomposites were obtained by reacting the $MgO@Mg(OH)_2$ in the toluene/1-octene suspension with 0.5-0.6 mmol of dibutyl magnesium (DBM) per gram filler for 15 min, i.e. before the addition of MAO (Figure 5.17). DBM also reacts with the surface protonic entities (liberation of butane). The amount of the co-catalyst MAO can be and was accordingly decreased to 0.75 $mmol{\cdot}Al{\cdot}g^{-1}$ $MgO@Mg(OH)_2$ while leading to a catalyst activity in the same range (Table 5.7).

Polymerizations were performed with the continuous addition of ethylene, keeping the pressure at 2 bar with the restriction that the ethylene mass flow was limited to 5000 $mL{\cdot}min^{-1}$ (Figure 5.18). The temperature could thus be kept in the interval of 60 to 67 °C with most of the product obtained almost isothermally at 66 °C. LLDPE and LLDPE nanocomposites with about 5 wt% and 8 wt% filler content were obtained with average catalytic activities of about 40-50 $t{\cdot}mol^{-1}{\cdot}h^{-1}$.[182] The degree of branching for LLDPE/$MgO@Mg(OH)_2$ nanocomposites is found in a narrow range of 2.3-3.3 mol%, respectively 3.8-4.7 mol% for reference LLDPE. High-temperature size exclusion chromatography (SEC) gave molecular weights of $M_w = 130$ $kg{\cdot}mol^{-1}$ for reference LLDPE. Molecular weights for nanocomposites polymerized under same conditions are expected to have similar molecular weights. It is difficult to get correct information on the molecular mass by SEC on account of the presence of the encapsulated filler. Nanoparticles would interact with the column and possibly block pores, and polymer chains surrounding a particle may be not completely disentangled.

The difference of 1-2 mol% 1-octene incorporation might be related to the presence of the catalyst near the nanofiller surface, more hindering 1-octene incorporation relative to a homogeneous polymerization. The co-monomer content in the composites of DBM pre-treated filler has a lower average and median than in MAO only based composites. The differences are small though, and a larger data base is necessary to assess the relevance of these observations.

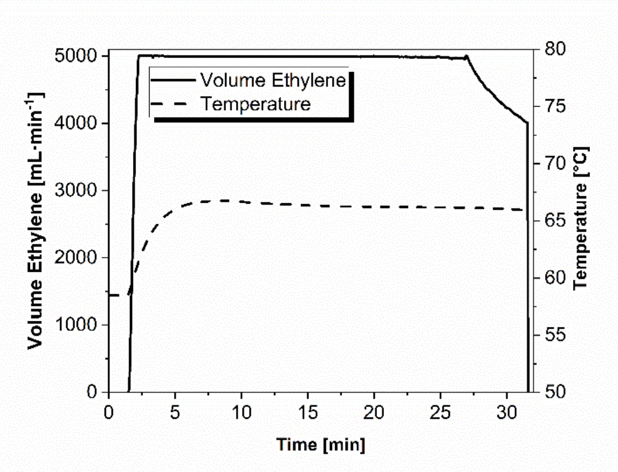

Figure 5.18. Mass flow of ethylene and reactor temperature during the preparation of LLDPE/ $MgO@Mg(OH)_2$/DBM in a 10 L reactor.

SEC gave molecular weights of $M_w = 130\ kg\cdot mol^{-1}$ for reference LLDPE. Molecular weights for nanocomposites polymerized under same conditions are expected to have similar molecular weights. It is difficult to get correct information on the molecular mass by SEC on account of the presence of the encapsulated filler. Nanoparticles would interact with the column and possibly block pores, and polymer chains surrounding a particle may be not completely disentangled.

Table 5.6. LLDPE obtained by ethylene and 1-octene co-polymerization

Sample number	**Average activity [kg·mol^{-1} h^{-1}]**	**Yield [g]**	**M_n [kg·mol^{-1}]**	**M_w [kg·mol^{-1}]**	**Đ**	**X_c [%]**	**T_c [°C]**	**T_m [°C]**	**1-Octene content [mol%]**
LLDPE									
1	45 400	452	43.2	132.9	3	39.6	100.9	112.4	4.7
2	46 800	466	45.0	135.0	3	37.5	97.7	111.6	3.8

Table 5.7. LLDPE nanocomposites obtained by *in situ* polymerization

Sample number	**Filler content [wt%]**	**Average activity [kg·mol^{-1}·h^{-1}]**	**Yield [g]**	**X_c [%]**	**T_c [°C]**	**T_m [°C]**	**1-Octene content [mol%]**
	with DBM pre-treatment						
3	4.9	39 100	390	37.2	96.2	113.5	2.9
4	5.3	36 100	360	40.8	104.0	117.0	2.3
5	8.2	44 800	223	40.0	101.7	117.7	2.3
6	8.6	42 900	214	47.5	108.9	125.0	3.3
7	8.7	42 100	210	40.0	101.1	119.2	2.5
	MAO only						
8	7.7	48 000	240	37.6	95.6	116.1	2.8
9	7.8	47 700	238	33.7	92.2	116.8	3.0
10	7.8	47 500	237	39.8	99.5	115.8	2.8

The melting points of the “DBM” samples and the “MAO-only” samples are found in a narrow range of 116-117 °C in non-isothermal crystallizations, which is interpreted in terms of a comparable microstructure (except for sample 6, which also has a little higher co-monomer content). This is in contrast to a comparable investigation using titania as filler.[184] The degree of crystallization normalized to co-polymer content follows more or less the temperature of crystallization, i.e. higher crystallinities are found for samples crystallizing at a higher temperature. Again, subtle differences between composites based on DBM and MAO-only treated filler were found. Samples with DBM pre-treated filler are in average crystallizing at somewhat higher temperatures, suggesting that nucleation – probably arising from the surface contact to alumina - is more effective.[182] The differences, however, are small also in relation to reference LLDPE that contains residual alumina, too.

The normalized WAXS patterns of the composites with sample 3 and 5 resemble the addition of the patterns of MgO@Mg(OH)$_2$ and LLDPE (Figure 5.19). The two sharp characteristic reflections at 2θ = 21.5° and 23.9° of neat LLDPE are assigned to the 110 and 200 reflections of the Bunn orthorhombic subcell of polyethylene.[181] The positions of the two main peaks are unchanged in the composite, indicating that the crystal lattice of the LLDPE does not change in the presence of the MgO nanoparticles.

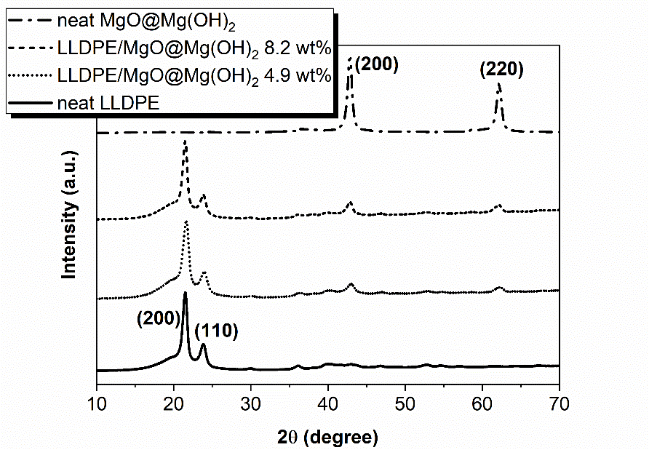

Figure 5.19. Wide-angle X-ray scattering patterns of LLDPE, $MgO@Mg(OH)_2$ and LLDPE/ $MgO@Mg(OH)_2$ nanocomposites.

Melt compounding of the nanoparticles with a comparable commercial grade LLDPE led to a further type of LLDPE/$MgO@Mg(OH)_2$ composite. Melt compounding was performed in a corotating double screw extruder using a typical barrel configuration for processing PE.[185] The initially formed material was run again through the extruder to ensure a good mixing. The highest level attained was 5 wt%. Processing higher amounts of filler into the polymer was not possible due to the increase in polymer viscosity in combination with the limited torque of the lab scale extruder.

5.2.2 Composite Morphology

The in situ polymerization of ethylene on DBM impregnated $MgO@Mg(OH)_2$ nanoparticles separates the nanoparticles effectively (Figure 5.20). The nanoparticles in composites prepared with MAO only end up not as thorough separated as those in product with DBM pre-treated filler (Figure 5.21d, f).

In both cases, it can be observed that the $MgO@Mg(OH)_2$ nanoparticles are encased in polymer matrix. No voids between matrix and filler are observed, indicating a good contact between polymer and filler. The nanoparticles pre-treated with DBM in the composites are more homogeneously distributed and separated. The encased nanoparticles also appear here as small clusters 100 nm in size of individual single particles (Figure 5.2). AFM images are consisted with this interpretation (Figure 5.20c). Areas of higher $MgO@Mg(OH)_2$ concentration are reminiscent of a separation of the agglomerates into single primary particles on account of the pressure executed by the formation of polymer between them. EDX mapping of composite with 8 wt% MgO impregnated with DBM again shows a fine distribution of Mg at 1.04 wt% (Figure 5.21b).

Composites based on MgO@Mg$(OH)_2$ treated with MAO only also contain agglomerates with a size up to 1 µm, but without an obvious continuous separation and encapsulation of the primary particles (Figure 5.20b, d). Thus, the impregnation of MgO nanoparticles with DBM is not only useful to reduce the amount of MAO necessary for polymerization reaction like described in chapter 5.1, it is in fact helping to achieve a nanocomposite with a finer particle distribution. It may be hypothesized that the distribution of the MAO over the filler surface is more homogeneous, and thus that the copolymerization is taken place at more positions on the surface.

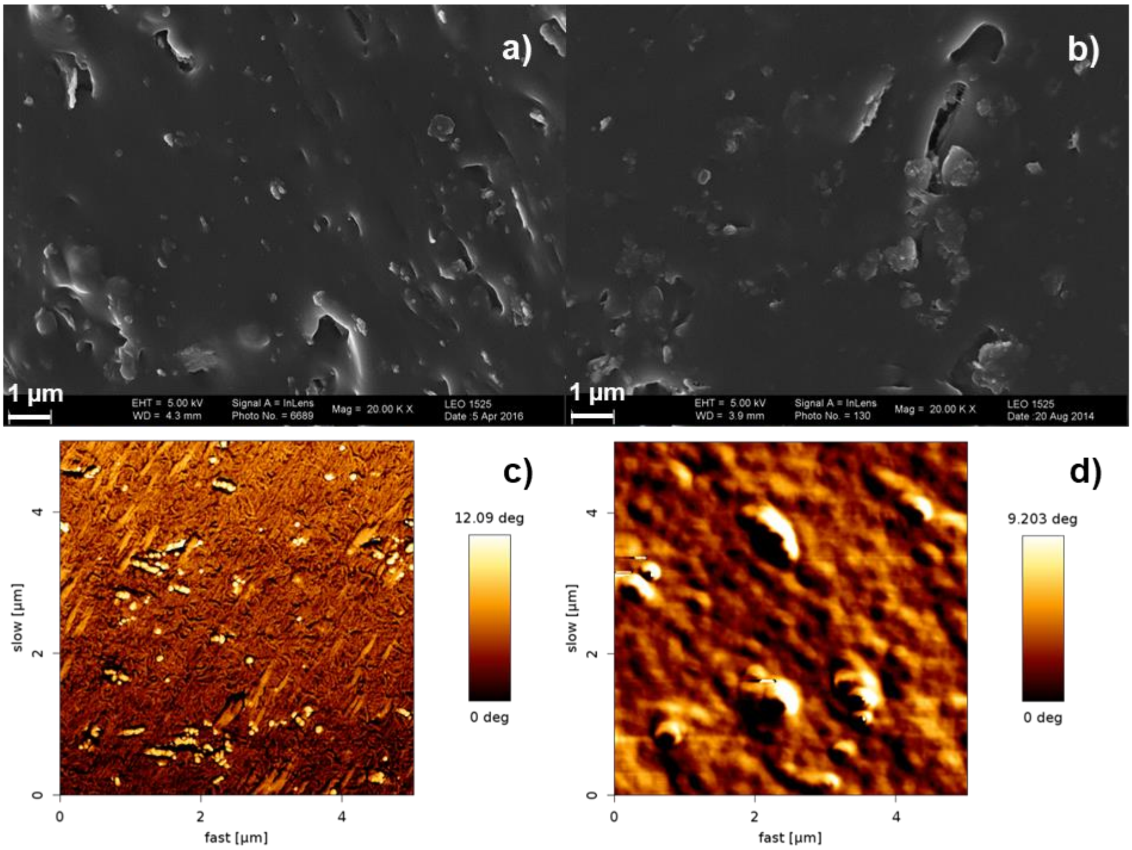

Figure 5.20 SEM images of *in situ* LLDPE/MgO@Mg$(OH)_2$ nanocomposite cross sections at a magnification of 20k (a) with 8.2 wt% MgO@Mg$(OH)_2$ pretreated with DBM and (b) with 7.7 wt% MgO@Mg$(OH)_2$ and MAO only impregnation, and the corresponding AFM images in (c) resp. (d).

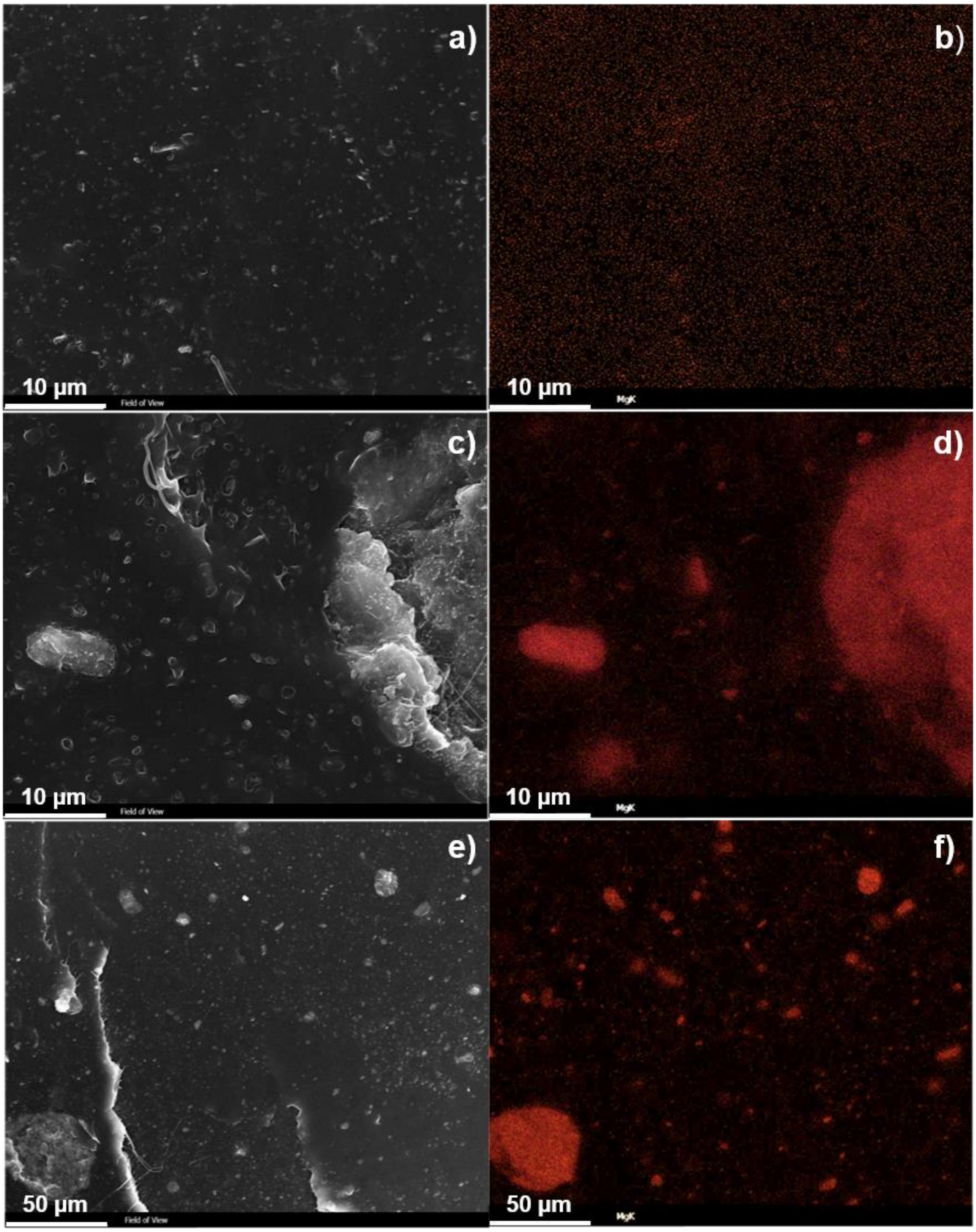

Figure 5.21. EDX mapping (red = Mg) of LLDPE/MgO@Mg(OH)$_2$ (4.9 wt%) nanocomposite filler cross sections at a magnification of 5k resp. 1k and SEM images (field of view) reached by *in situ* polymerization with application of DBM (a, b) and by melt extrusion (4.8 wt%) (c-f).

Melt compounds show MgO@Mg(OH)$_2$ nanoparticles that are not in good contact to the polymer matrix (Figure 5.22). Micrometer-sized filler agglomerates can also be observed in EDX measurements (1.13 at% Mg) with high local concentrations of Mg

(Figure 5.21d, f). Voids around those agglomerates indicate a phase separation between filler and polymer matrix. The nanoparticles are highly polar and tend to agglomerate more strongly without a further surface modification. The absence of alumina on (parts of) the surface may be the decisive factor for the differences in matrix-filler interaction.

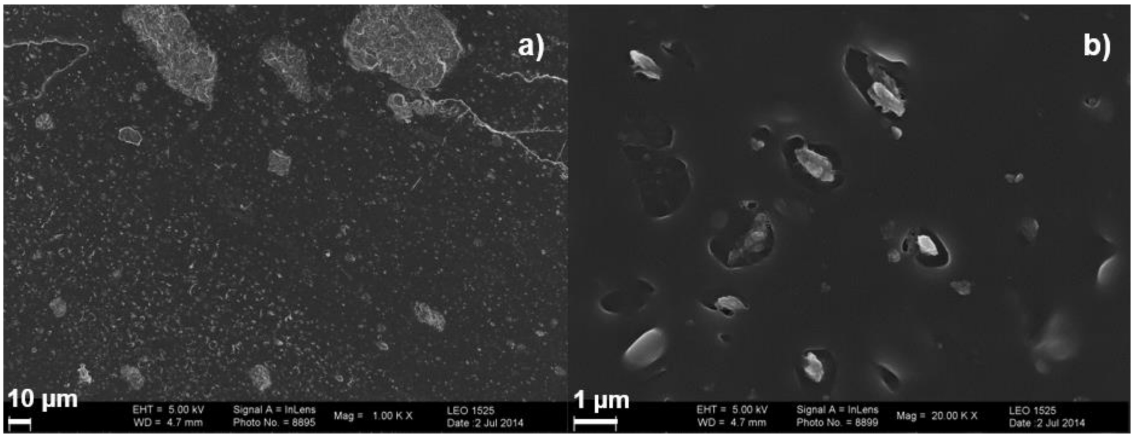

Figure 5.22. SEM images of LLDPE/MgO@Mg$(OH)_2$ (4.8 wt%) nanocomposite cross sections at a magnification of 1k (a) and 20k (b) reached by melt compounding with MgO@Mg$(OH)_2$ nanoparticles.

5.2.3 Mechanical Properties

Mechanical properties were determined from tensile testing of A5 type samples prepared by injection moulding (Table 5.8, Figure 5.23). Stress-strain curves show the usual behavior of a filled semi-crystalline thermoplastic polymer. The results of the evaluation are indicative of a good adhesion over the polymer-filler interface for the *in situ* prepared composites and good dispersion, especially for those containing DBM pre-treated filler (Figure 5.23).[186] This was already indicated in the SEM micrographs (Figure 5.20).[187] Thus, the ineffective deagglomeration of the MgO@Mg$(OH)_2$ nanoparticles in melt compounding results in a deterioration of mechanical performance.

The elongation at break decreases with the filler content and with the quality of dispersion. The smallest elongation at break is hence found for composites based on MgO@Mg$(OH)_2$ pre-treated with DBM, which seems to have the best dispersion. Low but reasonable values of 61% are found for sample 5, a composite with 8.2 wt% MgO@Mg$(OH)_2$. The comparable composite prepared by the *in situ* procedure using only MAO shows a mean elongation at break of 241% with a much larger standard deviation. The material is also less homogeneous. A similar picture arises from the comparison of the composites with a filler content of about 5 wt%. The composite based on DBM treated filler has a maximum elongation of 124% versus 548% in a reference LLDPE and the one from melt blending 295% versus 326% in the virgin material.

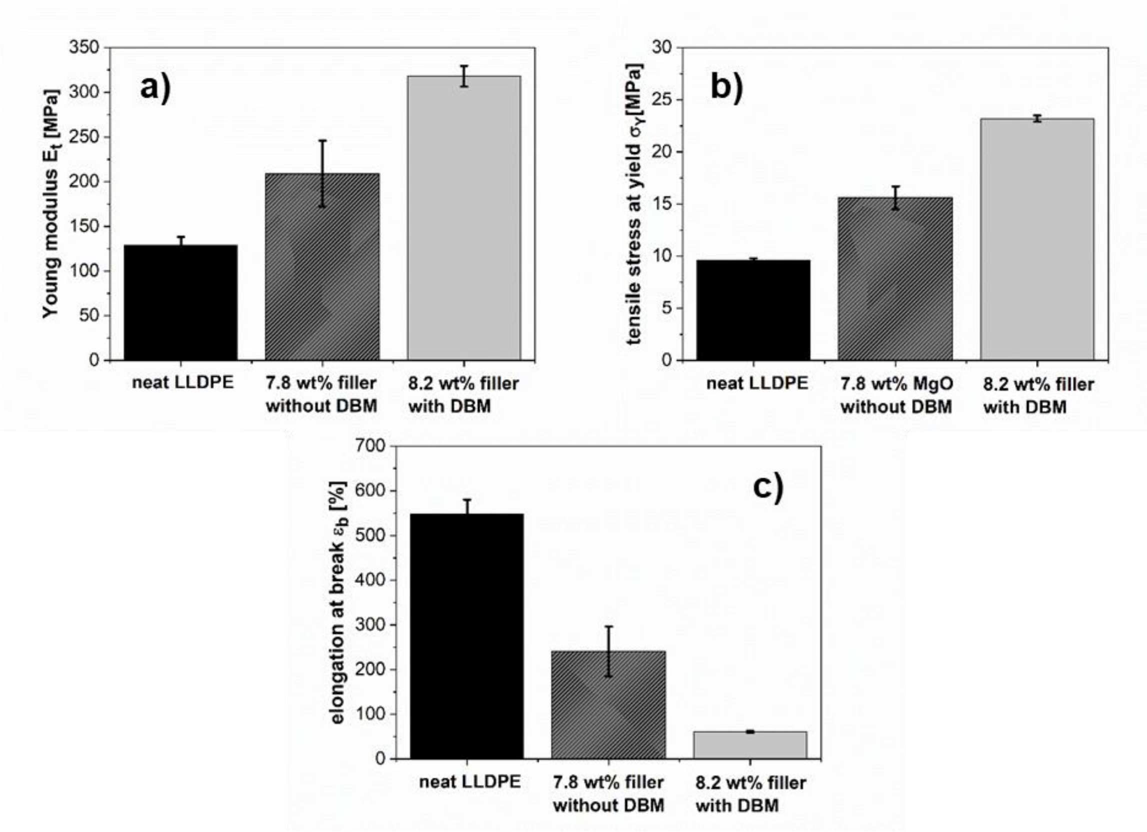

Figure 5.23. Young modulus E_{mod} (a), yield stress at yield σ_Y (b) and elongation at break ε_B (c) for LLDPE and LLDPE/MgO@Mg(OH)$_2$ nanocomposites containing MgO@Mg(OH)$_2$ nanoparticles with or without DBM impregnation.

Table 5.8 Mechanical properties of LLDPE/MgO@Mg(OH)$_2$ nanocomposites.

Sample	**Filler content [wt%]/[vol%]**	**Young modulus E_t [MPa]**	**Yield strength σ_Y [MPa]**	**Elongation at break ε_b [%]**
in situ polymerization				
LLDPE (homogeneous)	-	129 ± 9	9.6 ± 0.2	548 ± 33
LLDPE/MgO@Mg(OH)$_2$/DBM	4.9/1.3	151 ± 34	17.7 ± 1	124 ± 25
LLDPE/MgO@Mg(OH)$_2$/DBM	8.2/2.2	318 ± 12	23.2 ± 0.3	61 ± 2
LLDPE/MgO@Mg(OH)$_2$	7.7/2.0	209 ± 37	15.6 ± 1.1	241 ± 56
melt extrusion				
LLDPE C6 (*Sabic*)	-	252 ± 17	17 ± 1	326 ± 17
LLDPE C6/MgO@Mg(OH)$_2$	4.8/1.2	282 ± 36.5	14.7 ± 0.5	295 ± 30

It is also found that the yield strength is increased in the *in situ* composites and again most extensively in those with a DBM pre-treated filler. The composite by melt extrusion shows a smaller yield strength as the matrix polymer, which is an expected behavior for an inorganic filler such as $CaCO_3$ in a polyolefin.[97, 145, 188–190] The Young's modulus - determined from the slope of the initial elastic response - of LLDPE/MgO@Mg(OH)$_2$ *in situ* nanocomposite with about 8 wt% of filler also shows the largest enforcement for the composite with DBM pre-treated filler of 318 ± 12 MPa versus 209 ± 37 MPa for the comparable *in situ* composite with no DBM pre-treatment. The Young modulus with a filler content of 5 wt% is close to that of LLDPE. This may be related to the thermal properties, which are also comparable (sample 3).

5.2.4 Conclusion

LLDPE/MgO@Mg(OH)$_2$ nanocomposites with 5 wt% and 8 wt% filler were successfully prepared on a 400-500 g scale by an *in situ* polymerization using MgO@Mg(OH)$_2$ nanoparticles as support for bis(*n*-butyl cyclopentadienyl)zirconium dichloride. *In situ* copolymerization of ethylene/1-octene in the presence of MgO@Mg(OH)$_2$ nanoparticles pre-treated with DBM is an efficient way to obtain composites with good filler distribution in a one-pot synthesis route, which can be scaled up by a factor of 10. Average catalyst activity shows a good reproducibility in the range of 40 000 – 50 000 $kg \cdot mol^{-1} \cdot h^{-1}$. No reactor fouling was observed indicating of the action of a heterogeneous catalyst system.

The temperature could be controlled by limiting the ethylene feeding rate. The pre-treatment of the filler with DBM allows to reduce the amount of MAO, and consequently the alumina interface between filler and matrix is smaller/thinner, and more homogenous as initial filler agglomerates are broken up by the inner particle polymer formation. It seems that this has an overall positive effect on the mechanical properties with respect to tensile strength and Young modulus. Related to that may be the crystallization behavior, the surface is a better nucleating agent, and the crystallinity is the highest in the series. It is not known, whether the distribution of the co-monomer is different too, as a further reason for the crystallization behavior may be found in that. Melt compounded composites show a weak adhesion between filler and matrix indicated by voids and agglomerates in micrometre scale. They show no reinforcing effect and yield stress is decreased.

5.3 iPP Nanocomposites comprising *in situ* Olefin Polymerization and Melt Compounding

The objective of the research presented in the following chapter was to obtain iPP nanocomposites with low content (0.5 wt%) and without agglomerates of MgO@$Mg(OH)_2$, SiO_2 or $BaTiO_3$ filler. These oxidic nanofillers were chosen for reasons of modifying the dielectrical properties of polypropylene.[154, 191] It is known that only small amounts of nanofiller are necessary to observe a significant impact on mechanical, thermal or dielectric properties.[97, 122, 133, 135, 145, 192] A constraint of this research was to avoid the addition of dispersing agents or functionalized polyolefins as compatibilizers as normally used for polar fillers. A two-step strategy was chosen to prepare such nanocomposites (Figure 5.24). In the first step, nano-composites with a filler content of about 5 wt% were produced by an *in situ* olefin polymerization using a metallocene/MAO catalyst system. In the second step, the obtained nanocomposites were used as masterbatches, and were diluted with commercial iPP via melt compounding. The advantage of *in situ* polymerization in combination with the ease of melt compounding constitutes a versatile route to homogeneous dispersed nanoparticles in an iPP matrix.

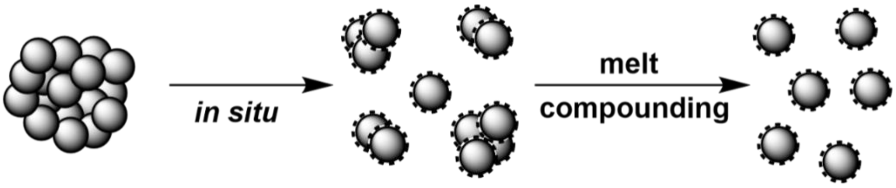

Figure 5.24. Two-step approach to obtain oxidic nanocomposites (grey: nanofiller, dashed: polymer).

5.3.1 Nanocomposite Preparation

The primary particles of the oxide fillers of this study are in of a size below 60 nm (Table 5.9), which make them potentially useful in films thinner than 5 µm. These types of oxides are known to have relatively high surface energies (polarity) and they tend to agglomerate in an apolar matrix such as iPP. The core-shell MgO@$Mg(OH)_2$ nanoparticles consists of small cubic particles with an edge length of about 20-40 nm (Figure 5.25a).[182] SiO_2 nanoparticles consist of particles 15-40 nm in size (Figure 5.25b) and $BaTiO_3$ nanoparticles are platelets with a slightly larger particle size of about 40-60 nm (Figure 5.25c). These primary oxide nanoparticles in the as-received powdery state coexist in larger agglomerates (Figure 5.26). Therefore, the formation of nanocomposites with well-distributed, single primary particles profits from a method of preparation that de-agglomerates and disperses the primary nanoparticles in an effective way.

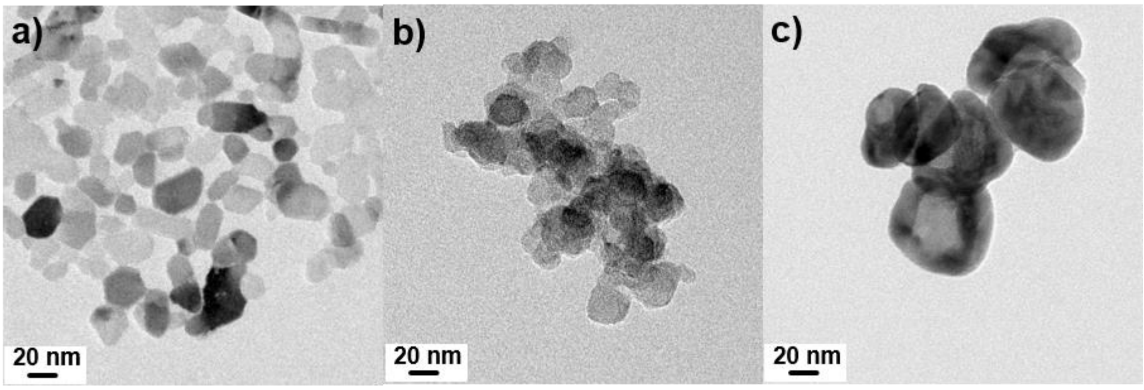

Figure 5.25. TEM images of fillers used in this work suspended in ethanol (a) MgO@Mg$(OH)_2$ MgO@Mg$(OH)_2$, (b) SiO_2 (c) $BaTiO_3$.

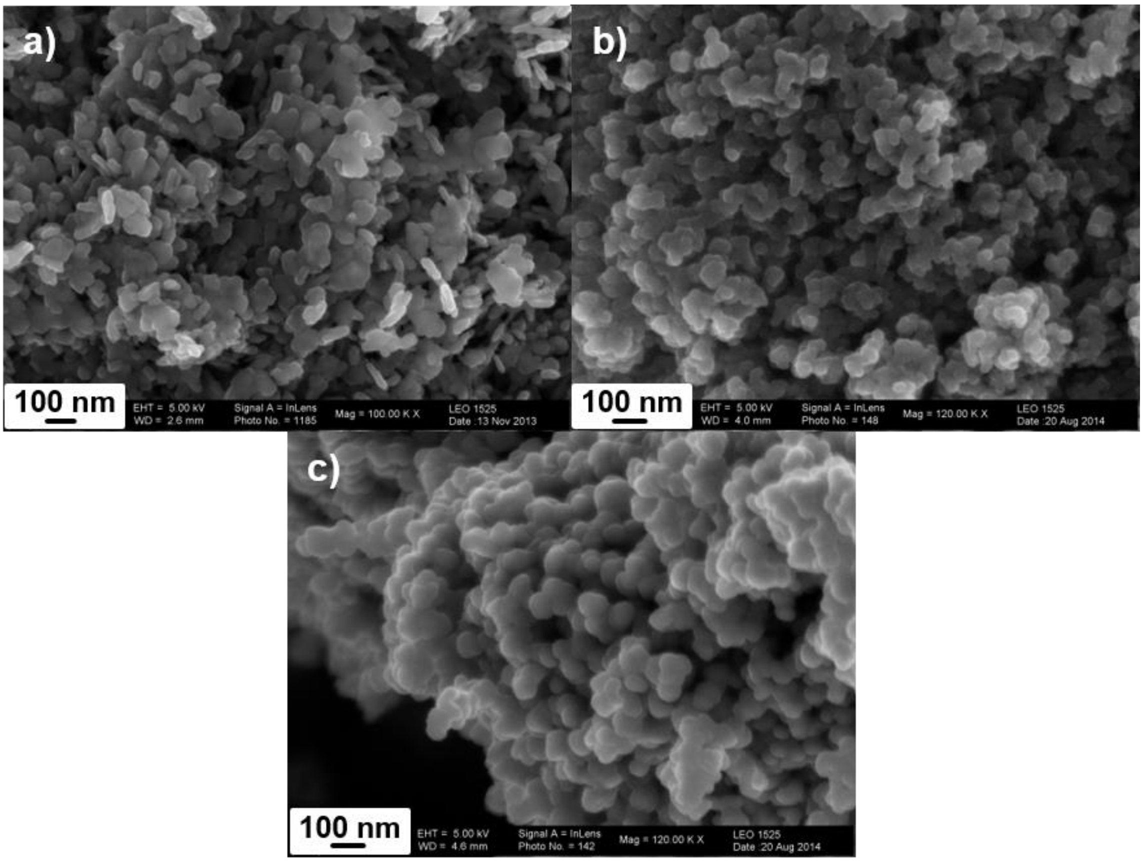

Figure 5.26. SEM images of fillers used in this work (a) MgO@Mg$(OH)_2$, (b) SiO_2 (c) $BaTiO_3$.

Table 5.9. Oxidic nanofillers used in this chapter.

Filler	**Size [nm]$^{a)}$**	**Surface [m^2·g^{-1}]$^{b)}$**	**Density [g·cm^{-3}]$^{a)}$**
MgO@Mg(OH)$_2$	35	51	3.6
SiO$_2$	20-60	430	2.2 – 2.6
BaTiO$_3$	50	19	5.9

$^{a)}$: Datasheet; $^{b)}$: determined by BET

The iPP/oxide nanocomposites masterbatches were prepared by *in situ* polymerization under the action of a metallocene/MAO system.[122] The co-catalyst MAO is reactive towards the hydroxyl groups present on the surface of the fillers; methane is evolved and covalent Al-O bounds are formed.[122, 192] Further, MAO will interact with the new surface and will be preferentially located on that surface, i.e. as long as its remaining concentration is below a certain level. MAO anchored by this method to the surface is potent enough to form an active polymerization catalyst from the metallocene [dimethylsilane diyl-bis(2-methyl-4-phenylindenyl)]zirconium(IV) dichloride **1**.[122, 143, 144]

The amount of MAO relative to the amount of filler was adjusted with the aim of reaching a powdery product – typical for the action of a supported catalyst with most of the MAO near the particle surface – and an average activity of the catalyst in the range of 3-6·10^5 kg iPP mol^{-1}·h^{-1}. MAO activates the metallocene dichloride, thereby, generating the near surface-anchored active catalyst species, which induces polymer formation close to the filler surface. It is inferred that this procedure leads to the powdery product.[97, 121, 144] The MAO was allowed to interact with the filler surface for 45-60 min prior to injection of the catalyst precursor. When the MAO is distributed evenly over the surface of the primary particles, the nanoparticles may effectively be de-agglomerated by the force of the growing layer of polymer on the surface.[159] The solid agglomerates of SiO$_2$ and BaTiO$_3$ nanoparticles were dispersed in toluene and subsequently subjected to ultrasound before they were contacted with MAO. MAO is thought to become more homogenously distributed over the surface in that way. Omitting this step leads to composites with the agglomerates of the primary particles (Figure 5.27).

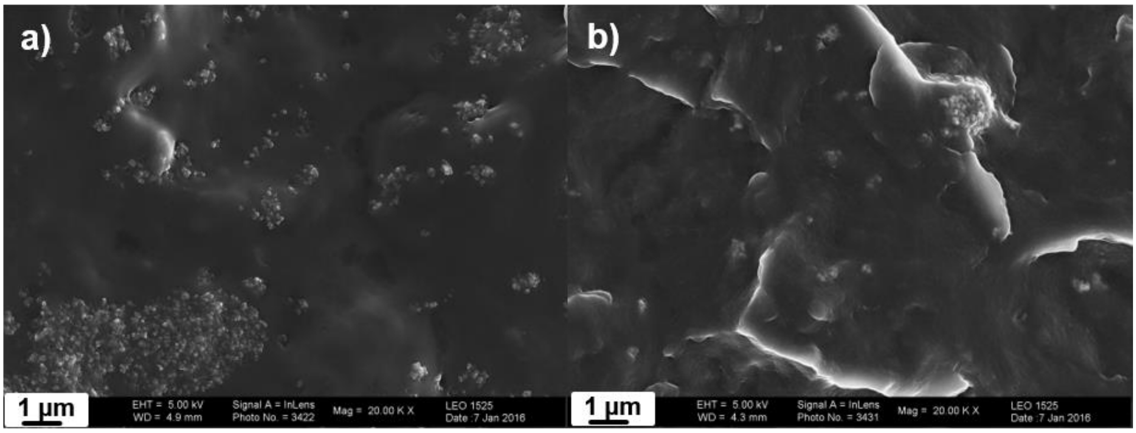

Figure 5.27 SEM images of iPP nanocomposite cross sections at a magnification of 20k reached by *in situ* polymerization (a) SiO2 4.8 wt% and (b) BaTiO3 4.5 wt%.

MgO@Mg$(OH)_2$ particles were pre-treated with 0.5 mmol of DBM per gram of filler. This allows a reduction in the amount of MAO necessary for inducing polymerization and leads to a good dispersion of MAO over the surface. As described in chapter 5.1 and 5.2, this method was developed for obtaining linear low-density PE/MgO@Mg$(OH)_2$ nanocomposites.[182] Pre-treating SiO_2 and $BaTiO_3$ nanoparticles using the same procedure with DBM results in a significant decrease of the catalytic activity of the metallocene, or results in a complete absence of PP formation.

Masterbatches were accordingly prepared by suspending 25 g of the oxide filler in toluene, adding MAO, propylene and metallocene dichloride. Reactions were carried out with continues addition of propylene, keeping the reactor internal pressure at 2 bar. The amount of propylene was metered. The flow of propylene was stopped after the desired amount of propylene was admitted for reaching over 500 g of composite with about 5 wt% of filler (Table 5.10). Changing the reaction conditions allows to prepare composites with higher contents. The composites with 5 wt% of filler, however, were found convenient as masterbatches for obtaining composites with a filler content of about 0.5 wt%. The obtained nanocomposites were dispersed in a commercial grade of iPP by melt extrusion compounding. Preparation and dilution of the masterbatch reduce the overall efforts arriving at a composite with 0.5 wt% of filler.

Table 5.10. iPP- oxidic nanocomposites by *in situ* polymerization.

Type of filler	Amount of Al (in MAO) [mg]	t(poly) [min]	Yield [g]	Average activity [t mol^{-1} h^{-1}]	Filler content [wt%]^{c}	Tacticity [%mmmm]	X_c [%]$^{d)}$	T_m [°C]$^{d)}$	T_c [°C]$^{d)}$
(reference iPP)	1140$^{a)}$	210	540	102	-	98.2	54.1	158.9	122.9
MgO@Mg(OH)$_2$/DBM	1580$^{b)}$	190	590	39	5.0	98.0	54.7	163.1	111.4
SiO$_2$	1960	110	530	30	4.8	98.1	57.6	156.0	122.3
BaTiO$_3$	1980	90	560	59	4.5	-	54.6	157.0	121.8

Polymerization conditions: 3.5 L dry toluene, 3 µmol catalyst, 60 °C, 25 g filler, 2 bar propylene $^{a)}$: 1.5 µmol catalyst $^{b)}$: 0.5 mmol DBM·g^{-1} of filler, $^{c)}$: from residual mass in TGA, $^{d)}$: by DSC

The ^{13}C NMR spectrum (Figure 5.28), which allows one to infer the matrix PP, has a microstructure with about 98 ± 1% mmmm pentades, equal to that of reference iPP. The presence of the filler thus, does not influence the catalytic action of the iso-specific metallocene catalyst. Reference iPP was prepared under similar conditions as of the composites with no filler present. It did not have a powdery morphology.

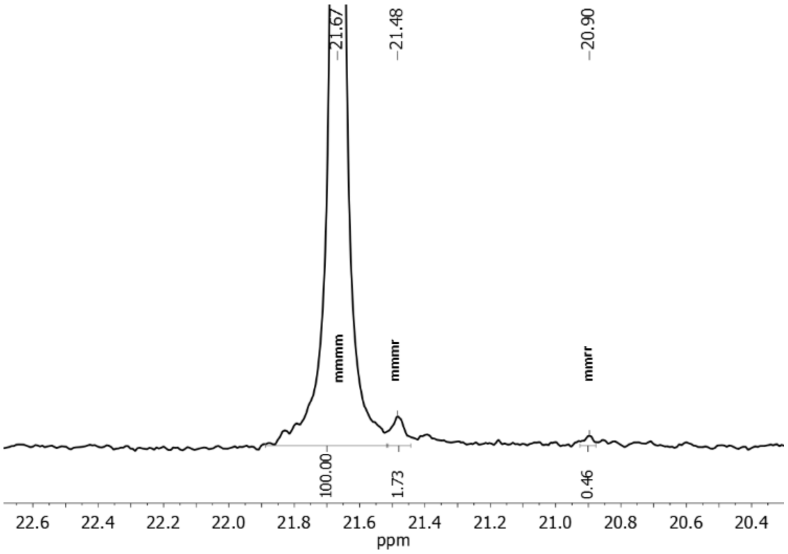

Figure 5.28 *Igated* ^{13}C-NMR spectrum of an iPP/MgO@Mg(OH)$_2$ nanocomposite with 5 wt% filler.

The thermal properties in terms of melting enthalpy, melting temperature and temperature of crystallization of the composites are also equal to that of the reference iPP, except for the MgO@Mg(OH)$_2$/DBM based composite (Table 5.10). The crystallinity is in between 54-57% with a crystallization setting in at 122-123 °C. The composite with

$MgO@Mg(OH)_2$/DBM needs a 10 °C larger undercooling in the non-isothermal DSC experiment (cooling rate of 20 $K \cdot min^{-1}$) for inducing crystallization. Nucleation is apparently more difficult and fewer nuclei may have formed, in accordance with the higher melting point of 163 °C of crystals that have grown larger. This may reflect the lower amount of nucleating alumina (originating from MAO) in the composite and/or shows that the alumina is more confined to the surface of the $MgO@Mg(OH)_2$/DBM than the other fillers and in reference iPP.

5.3.2 Composite Morphology

Single $MgO@Mg(OH)_2$ nanoparticles are seen in SEM images of the breaking edge of cryo-cracked samples of the iPP composite. In addition, some small clusters are present with average sizes of 200-300 nm (Figure 5.29a). The nanoparticles appear encased within the polymer matrix and no void or traces of filler pull-out processes are obvious. This is indicative of a reasonable compatibility between polymer and filler interface. The latter is tentatively mainly a shell of alumina surrounding the filler. This is believed to be the case for the primary particles making up the small clusters, too. They seem to be separately surrounded by polymer and still are very close to each other, reminiscent of the agglomerates from which they would originate. This is also observable in the 'raspberry' or 'cauliflower' constitution of supported ZIEGLER–NATTA catalysts.[193] Thus, major deagglomeration and effective nanoparticle dispersion is achieved. Similar holds true for composites containing SiO_2 and $BaTiO_3$ nanoparticles (Figure 5.29b and c). Here, the initial agglomerates (Figure 5.26) need to be broken up along with the addition of MAO, e.g. by the ultrasound of this work. MAO itself apparently is not penetrating the agglomerates extensively (at least not at the amount used) and the consecutive polymerization takes place at the surface of the agglomerates only. The pre-treatment of $MgO@Mg(OH)_2$ with DBM can thus be understood as a further procedure for decrease the binding within the agglomerates.

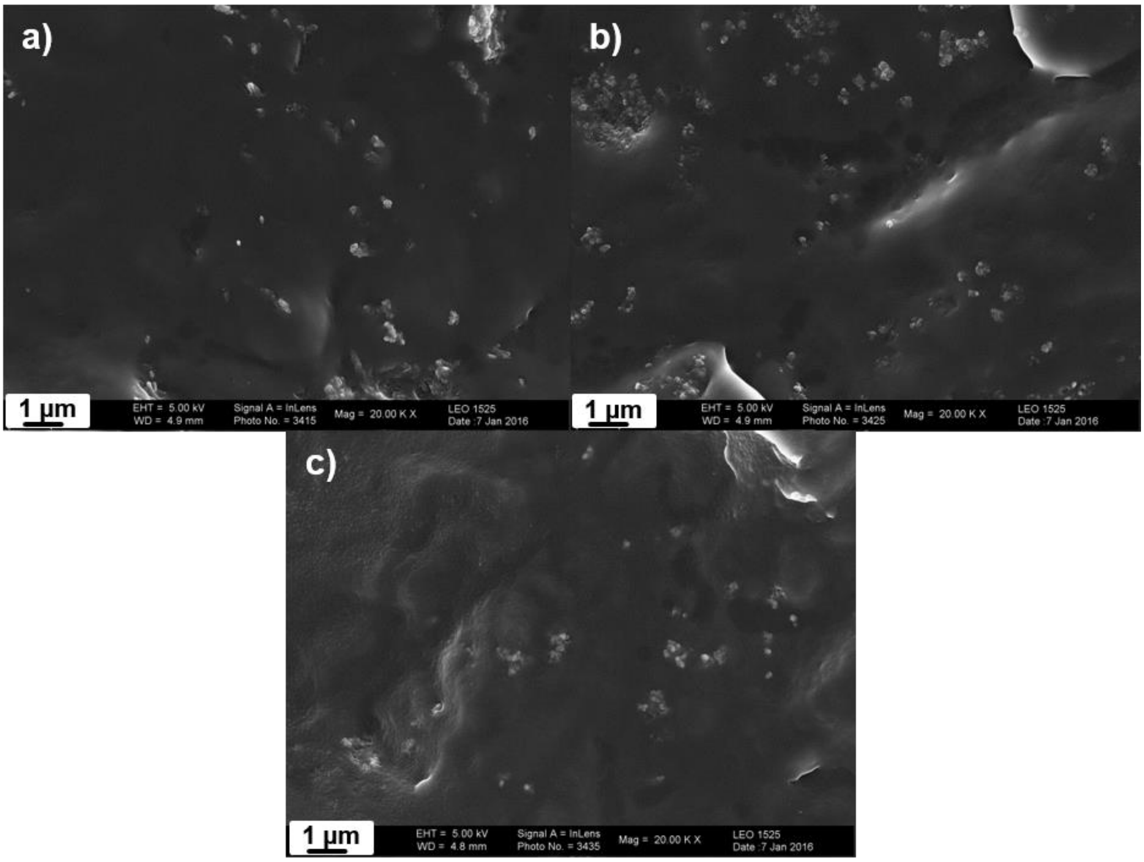

Figure 5.29 SEM images of iPP nanocomposite cross sections at a magnification of 20k reached by *in situ* polymerization a) MgO@Mg(OH)$_2$ 5 wt%, b) SiO2 4.8 wt% and c) BaTiO$_3$ 4.5 wt%.

It may be noticed that the cluster observed in case of the SiO$_2$ particles are larger and contain more primary particles (Figure 5.29b). The procedure of ultrasound treatment apparently is not as effective as for breaking up agglomerates of BaTiO$_3$ nanoparticles, and/or the re-agglomeration is faster. The surface area of the SiO$_2$ filler is also about one order of magnitude higher than of the other fillers of this study. It may be expected that the MAO will not only be on the particle surface, but also in pores. Since about the same amount of MAO is used in preparing SiO$_2$ and BaTiO$_3$ composites, the stabilizing surface coverage may be smaller for SiO$_2$ primary particles. The observation of cluster with a larger count of primary particles is also consistent with the higher crystallinity of the corresponding SiO$_2$ nanocomposite (Table 5.10), i.e. resulting from the less homogeneous distribution, leaving a more dynamic matrix back.

EDX mapping suggests that the MgO@Mg(OH)$_2$ nanoparticles are dispersed to the finest degree, followed by those of BaTiO$_3$ (Figure 5.30). In contrast, composites based on nanoparticular SiO$_2$ show cloudy areas with a higher Si concentration with an up to 15 µm. This is in accordance with the considerations arising from the SEM image. The

EDX mapping gives an average insight of volume below the surface; the analyzed area is larger and, particularly, spots of higher concentration are detected. The electron beam with an accelerating voltage of 20 kV will penetrate into the sample and a projection of the near-surface volume is obtained. Composites containing $BaTiO_3$ show a smaller amount of cloudy areas of smaller magnitude (< 4 µm). The Mg distribution in the composite presented in Figure 5.29a shows Mg well-dispersed in the sample with few areas of higher Mg concentration. The latter could be clusters of nanoparticles.

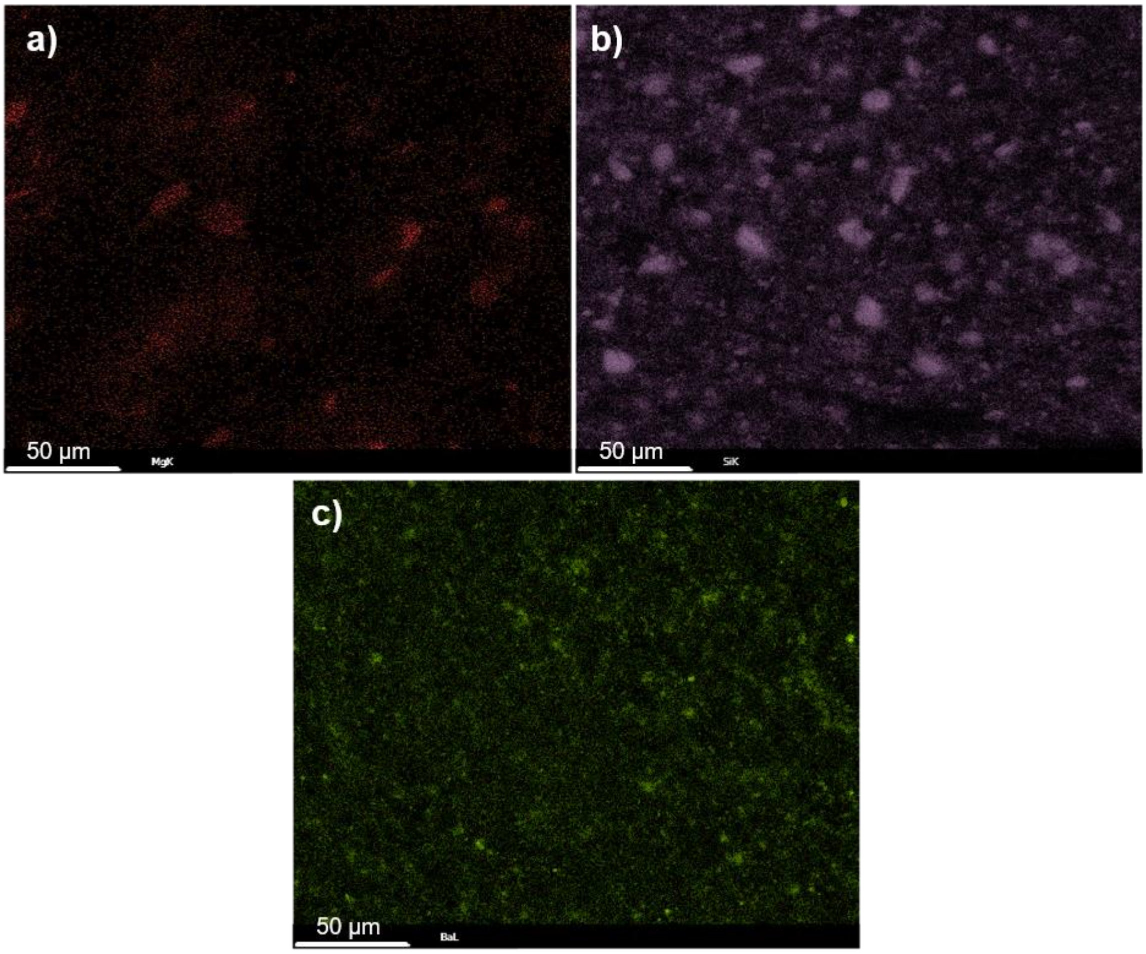

Figure 5.30 EDX mapping of iPP composites cross sections at a magnification of 5k a) red = Mg 5 wt%, b) magenta = Si 4.8 wt% and c) green = Ba 4.5 wt%.

SEM images show well-dispersed nanoparticles in the nanocomposites after diluting the masterbatches with 9 parts of iPP (Figure 5.31*).* Single nanoparticles are exclusively found after melt extrusion in the resulting composites with 0.5 wt% filler content, although it cannot be ruled out that small agglomerates of nanoparticles are still present somewhere in the nanocomposite. EDX mapping of the nanocomposite samples after melt extrusion gave no signals; the limit of the detection is too high for such a small particle/element concentration (0.5 wt%).

The thermal properties of the nanocomposites with 0.5 wt% of MgO@Mg(OH)$_2$ and BaTiO$_3$ are again very similar. The temperature of crystallization is a little higher than that of iPP showing a smaller nucleation effect of the filler surface (most likely of alumina, Table 5.11). This results in smaller crystals and a higher overall crystallinity. A comparable nucleation is not induced by the SiO$_2$ nanoparticles with tentatively less alumina in contact with the matrix. The thermal behavior resembles that of iPP, except for the lower crystallinity resulting from the presence of filler particles, reducing the mobility of the PP chain segments (Table 5.11).

Table 5.11. iPP oxidic nanocomposites prepared by melt compounding of nanocomposite masterbatches.

Filler type	**Filler content [wt%]$^{a)}$**	**X_c [%]$^{b)}$**	**T_m [°C]$^{b)}$**	**T_c [°C]$^{b)}$**
-	0	43.5	167.8	108.4
MgO	0.5	46.3	163.0	111.0
SiO$_2$	0.5	39.0	166.1	108.9
BaTiO$_3$	0.5	46.9	163.8	110.5

$^{a)}$: from residual mass in TGA, $^{b)}$: by DSC

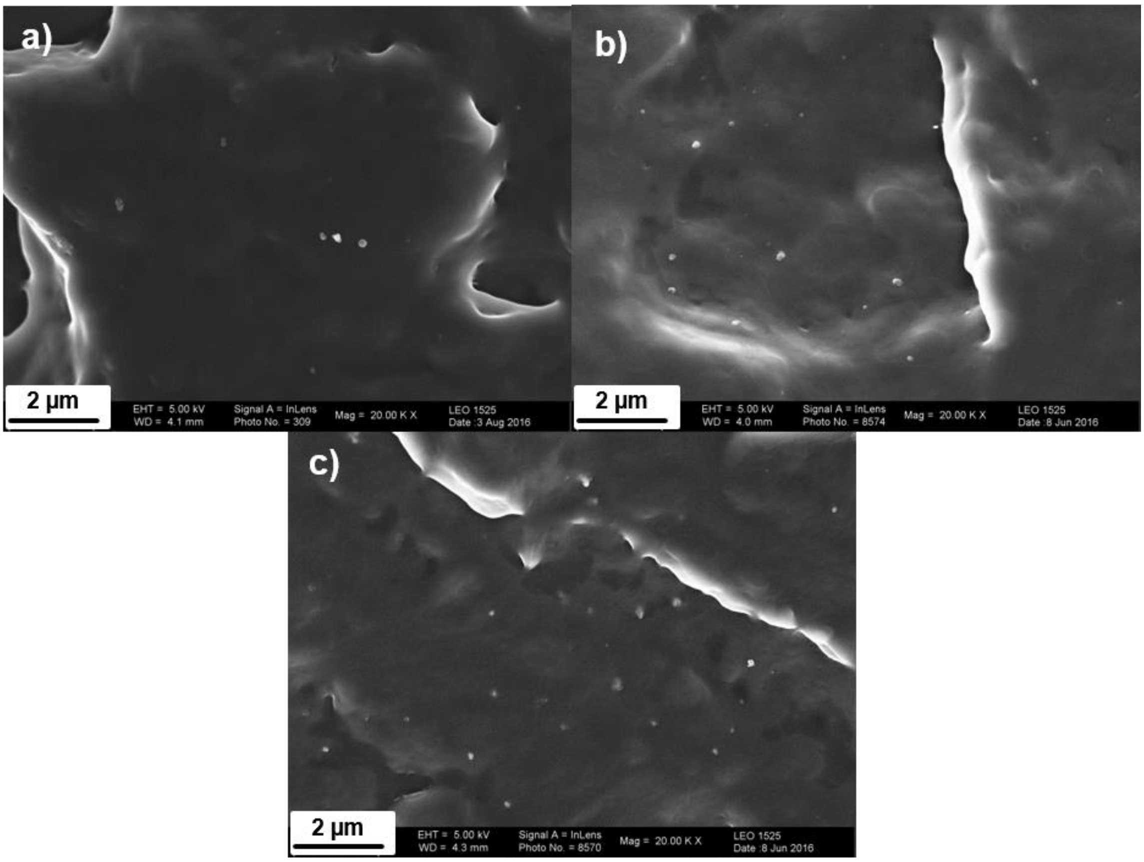

Figure 5.31 SEM images of iPP nanocomposite (0.5 wt%) cross sections at a magnification of 20k a) MgO@Mg(OH)$_2$, b) SiO$_2$ and c) BaTiO$_3$.

5.3.3 Mechanical Properties

The mechanical properties of the composites were evaluated from stress-strain measurements (Table 5.12). It is of importance for applications with electrical aspects - like insulation - that these are not negatively influenced by the presence of the fillers. Nanocomposites with about 5 wt% of filler (masterbatches) show no significant change in Young modulus E_t (2130 MPa for reference iPP) or yield stress σ_Y (43.3 MPa for iPP). The smaller and in part not significant differences are in line with the similar thermal properties of the composites. In contrast to, for example, carbon nanotubes with high aspect ratios, the volume of the isotropic fillers is too small for filler–filler interactions and thus, there is no major influence on the E-modulus and yield stress.[139, 194] The presence of agglomerates within the composite could lead to a noticeable loss of yield strength, which consistently seems not the case in the obtained materials. The elongation at break ε_B decreases from 234% for reference iPP to 49.7% for MgO, 17.4% for SiO$_2$ and 9.2% for BaTiO$_3$ nanoparticles in the case of 5 wt% oxide filler content. The decrease is typically caused by hydrodynamic effects, a reduced mobility of polymer chains within the composite,[97] i.e. if, like here, no strong filler-matrix interactions are present. Interestingly, the elongation at break in iPP/MgO@Mg(OH)$_2$ is not decreasing as much as for iPP/SiO$_2$ or iPP/BaTiO$_3$. Possibly, the modified surface of MgO@Mg(OH)$_2$ is more compatible to the matrix than that of BaTiO$_3$. Nanocomposites obtained from melt compounding of the masterbatches show similar results in the mechanical behavior with the exception of the elongation at break, which is also not affected by the nanoparticles (Table 5.12). The volume fraction of nanoparticles (0.21-0.08 vol%) are too low for an impact in the mechanical properties. Such low volume fractions are typically used in dielectric applications with enhanced requirements.

Table 5.12. Mechanical properties of iPP/oxidic nanocomposite masterbatches and prepared by melt compounding of nanocomposite masterbatches.

Filler	**Filler content [wt%]**	**Volume fraction [vol%]**	**Young-modulus E_t [MPa]**	**Yield stress σ_Y [MPa]**	**Elongation at break ε_B [%]**
ref. iPP[a]	-	-	2130 ± 180	43.3 ± 0.4	234 ± 64
MgO	5.0	1.11	2190 ± 180	42.5 ± 0.4	49.7 ± 15.7
SiO$_2$	4.8	1.71 - 2.02	2140 ± 180	41.7 ± 0.8	17.4 ± 5.8
BaTiO$_3$	4.5	0.72	1970 ± 490	44.2 ± 0.2	9.2 ± 1.6
comm. iPP[b]	-	-	1900 ± 190	44.1 ± 0.4	370 ± 11
MgO	0.5	0.13	1890 ± 140	43.6 ± 0.8	360 ± 8
SiO$_2$	0.5	0.17-0.21	1880 ± 90	44.1 ± 0.4	371 ± 17
BaTiO$_3$	0.5	0.08	1930 ± 120	44.7 ± 0.3	360 ± 36

a) prepared by metallocene/MAO catalyst b) HB311BF by *Borealis*

5.3.4 Conclusion

Isotactic PP nanocomposites containing MgO@Mg(OH)$_2$ (35 nm), SiO$_2$ (20-60 nm) or BaTiO$_3$ nanoparticles (50 nm) with a fine distribution were obtained in a two-step process. The first step was an *in situ* polymerization, using the catalytic action of a metallocene/MAO catalyst system to cover the primary filler particles with some iPP. The originally formed agglomerates of the filler nanoparticles are broken down in case of MgO@Mg(OH)$_2$ by treating the surface with DBM (chapter 5.1), and by MAO and ultrasound impact in case of SiO$_2$ and BaTiO$_3$. The most homogeneous distribution in a masterbatch with 5 wt% filler content is reached for MgO@Mg(OH)$_2$, followed by that for

$BaTiO_3$. The separation of the agglomerates was rudimentary in SiO_2, which was related to its higher surface area, leading to lower densities of MAO on the surface. The scale of about 500 g of the preparation of the masterbatches gives access to about 5 kg of a nanocomposite with 0.5 wt% nanofiller content after melt compounding with commercial iPP. SEM analysis and mechanical parameter are consistent with a predominantly single-particle distribution of the oxides. The E-modulus and yield strength are those of iPP. The elongation at break is likewise at the level of the matrix polymer. A relatively small elongation at break (below 49%) is only found in the nanocomposites with 5 wt%, showing the decreased mobility of polymer matrix segments, typical for a composite with a well-distributed filler. Thus, an effective two step procedure was elaborated to arrive at multi kilograms of an iPP composite with basically single nanoparticular $MgO@Mg(OH)_2$, SiO_2 or $BaTiO_3$. Functionalized polyolefins or compatibilizers were not used. These latter may negatively influence electrical properties (e.g. breakdown voltage). Their usage was avoided in this study, while reaching the goal of a very low – i.e. not detected - agglomerate content.

6 Materials and Methods

6.1 Materials

6.1.1 Gases

Argon used as protective gas with a purity of 99.996% (grade 5.0) was purchased from *Westfalen AG*.

Ethylene and **Propylene** were used as monomers for polymerization and obtained from *Gerling Holz+Co* with a purity of 99.8% (grade 3.0). Before use Ethylene resp. Propylene were passed through columns filled with *BASF* catalyst R3-11/G and molecular sieve (4 Å).

6.1.2 Chemicals

Toluene was distilled from KOH before use and subsequently purified over columns filled with *BASF* catalyst R3-11/G and molecular sieve (4 Å). It was purchased from *BASF*.

Dibutyl magnesium (**DBM**) (1 molL^{-1} in heptane) was purchased from *Sigma Aldrich* and used as received.

1-Octene (98%; *Sigma Aldrich*) was used as comonomer for LLDPE polymerization. It was dried over mol sieves and distilled before use.

Linear low-density polyethylene (LLDPE) for melt extrusion was provided from *SABIC* (SABIC PCG61).

Isotactic Polypropylene (iPP) used for diluting obtained masterbatches by melt extrusion was obtained from *Borealis* (HB311BF grade).

6.1.3 Filler

Magnesium oxide/hydroxide nanoparticles MgO@Mg(OH)$_2$ with 31 mol% MgOH (calculated from TGA) (100 nm) purchased from *Iolitec GmbH* were dried in a glass autoclave for 2h under static vacuum and 80 °C before use.

MgO nanoparticles of other qualities <100 nm were obtained from *US Research Nanomaterials Inc.* inclusive a silane treated grade.

SiO_2 and **$BaTiO_3$ nanoparticles** were provided by *Iolitec GmbH* (Table 6.1). They were dried overnight in a glass autoclave under static vacuum and 80 °C before use

Table 6.1 Grades of oxidic nanofillers used in this work.

Filler	Size [nm][a)]	Surface [$m^2 \cdot g^{-1}$][b)]	Density [$g \cdot cm^{-3}$][a)]
$MgO@Mg(OH)_2$	35	51	3.6
SiO_2	20-60	430	2.2 – 2.6
$BaTiO_3$	50	19	5.9

[a)]: Datasheet; [b)]: determined by BET

6.1.4 Catalysts

Bis(*n*-butyl cyclopentadienyl)zirconium(IV) dichloride 1 was purchased from *ABC Chemicals*. It was used as 1 mmol L^{-1} solution in toluene, which was subsequently purified over columns filled with *BASF* catalyst R3-11/G and molecular sieve (4 Å).

[dimethylsilane diyl-bis(2-methyl-4-phenylindenyl)]zirconium(IV) dichloride 2 (rac:meso = 20:1) was purchased from *ABC Chemicals* and used as received. The catalyst was used as 1.5-2 mmol L^{-1} solution in toluene, which was subsequently purified over columns filled with *BASF* catalyst R3-11/G and molecular sieve (4 Å).

6.1.5 Co-catalyst

Methylaluminoxane (MAO) (10% solution in toluene, 1.7 mol L^{-1} aluminum in solution, 5.24 wt% Al content, AXION® CA 1310) was purchased from *Chemtura Organometallics GmbH* and used as received.

6.2 Methods of Characterization

6.2.1 Static Sedimentation

A suspension of 50 mg of MgO@Mg$(OH)_2$ nanoparticles were stirred in 3 mL of toluene containing 0.25 mL of a MAO solution (10 wt%) for 12 hours in a nitrogen atmosphere. The time of sedimentation was subsequently measured in a cuvette placed in a *Jasco V-630* UV-Vis spectrometer by detection of the transmission at a wavelength of 550 nm.

6.2.2 ^{27}Al MAS NMR

^{27}Al magic angle spinning nuclear magnetic resonance (MAS NMR) experiments were performed at an operating frequency of 104.30 MHz on a *Bruker Avance II 400* spectrometer equipped with a 4 mm double resonance probe. A single pulse sequence with a 15° pulse length of 0.66 µs and a recycle delay of 2 s was used in order to obtain quantitative information. Measurements were performed at room temperature and with the MAS frequency of 13 kHz. 4000 transients were acquired for all the samples. Spectra were externally referenced to an 1 M $Al(NO)_3$ aqueous solution, at 0 ppm. Samples were prepared by impregnating MgO@Mg$(OH)_2$ nanoparticles with MAO for 60 min or with DBM for 15 min before impregnation with MAO. Both samples together with a sample of MAO solution were hydrolyzed by washing the samples with water-saturated toluene.

6.2.3 ^{1}H and ^{13}C-NMR

The degree of branching in LLDPE was evaluated from ^{1}H and ^{13}C-NMR spectra. The spectra were recorded on a *Bruker AV3600* spectrometer at 120 °C in 1,2,4-trichlorobenzene and 1,1,2,2-tetrachloroethane-d_2 with 256 scans at 3 seconds relaxation delay for ^{1}H-NMR and with 3076 scans at 2 seconds relaxation delay for ^{13}C-NMR. ^{13}C-NMR spectra were evaluated following actual literature.[172] A representative spectra is given in Figure 6.1.

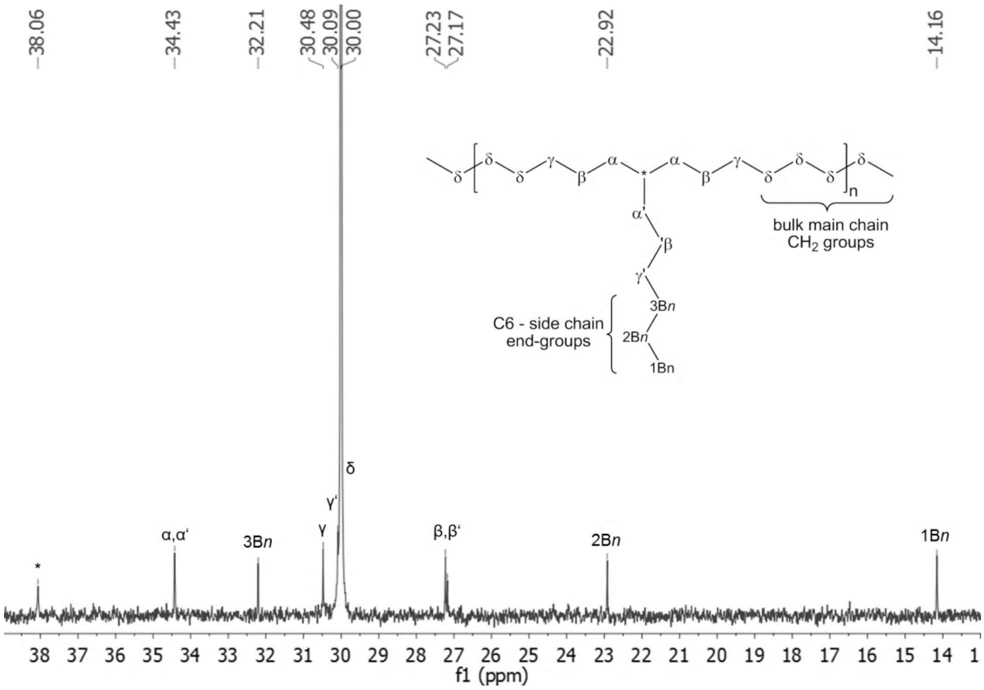

Figure 6.1. Representative ^{13}C-NMR spectra of C8-LLD-PE with 8.7 wt% MgO@Mg(OH)$_2$ content measured in 1,2,4-TCB and 1,1,2,2-tetrachloroethane-d2 at 120 °C.

To determine the tacticity of iPP ^{13}C-NMR spectroscopy was carried out on a *Bruker Avance 400* spectrometer; measurements were at 120 °C. Samples were prepared by dissolving 200 mg of polymer in 5 mL of 1,2,4-trichlorobenzene at 120 °C. 1,1,2,2-tetrachloroethane-d$_2$ (0.6 mL) was added as lock standard as soon as a homogenous solution had formed. Spectra are based on 3076 acquisitions of FIDs; the relaxation delay was 3 s.

6.2.4 Scanning Electron Microscopy (SEM) and Energy-Dispersive X-ray Spectroscopy (EDX)

Nanoparticle size and composite morphologies were investigated by scanning electron microscopy (SEM) (*Gemini Leo 1525* field emission microscope). Test specimen of type 5A obtained from injection molding with a *Haake Minijet* (T_{melt} = 270 °C, T_{mold} = 80 °C, p = 700 bars) were used. These were cooled to liquid nitrogen temperature and cryo-cracked. SEM-EDX measurements of the cross sections were conducted at 20 kV electron acceleration utilizing an *Octane plus* silicon drift detector with 20 scans the latter is limited by the sample starting to melt). Atomic consistence of the samples was averaged after measuring three different spots in each sample utilizing *Team V 4.1* software.

6.2.5 Atomic Force Microscopy (AFM)

Nanoparticle size and composite morphologies were investigated by atomic force microscopy (AFM, *JPK Nanowizard II*). Test specimen of type 5A (DIN EN ISO527-2) were obtained from injection moulding using a *Haake Mini-jet* (T_{melt} = 270 °C, T_{mold} = 80 °C, p = 700 bars). Some of the testing bars were cooled down in liquid nitrogen temperature and cryo-cracked. Cross sections were investigated. A plane cross section was prepared with a cryo ultramicrotom at -70 °C.

6.2.6 Transmission Electron Microscopy (TEM)

TEM imaging was conducted using a *Jeol JEM 2200FS* at 200 kV with two C_s-correctors (*CEOS: CETCOR, CESCOR*). For sample preparation samples of oxidic nanoparticles were suspended in ethanol and pre-treated in an ultrasonic bath for 5 min.

6.2.7 Wide-Angle X-ray Diffraction (WAXD)

Wide-angle X-ray diffraction (WAXD) measurements were carried out on a *PHILIPS X´Pert Pro MPD* Powder Diffractometer with BRAGG-BRENTANO geometry (Cu-K_α: 0.154 nm) with a step size of 0.0334° and 74.93 s time per step.

6.2.8 Thermogravimetric Analysis (TGA)

Thermal weight loss experiments were performed by using a *Mettler Toledo TGA1* equipped with a *GC 200* gas controller. Samples of 10 ± 1 mg were measured in ceramic crucibles with a temperature program starting at room temperature and heated to 600 °C at 10 K min^{-1} under 20 mL min^{-1} air or nitrogen flow.

6.2.9 Differential-Scanning-Calorimetry (DSC)

Melting and crystallization behavior of the materials were investigated by differential scanning calorimetry (DSC) with a *Mettler Toledo DSC1*. Non-isothermal crystallization experiments were started by heating of the samples from 25 °C to 200 °C at 20 $K \cdot min^{-1}$ heating rate. The temperature was maintained at 200 °C for 5 min to remove the thermal history. The samples were then cooled from 200 °C to 25 °C with a cooling rate of 20 $K \cdot min^{-1}$ and the temperature subsequently hold at 25 °C for 5 min. The second melting cycle was performed by heating from 25 °C to 200 °C at a heating rate of 20 K·min^{-1}. Data were extracted from the first endothermic and the second exothermic transitions. The percentage of crystallinity was calculated as the enthalpy of fusion taken from DSC divided by the enthalpy of 100% crystalline PE/iPP. Latter was takes as 293 J·g^{-1}[195] for PE and 207 J·g^{-1}[196] for iPP.

6.2.10 Reaction Tracking of DBM and MgO@Mg(OH)$_2$

A custom-made gas burette was used to record the formation of *n*-butane gas in the reaction of DBM (0.6 mmol) with MgO@Mg(OH)$_2$ nanoparticles as they were delivered (1 g) in 20 mL of toluene. The volume was determined every 30 seconds for 10 minutes.

6.2.11 High-Temperature Size Exclusion Chromatography (SEC)

Molecular weight distributions of neat LLDPE and iPP were obtained from high-temperature size exclusion chromatography (SEC) performed on a *PL-GPC 220* with a refractive index detector. A polystyrene calibration curve was used to obtain relative molecular masses.[197] Samples were measured in 1,2,4-trichlorobenzene at 130 °C and using a flow rate of 1 mL·min^{-1}.

6.2.12 Tensile Strain Measurements

Tensile test measurements were performed following DIN EN ISO 527 in an air-conditioned measuring room on a *Zwick-Roell Zwicki-Line Z1.0* machine equipped with a 1 kN force-transducer and *VideoXtense* detection of the elongation. Test specimen of type 5A prepared by injection molding were used for mechanical tests. The crosshead speed was 1 mm min^{-1} for determination of Young's modulus and 50 mm·min^{-1} for determination of yield stress and elongation at break. Yield stress and Young's modulus were calculated with a *Zwick Test Xpert II* software version 2.4 according to ISO 527. Values of volume fractions of oxidic fillers were calculated by converting weight fractions to volume fractions taking the density of LLDPE (0.92 g·cm^{-3}) resp. iPP (0.90 g·cm^{-3}), and MgO@Mg(OH)$_2$ as 3.6 g·cm^{-3}, for SiO$_2$ as 2.2 – 2.6 g·cm^{-3} and for BaTiO$_3$ as 5.9 g·cm^{-3}.

6.3 Polyolefin Polymerization

Polymerization reaction in this work were carried out using standard SCHLENK techniques under argon atmosphere.

6.3.1 Preparation of LLDPE and LLDPE/MgO@Mg(OH)$_2$ Nanocomposites in 1 L Glass Autoclave

Linear low-density polyethylene (LLDPE) and LLDPE/MgO nanocomposites were synthesized in 1 L glass autoclave reactors (*Büchi Glas Uster AG*). Reactors were kept at 80 °C under a dynamic vacuum (10^{-2} mbar) for two hours before use. LLDPE was prepared by filling the reactor at room temperature with 300 mL of purified toluene, adding 8 mL of octene and the appropriate amount of MAO solution. The content of the reactor was subsequently heated to 60 °C. After saturating the solution with ethylene at 2 bar pressure while stirring at 270 rpm (60 min), the polymerization was started by injecting with syringe 0.5 mL of an 1 mmol·L^{-1} toluene solution of bis(*n*-butyl cyclopentadienyl)zirconium(IV) dichloride **1**. Composites of LLDPE/MgO were synthesized accordingly. In those cases, the reactor filled with MgO (0.5 – 2 g) was held at 80 °C under dynamic vacuum (10^{-2} mbar) over night to condition the filler. Various amounts of DBM solution (1 mol·L^{-1} in heptane) were added to the stirred mixture of filler, toluene and 1-octene at 60 °C. MAO and ethylene were added after 15 min, and subsequently after 45 min the catalyst solution. Reactions were terminated after 30 min by removal of ethylene and addition of 20 mL of ethanol. The solid polymeric materials were collected on a frit, washed with ethanol and subsequently dried to constant weight (at least 48 hours) in a vacuum oven at 40 °C.

6.3.2 Preparation of LLDPE and LLDPE/MgO@Mg(OH)$_2$ Nanocomposites in 10 L scale

Linear low density polyethylene and LLDPE/MgO@Mg(OH)$_2$ nanocomposites were prepared in a 10 L double walled stainless steel reactor (*Karl Kurt Juchheim Laborgeräte GmbH*). The reactor was heated and cooled using a thermostat and had an additional external cooling circuit. The reactor was cleaned, closed and dried at 80 °C under a dynamic vacuum (10^{-2} mbar) for at least two hours before use. LLDPE was prepared by first filling the reactor with 3.5 L of purified toluene, 80 mL resp. 160 mL of 1-octene (depending on reaction time) and the appropriate amount of MAO solution. After saturating the solution at 60 °C with ethylene at 2 bar pressure while stirring at 200 rpm (60 min), the polymerization was started by injecting (by syringe) 5 mL of an 1 mM toluene solution of bis(*n*-butyl cyclopentadienyl)zirconium(IV) dichloride **1**. Reactions were carried out in semibatch mode with respect to ethylene at 2 bars with a limitation of 5000 $mL \cdot min^{-1}$ to keep the temperature of the reactor in the range of 60-67 °C. Reactions were terminated after 30-60 min by removal of ethylene (*in vacuo*) and addition of 250 mL of ethanol. The solid polymeric materials were collected on a frit, washed with ethanol and subsequently dried to constant weight (at least 48 hours) in a vacuum oven at 40 °C.

Composites of LLDPE/$MgO@Mg(OH)_2$ were synthesized accordingly. In those cases, the reactor filled with $MgO@Mg(OH)_2$ (ca 20 g) was held at 80 °C under a dynamic vacuum of 10^{-2} mbar overnight in order to condition the filler, before addition of toluene and 1-octene. Optionally, the relevant amount of DBM in heptane solution (0.5 $mL \cdot g^{-1}$ filler) was added to the stirred mixture 15 min before the addition of MAO, heating to 60 °C and saturating with ethylene for at least 45 min.

6.3.3 Preparation of isotactic Polypropylene (iPP) and iPP/Nanocomposites

Reference isotactic polypropylene (iPP) and iPP/nanocomposites were synthesized in a 10 L steel reactor (*Karl Kurt Juchheim Laborgeräte GmbH*). The reactor was kept at 80 °C under a dynamic vacuum (approx. 10^{-2} mbar) overnight before use. Reference iPP was prepared by filling the reactor at room temperature with 3.5 L of purified toluene and an appropriate amount of MAO solution. After saturating the solution with propylene at 2 bar pressure while stirring at 200 rpm (60-120 min), the polymerization was started by injecting 1 mL of an 1.5 mmol solution of [dimethylsilane diyl-bis(2-methyl-4-phenylindenyl)]zirconium(IV) dichloride **2** by syringe. Polyreactions and impregnation were carried out at 45 °C starting temperature. Composites of iPP with $MgO@Mg(OH)_2$, SiO_2 and $BaTiO_3$ were prepared accordingly with 3 mL of the catalyst solution. In those cases, the reactor filled with 25 g of the filler was held at 80 °C under dynamic vacuum (10^{-2} mbar) overnight, also to condition the filler. In case of $MgO@Mg(OH)_2$, various amounts of DBM solution were added to the stirred mixture of filler and toluene for 15 min before addition of MAO and propylene. In case of SiO_2 and $BaTiO_3$ nanoparticles the filler was dispersed in toluene and pretreated with ultrasound for 20 min under argon atmosphere before impregnation with MAO. Reactions were terminated after 60-120 min by removal of propylene and addition of 100 mL of ethanol. The solid polymeric materials were collected on a frit, washed with ethanol and subsequently dried to constant weight (at least 48 hours) in a vacuum oven at 40 °C.

6.3.4 Preparation of LLDPE/MgO Nanocomposites by Melt Mixing

Composites of linear low density polyethylene (*SABIC* LLDPE C6) and MgO@Mg(OH)$_2$ were prepared in a co-rotating twin-screw extruder (*Thermo Scientific, Prism Eurolab 16, L/D 40:1*) at 280 °C barrel and 260 °C die temperature at 35 rpm rotation speed. Composites with filler contents of 5 wt% were prepared. LLDPE and MgO were manually premixed and subsequently fed to the extruder. The composite melt leaving the round die was run through a water bath, air dried, granulated and subsequently dried in a vacuum oven at 40 °C to constant weight. The initial composite was subsequently run through the extruder again to ensure a good mixing of the components. The residence time inside the extruder was recorded as minimum 3 minutes.

6.3.5 Preparation of iPP/Nanocomposites with 0.5 wt% Filler by Melt Mixing

Composites of iPP with 0.5 wt% filler were prepared in a co-rotating twin-screw extruder (*Thermo Scientific, Prism Eurolab 16, L/D 40:1*) at 280 °C barrel and 260 °C die temperature and 35 rpm rotation speed. Isotactic PP and the composite masterbatches were manually premixed and fed to the extruder. The resulting melt leaving the die was cooled in a water bath, air-dried, granulated and subsequently dried in a vacuum oven at 40 °C to constant weight. The melt mixing procedure was performed twice to ensure a homogeneous mixing of the components. The residence time inside the extruder was recorded at a minimum of 3 minutes.

7 References

1. H. Staudinger, *Ber. dtsch. Chem. Ges. A/B*, **53**, 1073 (1920).
2. H. Staudinger, *Ber. dtsch. Chem. Ges. A/B*, **57**, 1203 (1924).
3. L.L. Böhm, H.-F. Enderle, M. Fleissner, and F. Kloos, *Angew. Makromol. Chemie*, **244**, 93 (1997).
4. N. Pasquini and A. Addeo, *Polypropylene handbook,* 2nd edn., Carl Hanser Verlag, München (2005).
5. PlasticsEurope Market Research Group, *The Compelling Facts About Plastics 2009* (2016). http://www.plasticseurope.org/document/the-compelling-facts-about-plastics-2009.aspx.
6. PlasticsEurope Market Research Group, *Plastics – the Facts 2015* (2016). http://www.plasticseurope.org/Document/plastics---the-facts-2015.aspx.
7. A. Mariacher, “Downgauging boosts resin’s,” in *Modern plastics world encyclopedia 2008/ with buyers*, Canon Communications, Los Angeles (2008).
8. S. Thomas, *Recent advances in polymer nanocomposites: Synthesis and characterisation*, VSP, Leiden, Boston (2010).
9. R.B. Seymour and T. Cheng, *History of Polyolefins: The World's Most Widely Used Polymers*, Springer Netherlands, Dordrecht (1985).
10. K.B. Sinclair, *Macromol. Symp.*, **173**, 237 (2001).
11. M. Aulbach and F. Küber, *Chem. unserer Zeit*, **28**, 197 (1994).
12. W. Keim, *Kunststoffe: Synthese, Herstellungsverfahren, Apparaturen*, Wiley-VCH, Weinheim (2006).
13. A.H. Tullo, *C&E New*, **88** (2010).
14. M. Stürzel, S. Mihan, and R. Mülhaupt, *Chem. Rev.*, **116**, 1398 (2016).
15. W. Kaminsky, *Macromol. Chem. Phys.*, **209**, 459 (2008).
16. H. v. Pechmann, *Ber. Dtsch. Chem. Ges.*, **31**, 2950 (1898).
17. E. Bamberger and F. Tschirner, *Ber. Dtsch. Chem. Ges.*, **33**, 955 (1900).
18. E.W. Fawcett, R.O. Gibson, M.W. Perrin, J.G. Paton, and E.G. Williams, GB471590 (A) (1936).
19. E. W. Fawcett, R. U. Gibson, M. W. Perrin, J. G. Paton, and E. G. Williams, *Chem. Abstr.*, **34**, 24330 (1940).
20. A.J. Peacock, *Handbook of polyethylene: Structures, properties, and applications*, Marcel Dekker, New York (2000).

21. K. Ziegler, *Angew. Chem.*, **76**, 545 (1964).

22. K. Ziegler, *Angew. Chem.*, **64**, 323 (1952).

23. K. Ziegler, E. Holzkamp, H. Breil, and H. Martin, *Angew. Chem.*, **67**, 426 (1955).

24. E.J. Arlman and P. Cossée, *J. Catal.*, **3**, 80 (1964).

25. Symposium "50 Jahre Ziegler-Katalysatoren", *Symposium "50 Jahre Ziegler-Katalysatoren"*, Schöningh, Paderborn (2004).

26. R. Mülhaupt, *Macromol. Chem. Phys.*, **204**, 289 (2003).

27. G. Natta, *Angew. Chem.*, **68**, 393 (1956).

28. G. Natta, P. Pino, G. Mazzanti, and U. Giannini, *J. Am. Chem. Soc.*, **79**, 2975 (1957).

29. G. Natta, G. Dall'Asta, G. Mazzanti, U. Giannini, and S. Cesca, *Angew. Chem.*, **71**, 205 (1959).

30. G. Natta, *Angew. Chem.*, **76**, 553 (1964).

31. P. Galli and G. Vecellio, *Prog. Polym. Sci.*, **26**, 1287 (2001).

32. P. Galli, *J. Macromol. Sci. Part A Pure Appl. Chem.*, **36**, 1561 (1999).

33. D.S. Breslow and N.R. Newburg, *J. Am. Chem. Soc.*, **79**, 5072 (1957).

34. A. Andresen, H.-G. Cordes, J. Herwig, W. Kaminsky, A. Merck, R. Mottweiler, J. Pein, H. Sinn, and H.-J. Vollmer, *Angew. Chem.*, **88**, 689 (1976).

35. H. Sinn, W. Kaminsky, H.-J. Vollmer, and R. Woldt, *Angew. Chem. Int. Ed. Engl.*, **19**, 390 (1980).

36. H. Sinn and W. Kaminsky, *Adv. Organomet. Chem.*, **18**, 99 (1980).

37. E.Y.-X. Chen and T.J. Marks, *Chem. Rev.*, **100**, 1391 (2000).

38. H.G. Alt and A. Köppl, *Chem. Rev.*, **100**, 1205 (2000).

39. W. Kaminsky and R. Steiger, *Polyhedron*, **7**, 2375 (1988).

40. C. Sishta, R.M. Hathorn, and T.J. Marks, *J. Am. Chem. Soc.*, **114**, 1112 (1992).

41. D.E. Babushkin, C. Naundorf, and H.H. Brintzinger, *Dalton Trans.*, 4539 (2006).

42. M. Brookhart and M.L.H. Green, *J. Organomet. Chem.*, **250**, 395 (1983).

43. R.H. Grubbs and G.W. Coates, *Acc. Chem. Res.*, **29**, 85 (1996).

44. P. Margl, L. Deng, and T. Ziegler, *J. Am. Chem. Soc.*, **121**, 154 (1999).

45. L. Resconi, S. Bossi, and L. Abis, *Macromolecules*, **23**, 4489 (1990).

46. R. Mülhaupt and B. Rieger, *Chimia*, **50**, 10 (1996).

47. J.C.W. Chien and B.-P. Wang, *J. Polym. Sci. A Polym. Chem.*, **28**, 15 (1990).

48. M. Hoff, *Polymerisation sterisch gehinderter Alkene mit single-site Katalysatoren*. Dissertation, Hamburg (2007).

49. F.R.W.P. Wild, L. Zsolnai, G. Huttner, and H.H. Brintzinger, *J. Organomet. Chem.*, **232**, 233 (1982).

50. W. Kaminsky, K. Külper, H.H. Brintzinger, and F.R.W.P. Wild, *Angew. Chem.*, **97**, 507 (1985).

51. J.A. Ewen, *J. Am. Chem. Soc.*, **106**, 6355 (1984).

52. J.A. Ewen, R.L. Jones, A. Razavi, and J.D. Ferrara, *J. Am. Chem. Soc.*, **110**, 6255 (1988).

53. G.W. Coates, *Chem. Rev.*, **100**, 1223 (2000).

54. T. Halbach, *Katalytische Olefinpolymerisation und in-situ Synthese von Böhmit- und Calciumcarbonat-Nanocompositen*. Dissertation, Freiburg (2008).

55. J. A. M. Canich and H. W. Turner, WO9212162 (1992).

56. J. C. Stevens, F. J. Timmers, D. R. Wilson, G. F. Schmidt, P. N. Nickias, R. K. Rosen, G. W. Knight, and S.-Y. Lai, EP0416815 (1991).

57. A.L. McKnight and R.M. Waymouth, *Chem. Rev.*, **98**, 2587 (1998).

58. P.S. Chum, W.J. Kruper, and M.J. Guest, *Adv. Mater.*, **12**, 1759 (2000).

59. L.K. Johnson, C.M. Killian, and M. Brookhart, *J. Am. Chem. Soc.*, **117**, 6414 (1995).

60. S.D. Ittel, L.K. Johnson, and M. Brookhart, *Chem. Rev.*, **100**, 1169 (2000).

61. S. Mecking, *Angew. Chem. Int. Ed.*, **40**, 534 (2001).

62. T.R. Younkin, *Science*, **287**, 460 (2000).

63. B.L. Small, M. Brookhart, and A.M.A. Bennett, *J. Am. Chem. Soc.*, **120**, 4049 (1998).

64. G.J.P. Britovsek, V.C. Gibson, S.J. McTavish, G.A. Solan, A.J.P. White, D.J. Williams, B.S. Kimberley, and P.J. Maddox, *Chem. Commun.*, 849 (1998).

65. G.J.P. Britovsek, M. Bruce, V.C. Gibson, B.S. Kimberley, P.J. Maddox, S. Mastroianni, S.J. McTavish, C. Redshaw, G.A. Solan, S. Strömberg, A.J.P. White, and D.J. Williams, *J. Am. Chem. Soc.*, **121**, 8728 (1999).

66. J. Heinemann, R. Mülhaupt, P. Brinkmann, and G. Luinstra, *Macromol. Chem. Phys.*, **200**, 384 (1999).

67. V.C. Gibson and S.K. Spitzmesser, *Chem. Rev.*, **103**, 283 (2003).

68. T. Yasumoto, T. Yamagata, and K. Mashima, *Organometallics*, **24**, 3375 (2005).

69. H. Makio, N. Kashiwa, and T. Fujita, *Adv. Synth. Catal.*, **344**, 477 (2002).

70. G.W. Coates, P.D. Hustad, and S. Reinartz, *Angew. Chem. Int. Ed.*, **41**, 2236 (2002).

71. G.G. Hlatky, *Chem. Rev.*, **100**, 1347 (2000).

72. A.-M. Uusitalo, T.T. Pakkanen, and E.I. Iskola, *J. Mol. Catal. Chem.*, **177**, 179 (2002).

73. K. Soga and M. Kaminaka, *Makromol. Chem.*, **194**, 1745 (1993).

74. Y.S. Ko, T.K. Han, J.W. Park, and S.I. Woo, *Macromol. Rapid Commun.*, **17**, 749 (1996).

75. B. Jongsomjit, S. Ngamposri, and P. Praserthdam, *Catalysis Letters*, **100**, 139.

76. De Fátima V. Marques, Maria and A. Conte, *J. Appl. Polym. Sci.*, **86**, 2054 (2002).

77. S. Sensarma and S. Sivaram, *Polym. Int.*, **51**, 417 (2002).

78. P.G. Belelli, M.L. Ferreira, and D.E. Damiani, *Appl. Catal., A.*, **228**, 189 (2002).

79. J.-T. Xu, Y.-B. Zhu, Z.-Q. Fan, and L.-X. Feng, *J. Polym. Sci. A Polym. Chem.*, **39**, 3294 (2001).

80. L. Korach and K. Czaja, *Polymer Bulletin*, **46**, 67.

81. A. Köppl and H.G. Alt, *J. Mol. Catal. Chem.*, **165**, 23 (2001).

82. B. Jongsomjit, P. Praserthdam, and P. Kaewkrajang, *Mater. Chem. Phys.*, **86**, 243 (2004).

83. H.G. Alt, *J. Chem. Soc., Dalton Trans.*, 1703 (1999).

84. A.J.D. de Freitas, J.H.Z. dos Santos, S.M.P. Meneghetti, and M.R. Meneghetti, *J. Appl. Polym. Sci.*, **119**, 3051 (2011).

85. S. Abedi and M. Abdouss, *Appl. Catal., A.*, **475**, 386 (2014).

86. K.A. Carrado and L. Xu, *Chem. Mater.*, **10**, 1440 (1998).

87. S.-W. Kuo, W.-J. Huang, S.-B. Huang, H.-C. Kao, and F.-C. Chang, *Polymer*, **44**, 7709 (2003).

88. J.R. Severn, J.C. Chadwick, R. Duchateau, and N. Friederichs, *Chem. Rev.*, **105**, 4073 (2005).

89. M. Xanthos, *Functional fillers for plastics*, Wiley-VCH, Weinheim (2005).

90. R.N. Rothon, *Adv. Polym. Sci.*, **139**, 67 (1999).

91. B. Pukánszky and E. Fekete, *Adv. Polym. Sci.*, **139**, 109 (1999).

92. H.R. Fischer, L.H. Gielgens, and T.P.M. Koster, *Acta Polym.*, **50**, 122 (1999).

93. G.H. Michler, *Kunststoff-Mikromechanik: Morphologie, Deformations- und Bruchmechanismen von Polymerwerkstoffen*, Carl Hanser Verlag, München, Wien (1992).

94. R. Mülhaupt, T. Engelhardt, and N. Schall, *Kunstst.-Plast Eur.*, **91**, 178-190 (2001).

95. R. Mülhaupt, *Kunstst.-Plast Eur.*, **94**, 76-88 (2004).

96. J. Qian and C.-Y. Guo, *TOMACROJ*, **4**, 1 (2010).

97. T.S. Halbach, Y. Thomann, and R. Mülhaupt, *J. Polym. Sci. A Polym. Chem.*, **46**, 2755 (2008).

98. P.N. Khanam and M.A.A. AlMaadeed, *Adv. Manuf. Polym. Compos. Sci.*, **1**, 63 (2015).

99. J. Aalaie, A. Rahmatpour, and S. Maghami, *J. of Macromolecular Sc., Part B*, **46**, 877 (2007).

100. Y. Song, L. Zeng, A. Guan, and Q. Zheng, *Polymer*, **121**, 106 (2017).

101. C.L. Wu, M.Q. Zhang, M.Z. Rong, and K. Friedrich, *Compos. Sci. Technol.*, **62**, 1327 (2002).

102. H.-s. Lee, P.D. Fasulo, W.R. Rodgers, and D.R. Paul, *Polymer*, **46**, 11673 (2005).

103. M. Alexandre and P. Dubois, *Mater. Sci. Eng. R Rep.*, **28**, 1 (2000).

104. G. Kickelbick, *Chem. unserer Zeit*, **39**, 46 (2005).

105. J.-C. Huang, Z.-k. Zhu, J. Yin, X.-f. Qian, and Y.-Y. Sun, *Polymer*, **42**, 873 (2001).

106. G. Gorrasi, M. Tortora, V. Vittoria, D. Kaempfer, and R. Mülhaupt, *Polymer*, **44**, 3679 (2003).

107. R.K. Bharadwaj, *Macromolecules*, **34**, 9189 (2001).

108. M. Tortora, G. Gorrasi, V. Vittoria, G. Galli, S. Ritrovati, and E. Chiellini, *Polymer*, **43**, 6147 (2002).

109. F. Dietsche and R. Mülhaupt, *Polym. Bull.*, **43**, 395 (1999).

110. J.W. Gilman, C.L. Jackson, A.B. Morgan, R. Harris, E. Manias, E.P. Giannelis, M. Wuthenow, D. Hilton, and S.H. Phillips, *Chem. Mater.*, **12**, 1866 (2000).

111. M. Zanetti, T. Kashiwagi, L. Falqui, and G. Camino, *Chem. Mater.*, **14**, 881 (2002).

112. J.W. Gilman, *Appl. Clay Sci.*, **15**, 31 (1999).

113. H.-J. Gläsel, E. Hartmann, L. Wennrich, T. Höche, and M.R. Buchmeiser, *Macromol. Mater. Eng.*, **292**, 70 (2007).

114. H.-J. Gläsel, E. Hartmann, R. Mehnert, L. Wennrich, A. Prager-Duschke, H. Khalil, K.H. Hallmeier, L. Makhova, C. Thieroff, and M.R. Buchmeiser, *Macromol. Mater. Eng.*, **292**, 1140 (2007).

115. F. Bauer, V. Sauerland, H.-J. Gläsel, H. Ernst, M. Findeisen, E. Hartmann, H. Langguth, B. Marquardt, and R. Mehnert, *Macromol. Mater. Eng.*, **287**, 546 (2002).

116. F. Bauer, R. Flyunt, K. Czihal, M.R. Buchmeiser, H. Langguth, and R. Mehnert, *Macromol. Mater. Eng.*, **291**, 493 (2006).

117. O. Meincke, D. Kaempfer, H. Weickmann, C. Friedrich, M. Vathauer, and H. Warth, *Polymer*, **45**, 739 (2004).

118. R.A. Vaia, S. Vasudevan, W. Krawiec, L.G. Scanlon, and E.P. Giannelis, *Adv. Mater.*, **7**, 154 (1995).

119. T. Tanaka, A. Nose, Y. Ohki, and Y. Murata, "PD Resistance Evaluation of LDPE/MgO Nanocomposite by a Rod-to-Plane Electrode System," in *IEEE Conference 2006*.

120. D. Ma, R.W. Siegel, J.-I. Hong, L.S. Schadler, E. Mårtensson, and C. Önneby, *Journal of Materials Research*, **19**, 857 (2004).

121. S. Zakrzewska, A.C. dos Ouros, N. Schramm, d. Jehnichen, L. Häussler, d. Pospiech, B. Voit, U. Schulze, and H.O. Pastore, *Eur. Polym. J.*, **65**, 238 (2015).

122. W. Kaminsky, *Materials*, **7**, 1995 (2014).

123. S.B. Amin and T.J. Marks, *Angew. Chem. Int. Ed.*, **47**, 2006 (2008).

124. W. Kaminsky, *J. Polym. Sci. A Polym. Chem.*, **42**, 3911 (2004).

125. W. Caseri, *Macromol. Rapid Commun.*, **21**, 705 (2000).

126. R. Xalter, F. Pelascini, and R. Mülhaupt, *Macromolecules*, **41**, 3136 (2008).

127. M. Etcheverry, M.L. Ferreira, N.J. Capiati, A. Pegoretti, and S.E. Barbosa, *Composites Part A*, **39**, 1915 (2008).

128. P.A. Zapata, R. Quijada, I. Lieberwirth, and R. Benavente, *Macromol. React. Eng.*, **5**, 294 (2011).

129. R.A. Vaia, H. Ishii, and E.P. Giannelis, *Chem. Mater.*, **5**, 1694 (1993).

130. X. Zhang and L.C. Simon, *Macromol. Mater. Eng.*, **290**, 573 (2005).

131. R.S.A. Meyer and G.A. Luinstra, "Iron Catalyst in the Preparation of Polyolefin Composites," in *Polyolefins: 50 years after Ziegler and Natta II: Polyolefins by Metallocenes and Other Single-Site Catalysts,* W. Kaminsky, Ed., Springer Berlin Heidelberg, Berlin, Heidelberg (2013).

132. M. Alexandre, M. Pluta, P. Dubois, and R. Jérôme, *Macromol. Chem. Phys.*, **202**, 2239 (2001).

133. D. Bonduel, S. Bredeau, M. Alexandre, F. Monteverde, and P. Dubois, *J. Mater. Chem.*, **17**, 2359 (2007).

134. D. Bonduel, M. Mainil, M. Alexandre, F. Monteverde, and P. Dubois, *Chem. Commun.*, 781 (2005).

135. A. Funck and W. Kaminsky, *Compos. Sci. Technol.*, **67**, 906 (2007).

136. T. Sun and J.M. Garcés, *Adv. Mater.*, **14**, 128 (2002).

137. J. Ma, Z. Qi, and Y. Hu, *J. Appl. Polym. Sci.*, **82**, 3611 (2001).

138. R. Barranco-Garcia, A.E. Ferreira, M.R. Ribeiro, V. Lorenzo, A. Garcia-Penas, J.M. Gomez-Elvira, E. Perez, and M.L. Cerrada, *Polymer*, **151**, 218 (2018).

139. M. Asensio, M. Herrero, K. Nunez, R. Gallego, J.C. Merino, and J.M. Pastor, *Eur. Polym. J.*, **100**, 278 (2018).

140. H.-X. Zhang, X.-Q. Zhang, and K.-B. Yoon, *Polymers (Basel, Switz.)*, **9**, 490/1-490/10 (2017).

141. L.A. Almeida, M.D.F.V. Marques, and K. Dahmouche, *J. Appl. Polym. Sci.*, **135** (2018).

142. Vieira Marques, Maria de Fatima, da Silva Rosa, Jefferson Luis, and da Silva, Marcelo Cosme Vasconcelos., *Polym. Bull. (Heidelberg, Ger.)*, **74**, 2447 (2017).

143. D.M. González, R. Quijada, M. Yazdani-Pedram, J.P. Lourenço, and M.R. Ribeiro, *Polym. Int.*, **65**, 320 (2016).

144. M.D.F.V. Marques and R.M. Fernandes, *J. Nanosci. Nanotechnol.*, **17**, 5095 (2017).

145. P. Dubois, M. Alexandre, F. Hindryckx, and R. Jérôme, *J. Macromol. Sci., Polym. Rev.*, **38**, 511 (1998).

146. M. Alexandre, E. Martin, P. Dubois, M.G. Marti, and R. Jérôme, *Chem. Mater.*, **13**, 236 (2001).

147. M. Alexandre and P. Dubois, “Nanocomposites,” in *Macromolecular engineering: Precise Synthesis, Materials Properties, Applications*, 4th edn., K. Matyjaszewski, Y. Gnanou, and L. Leibler, Eds., Wiley-VCH, Weinheim (2007).

148. N. Ogata, G. Jimenez, H. Kawai, and T. Ogihara, *J. Polym. Sci. B Polym. Phys.*, **35**, 389 (1997).

149. N. Ogata, S. Kawakage, and T. Ogihara, *J. Appl. Polym. Sci.*, **66**, 573 (1997).

150. W. Kaminsky, *Macromol. Chem. Phys.*, **197**, 3907 (1996).

151. W. Kaminsky, J. Dutschke, M. Maedler, M. Miri, and M. Schlobohm, DE3240382 C2 (1982).

152. J. Heinemann, P. Reichert, R. Thomann, and R. Mülhaupt, *Macromol. Rapid Commun.*, **20**, 423 (1999).

153. Z. Li, L.A. Fredin, P. Tewari, S.A. DiBenedetto, M.T. Lanagan, M.A. Ratner, and T.J. Marks, *Chem. Mater.*, **22**, 5154 (2010).

154. N. Guo, S.A. DiBenedetto, D.-K. Kwon, L. Wang, M.T. Russell, M.T. Lanagan, A. Facchetti, and T.J. Marks, *J. Am. Chem. Soc.*, **129**, 766 (2007).

155. B.P. Moller, *Carbon Nanotube Dispersionen: Herstellung, Charakterisierung und Weiterverarbeitung von CNT-Dispersionen und CNT-Polymer-Kompositen,* 1st edn., Südwestdeutscher Verlag für Hochschulschriften, Saarbrücken (2013).

156. T. Takada, Y. Hayase, Y. Tanaka, and T. Okamoto, *IEEE Trans. Dielect. Electr. Insul.*, **15**, 152 (2008).

157. J. Yoshida, T. Maezawa, H. Miyake, Y. Tanaka, T. Takada, Y. Sekiguchi, Y. Murata, and C.C. Reddy, “Space charge accumulation and breakdown in LDPE and LDPE/MgO nano-composite under high dc stress at various temperatures,” in *IEEE CEIDP 2009*.

158. G. Fink, B. Tesche, F. Korber, and S. Knoke, *Macromol. Symp.*, **173**, 77 (2001).

159. R. Goretzki, G. Fink, B. Tesche, B. Steinmetz, R. Rieger, and W. Uzick, *J. Polym. Sci. A Polym. Chem.*, **37**, 677 (1999).

160. B. Wang, W. Zhang, W. Zhang, C. Yu, G. Wang, L. Huang, and A.S. Mujumdar, *Drying Technology*, **25**, 715 (2007).

161. M.S. Mel'gunov, V.B. Fenelonov, E.A. Mel'gunova, A.F. Bedilo, and K.J. Klabunde, *J. Phys. Chem. B*, **107**, 2427 (2003).

162. R. van Grieken, A. Carrero, I. Suarez, and B. Paredes, *Eur. Polym. J.*, **43**, 1267 (2007).

163. S. Pasynkiewicz, *Polyhedron*, **9**, 429 (1990).

164. C.J. Harlan, S.G. Bott, and A.R. Barron, *J. Am. Chem. Soc.*, **117**, 6465 (1995).

165. C. Janiak, B. Rieger, R. Voelkel, and H.-G. Braun, *J. Polym. Sci. A Polym. Chem.*, **31**, 2959 (1993).

166. I. Tritto, M.C. Sacchi, P. Locatelli, and S.X. Li, *Macromol. Chem. Phys.*, **197**, 1537 (1996).

167. L.A. O’Dell, S.L.P. Savin, A.V. Chadwick, and M.E. Smith, *Faraday Discuss*, **134**, 83 (2007).

168. X.M. Liu, G.Q. Lu, and Z.F. Yan, *J. Phys. Chem. B*, **108**, 15523 (2004).

169. C. Pecharromán, I. Sobrados, J. E. Iglesias, and T. González-Carreno and J. Sanz, *J. Phys. Chem. B*, **103**, 6160 (1999).

170. A.R. Ferreira, E. Küçükbenli, A.A. Leitão, and S. de Gironcoli, *Phys. Rev. B*, **84** (2011).

171. W. Kaminsky, A. Funck, and K. Wiemann, *Macromol. Symp.*, **239**, 1 (2006).

172. A.J. Brandolini and D.D. Hills, *NMR spectra of polymers and polymer additives*, Marcel Dekker, New York (2000).

173. P.C. Hiemenz, *Polymer Chemistry: The Basic Concepts*, Marcel Dekker, New York (1984).

174. C.-C. Chu, K.L. White, P. Liu, X. Zhang, and H.-J. Sue, *Carbon*, **50**, 4711 (2012).

175. M.-K. Seo, J.-R. Lee, and S.-J. Park, *Mater. Sci. Eng. A*, **404**, 79 (2005).

176. P. Kalakonda, G.S. Iannacchione, M. Daly, G.Y. Georgiev, Y. Cabrera, R. Judith, and P. Cebe, *J. Appl. Polym. Sci.*, **130**, 587 (2013).

177. Z. Bartczak, A.S. Argon, R.E. Cohen, and T. Kowalewski, *Polymer*, **40**, 2367 (1999).

178. A. Rahmatpour and J. Aalaie, *J. Macromol. Sci. B*, **47**, 929 (2008).

179. M. Trujillo, M.L. Arnal, A.J. Müller, E. Laredo, St. Bredeau, D. Bonduel, and P. Dubois, *Macromolecules*, **40**, 6268 (2007).

180. X. Huang, Q. Ke, C. Kim, H. Zhong, P. Wei, G. Wang, F. Liu, and P. Jiang, *Polym. Eng. Sci.*, **47**, 1052 (2007).

181. M. Joshi, B.S. Butola, G. Simon, and N. Kukaleva, *Macromolecules*, **39**, 1839 (2006).

182. S. Käselau, S. Scheel, L. Petersson, C.-H. Ho, and G.A. Luinstra, *Polym. Int.*, **67**, 1359 (2018).

183. G. Fink, R. Mülhaupt, and H.H. Brintzinger, *Ziegler Catalysts: Recent Scientific Innovations and Technological Improvements*, Springer Berlin Heidelberg, Berlin, Heidelberg (1995).

184. M. Daud, F. Shehzad, and M.A. Al-Harthi, *Arab J Sci Eng*, **43**, 6021 (2018).

185. H.G. Karian, *Handbook of polypropylene and polypropylene composites,* 2nd edn., Marcel Dekker, New York (2003).

186. X.L. Xie, B.G. Li, Z.R. Pan, R.K.Y. Li, and S.C. Tjong, *J. Appl. Polym. Sci.*, **80**, 2105 (2001).

187. A. Durmus, A. Kasgöz, and C. Macosko, *J. Macromol. Sci. B*, **47**, 608 (2008).

188. S.C. Tjong, *Mater. Sci. Eng. R Rep.*, **53**, 73 (2006).

189. X. Zhao, Q. Zhang, D. Chen, and P. Lu, *Macromolecules*, **43**, 2357 (2010).

190. H. Hu, L. Onyebueke, and A. Abatan, *JMMCE*, **09**, 275 (2010).

191. N. Guo, S.A. DiBenedetto, P. Tewari, M.T. Lanagan, M.A. Ratner, and T.J. Marks, *Chem. Mater.*, **22**, 1567 (2010).

192. W. Kaminsky and M. Arndt-Rosenau, “Reactions of Unsaturated Compounds,” in *Applied homogeneous catalysis with organometallic compounds: A comprehensive handbook in three volumes*, 2nd edn., B. Cornils and W.A. Herrmann, Eds., Wiley-VCH, Weinheim (2002).

193. L. Wu and S.E. Wanke, “Product Morphology in Olefin Polymerization with Polymer-Supported Metallocene Catalysts,” in *Handbook of transition metal polymerization catalysts,* R.E. Hoff and R.T. Mathers, Eds., Wiley, Hoboken, NJ (2010).

194. X. Wang, Q. Li, J. Xie, Z. Jin, J. Wang, Y. Li, K. Jiang, and S. Fan, *Nano letters*, **9**, 3137 (2009).

195. T. POLTIMÄE, E. TARASOVA, A. KRUMME, J. ROOTS, and A. VIIKNA, *Mater. Sci.*, **17** (2011).

196. A. van der Wal, J.J. Mulder, and R.J. Gaymans, *Polymer*, **39**, 5477 (1998).

197. J. Janák, K. Macek, and Z. Deyl, *Liquid Column Chromatography: A Survey of Modern Techniques and Applications*, Elsevier Science Limited (2007).

198. *Merck Millipore Chemicals* (2019). http://www.merckmillipore.com/DE/de.

199. IFA, *GESTIS Substance Database* (2019). http://gestis-en.itrust.de.

200. Merck, *Sigma-Aldrich* (2019). http://www.sigmaaldrich.com/technical-service-home/product-catalog.html.

8 Appendix

8.1 Safety and Disposal

Throughout the project, the following chemicals were used in the course of polyolefin nanocomposite samples production. The substances are listed with hazard symbols, H- and P-phrases in Table 8.1.[198–200] All hazardous waste materials were disposed in compliance with legal requirements.

Table 8.1: List of chemicals with their hazardous material characteristics used in this work.

Substance	Hazard pictograms	H-phrase	P-phrase
Acetic acid		H226, H290, H314	P210, P280, P301+P330+P331 P305+P351+P338 P308+P310
Aerosil R8200	substance not yet fully tested		
Argon	-	-	-
BaTiO$_3$ nanoparticles (60 nm)	substance not yet fully tested		
Bis(*n*-butyl cyclopentadienyl) zirconium(IV) dichloride	-	-	-
Dibutylmagnesium		H225, H250, H260, H304, H314, H336, H410, EUH014	P210, P231+P232, P280, P305+ P351+P338, P370+P378, P422
***rac*-dimethylsilyl-bis(2-methyl-4-phenyl-1-indenyl)zirconium(IV) chloride**	substance not yet fully tested		
Ethanol		H225, H319	P210, P240, P305+P351+P338, P403+P233
Ethylene		H220, H280, H336	P210, P260, P304+P340, P315, P377, P381, P405, P403
HCl (37 %)		H290, H314, H335	P260, P280, P303+P361+P353,

			P304+P340+P310, P305+P351+P338
HCl (7 %)		H290	P406
Isotactic polypropylene	-	-	-
Linear low-density polyethylene	-	-	-
Methylaluminoxane		H225, H260, H304, H314, H336, H361d, H373, H412, EUH014	P210, P231+P232, P280, P370+P378, P402+P404, P403+P235
$MgCl_2$	-	-	-
MgO nanoparticles (35 nm)	substance not yet fully tested		
MgOH nanoparticles (100 nm)	substance not yet fully tested		
NaOH		H290, H314	P280, P301+P330+P331, P305+P351+P338, P308+P310
1-Octene		H225, H304, H410	P210, P273, P301+P310, P331, P501
Propylene		H220, H280	P210, P377, P381, P403
SiO_2 nanoparticles (20-60 nm)	substance not yet fully tested		
1,1,2,2-Terachlorethane-d2		H310+H330, H411	P260, P273, P280, P284, P302+P350
1,2,4-Trichlorbenzole		H302, H315, H410	P273, P302+P352
Triisobutylamluminum		H250, H260, H304, H314, H336, H361f, H373, H411, EUH014	P222, P223, P231+P232, P261, P370+P378, P422
Trimethylaluminum		H225, H250, H260, H304, H314, H336, H361d, H373 EUH014	P210, P222, P223, P231+P232, P370+P378, P422
Toluene		H225, H361d, H304, H373, H315, H336	P210, P240, P301+P310+P330, P302+P352, P308+P313, P314, P403+P233

Table 8.2 Used CMR substances of category I+II (GHS).

CAS Number	Chemical name	Treatment and quantity	Number of experiments	Category
Toluene	108-88-3	Solvent for polymerization reaction 300 mL	511	R:2
Toluene	108-88-3	Solvent for polymerization reaction 3.5 L	45	R:2
1,1,2,2-Terachlorethane-d2	33685-54-0	NMR-standard 0.06 mL	35	K:2 M:2
1,1,2,2-Terachlorethane-d2	33685-54-0	NMR-standard 0.6 mL	21	K:2 M:2

8.2 Acknowledgements

An erster Stelle möchte ich mich bei meinem Doktorvater Professor Dr. Gerrit A. Luinstra für die Aufnahme in seinen Arbeitskreis und die fachliche Betreuung meiner Arbeit bedanken.

Professor Dr. Hans-Ulrich Moritz danke ich für die Übernahme des Zweitgutachtens. Dr. Saskia Scheel (ABB AG), Dr. Linnea Petterson (ABB AG) und Dr. Chau Hon Ho (ABB AG) möchte ich für die Unterstützung und den vielen Feedbacks über meine Arbeit danken.

Dr. Felix Scheliga danke ich für die GPC Messungen sowie für die fachliche Unterstützung bei meiner experimentellen Arbeit. Weiterhin möchte ich Renate Walter aus dem Institut für Zoologie für die vielen SEM und EDX Aufnahmen danken, Isabelle Nevoigt für die XRD Messungen, Andreas Konowski für die TEM Aufnahmen, sowie Dr. Young Joo Lee und Dr. Thomas Hackl für die ^{13}C und ^{27}Al-MAS NMR Messungen.

Ich bedanke mich bei dem gesamten Arbeitskreis Luinstra für die herzliche Aufnahme, die fachlichen Diskussionen, aber auch die gemeinsamen Kuchenpausen, Quake Runden und Fachsimpeln abseits der Chemie. Ein besonderer Dank gilt meinen Laborkollegen Dr. Jim Uther, Katharina Jörg und Carmen Spottog für die schöne Zeit in C316, an die ich gerne zurückdenke.

Ein großer Dank geht auch an meine Familie und meinen Freunden für die Unterstützung jenseits der Universität und ihr Verständnis dafür, dass ich in den vielen Jahren nicht immer genug Zeit für sie hatte. Mein größter Dank gilt meiner Freundin Olga, für ihren großen Rückhalt, ihre Geduld und ihr großes Herz. Danke, dass ihr alle für mich da seid.

8.3 Statutory Declaration

I hereby declare on oath that I have written the present dissertation by my own and have not used other than the acknowledged resources and aids. I hereby declare that I have not previously applied or pursued for a doctorate (Ph.D. studies).

Hamburg, 26. May 2019

Sven Käselau